Project Number: 5-C3418.00

Kaikōura Earthquake-Induced Landscape Dynamics Research

13 June 2023

CONFIDENTIAL

Theme 6 – Assessment Report

wsp

150 YEARS IN AOTEAROA

Contact Details

WSP
L9 Majestic Centre
100 Willis Street
Wellington 6011
+64 4 471 7000

Document Details:

Report No:	GER 2023/14
Date:	13 June 2023
Reference:	5-C3418.00
Status:	Rev A

Prepared by

Doug Mason

Reviewed by

P. Brabhaharan

Approved for release by

P. Brabhaharan

Document History and Status

Issue	Date	Author	Reviewed by	Approved by	Status
1	27/03/2023	Doug Mason	P Brabhaharan	P Brabhaharan	Draft
2	22/05/2023	Doug Mason	P Brabhaharan	P Brabhaharan	Rev A

Revision Details

Revision	Details
-	Draft issue
A	Appendix A added

Disclaimers and Limitations

This report ('**Report**') has been prepared by WSP exclusively for GNS Science ('**Client**') in relation to geotechnical site investigations carried out under the Kaikōura Earthquake-Induced Landslide Dynamics (EILD) research programme ('**Purpose**') and in accordance with the Short Form Agreement with the Client dated 22 August 2018. The findings in this Report are based on and are subject to the assumptions specified in the Report. WSP accepts no liability whatsoever for any reliance on or use of this Report, in whole or in part, for any use or purpose other than the Purpose or any use or reliance on the Report by any third party.

In preparing the Report, WSP has relied upon data, surveys, analyses, designs, plans and other information ('**Client Data'**) provided by or on behalf of the Client. Except as otherwise stated in the Report, WSP has not verified the accuracy or completeness of the Client Data. To the extent that the statements, opinions, facts, information, conclusions and/or recommendations in this Report are based in whole or part on the Client Data, those conclusions are contingent upon the accuracy and completeness of the Client Data. WSP will not be liable in relation to incorrect conclusions or findings in the Report should any Client Data be incorrect or have been concealed, withheld, misrepresented or otherwise not fully disclosed to WSP.

Contents

List of Figures

List of Tables

1 Introduction

The 14 November 2016 M_w 7.8 Kaikōura earthquake triggered over 30,000 landslides, hundreds of significant landslide dams and damaged hillslopes that are now susceptible to failure during rainstorms and aftershocks (Massey *et al.*, 2018). The damage caused by the earthquake included landslides, debris flows, rock falls, failure of retaining walls and bridges, fault rupture and slumping of embankments located over a 200 km long stretch of land in the northeastern part of the South Island. This resulted in severe disruption to transport infrastructure in the North Canterbury and Marlborough regions, with the Main North Line railway (MNL) closed for 10 months and State Highway 1 (SH1) closed for over a year.

The Ministry of Business Innovation and Employment (MBIE) has funded a programme of research into earthquake-induced landscape dynamics (EILD) following the Kaikōura earthquake under its Endeavour research programme. This is being led by GNS Science, with 7 research themes addressing different aspects of the landslides and sediment cascades triggered by that earthquake.

Under this research programme, WSP has been commissioned by GNS to investigate and analyse the performance of engineered and modified slopes in the earthquake, and to develop recommendations for resilient slope design and landslide hazard management.

The objectives of this research theme are to:

1 Map the locations and extents of failures of cut slopes, natural slopes, fill embankments, and retaining systems along the transport corridors affected by the 2016 Kaikōura earthquake;

2 Carry out site investigations at selected key slope failures triggered by the Kaikōura earthquake;

3 Analyse selected landslides from the Kaikōura event to characterise the slope failure mechanisms and relate these to the observed impacts;

4 Identify critical factors that contributed to the slope failures and develop recommendations or guidelines for measures to enhance resilience for the design of new slopes and in management of landslide hazards along existing corridors;

5 Disseminate the recommendations amongst the engineering profession.

This report presents the results of the assessment of selected landslides carried out as part of step 3 above. The results of steps 1 and 2 are presented in Mason and Brabhaharan (2023a) and Mason and Brabhaharan (2023b), respectively.

2 Study area

2.1 Location

This study focuses on the key transport corridors through the Kaikōura earthquake-affected region, as shown in Figure 1. These include State Highway 1 (SH1) and the Main North Line railway (MNL) between Picton and Waipara, State Highway 7 (SH7) between Hanmer Springs and Waipara, the Inland Route 70 between Culverden and Kaikōura, and Awatere Valley Road in Marlborough.

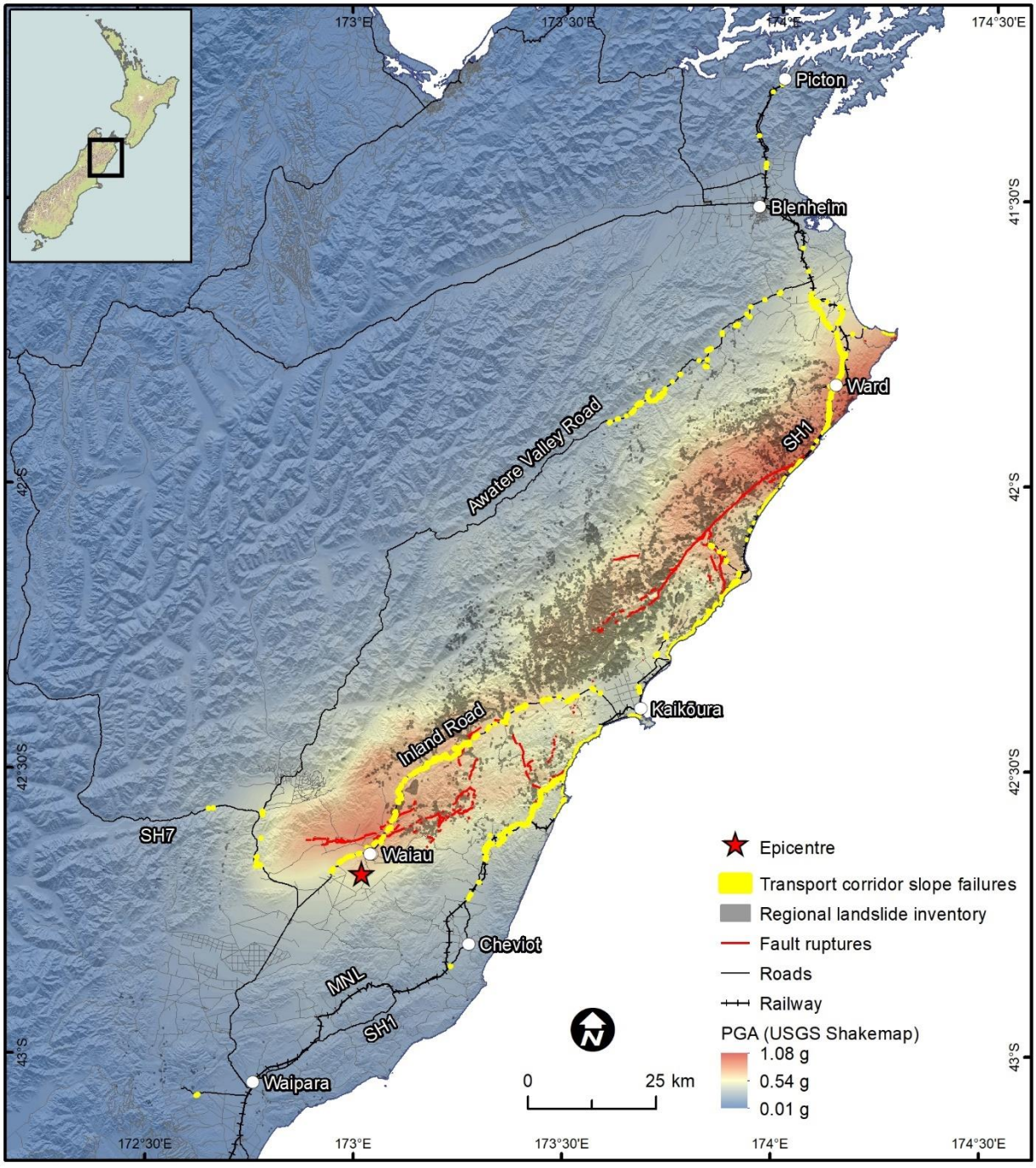

Figure 1: Transport corridors in the study area and locations of slope failures. Locations of landslides in the regional inventory are from Massey et al. (2018; 2020).

2.2 Regional geology

The geology of the study area can be grouped into four main geological units (Figure 2). These are described by Rattenbury *et al.* (2006) and are summarised below, in order of youngest to oldest:

1 Recent sediments

(a) Anthropogenic fill materials

Anthropogenic fill bodies placed for construction of the transport corridor and residential developments generally used material excavated from the local slopes. However, apart from large municipal landfills, the fill bodies are not differentiated and are not always shown on the regional geology map. The composition, thickness and extent of fill bodies at the study sites described in this report have been mapped using field mapping, historical information and high-resolution LiDAR terrain data.

(b) Quaternary deposits

These materials are dominated by alluvial terrace and floodplain deposits in Marlborough and North Canterbury. The alluvial sediments consist of well- to poorly-graded gravel with sand and silt, and the terrace surfaces are often overlain with extensive deposits of loess up to several metres thick.

Marine sand and gravel deposits underlie much of the coastal area, and are exposed in uplifted and dissected terraces and range fronts along the coast. Aeolian sand deposits occur along the coast and extend up-slope onto the fringing hills.

Quaternary-age colluvium is ubiquitous in the hilly terrain that covers much of the study area. The colluvial soils are commonly comprised of poorly sorted gravel, sand and silt derived from weathering and erosion of the Mesozoic and Neogene rocks that underlie the majority of the region.

2 Neogene sedimentary rocks

These materials are dominated by weakly indurated, massive to poorly bedded calcareous fine grained siltstone and mudstone, with minor sandstone, limestone and conglomerate.

3 Late Cretaceous and Paleogene sedimentary and volcanic rocks

Late Cretaceous sedimentary rocks are dominated by highly deformed, poorly bedded to massive sandstone, mudstone and minor conglomerate.

Paleocene to Eocene sedimentary rocks consist of strongly indurated limestone and chert, with minor calcareous mudstone. Volcanic rocks comprise basalt and volcaniclastic breccia, sandstone and conglomerate.

4 Mesozoic basement terranes

Much of the north Canterbury and Marlborough regions is underlain by Late Jurassic to Early Cretaceous greywacke of the Pahau terrane. These rocks are dominated by indurated, grey, quartzofeldspathic thin- to medium-bedded sandstone and mudstone, and very thick-bedded sandstone.

A particular characteristic of the greywacke rock masses in central New Zealand is the close spacing and non-systematic orientation of joints (Stewart, 2007) due to its complex geological history of deformation. Consequently, although the greywacke can have high intact rock material strength, the high degree of fracturing results in significantly weaker rock mass strength (Brideau et al., 2022). Sheared zones and faults are also common throughout the rock mass. Along the coastal hillslopes in the study area, these rocks are variably weathered and deformed, resulting in significant variability in geotechnical rock mass properties.

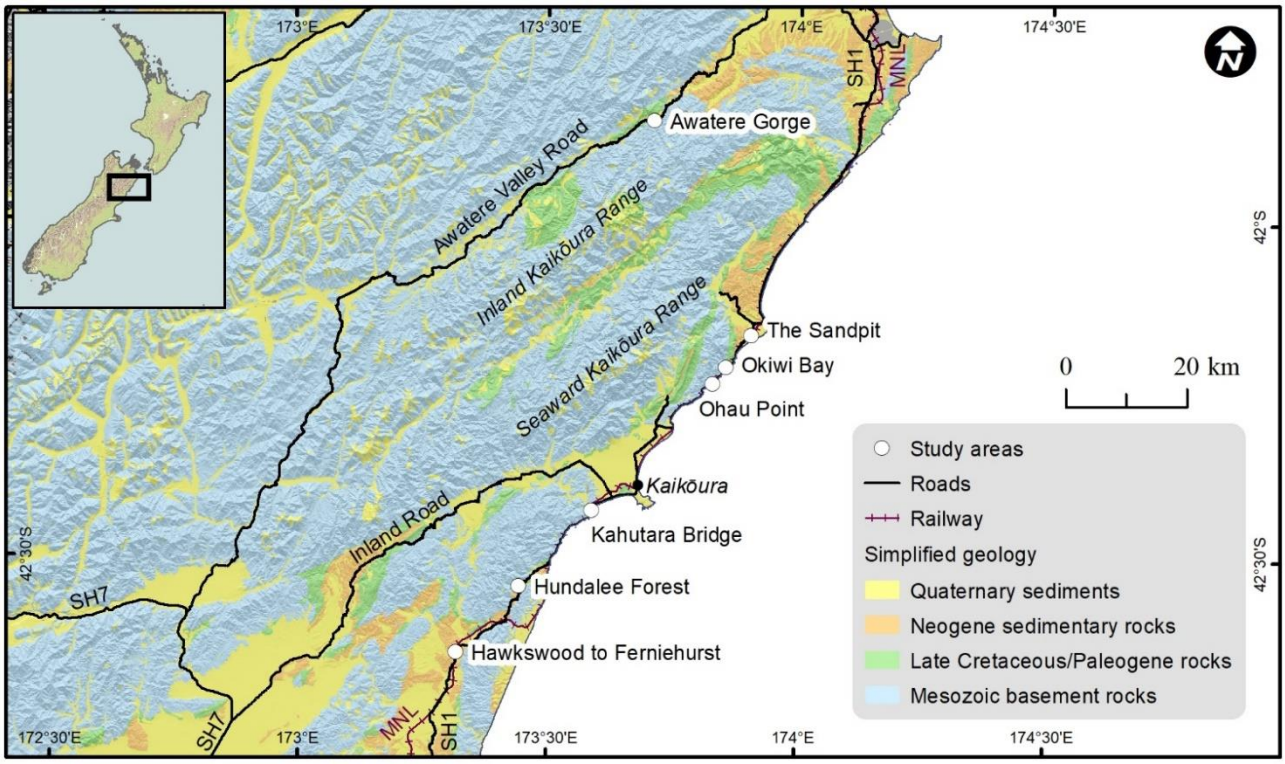

Figure 2: Regional geology

2.3 Geomorphology

The plate boundary between the Pacific and Australian plates passes through the north Canterbury and Marlborough regions in northeast South Island, and consequently this region is an area of active deformation and high seismicity. Obliquely convergent relative plate motion between the tectonic plates is accommodated through a series of dextral-slip faults in Marlborough and more slowly deforming faults and folds in Canterbury, which link the Alpine Fault transform plate boundary to the south with the westward-directed Hikurangi subduction margin to the northeast. The transpressional nature of the plate boundary motion in this part of New Zealand has resulted in uplift of the Kaikōura and Marlborough ranges during the Neogene (Rattenbury *et al.*, 2006). These ranges dominate the geomorphology of the study area and consist of very steep and high hills and mountains on the upthrown sides of the principal active faults in the region. The ranges are separated by major southwest-to-northeast flowing rivers that follow the faults.

To the south of the Kaikōura ranges, the tectonic deformation is slower and consequently the topography is more subdued (Rattenbury *et al.*, 2006). This area is characterised by basin and range topography in the areas around Culverden and Cheviot in north Canterbury, with undulating, moderately steep to steep hills surrounding infilled flat-lying basins.

The area to the north and northeast of the Kaikōura ranges around Seddon and Ward is dominated by uplifted late Tertiary to Quaternary sedimentary basins that have been incised into rolling hills and flights of alluvial terraces (Townsend, 2001). The areas surrounding Blenheim and Kaikōura consist of extensive Quaternary alluvial terraces, formed by aggradation of alluvial sediments shed from the uplifting greywacke ranges. The coastal margin around the study area consists of uplifted marine terraces and steep coastal cliffs, with ocean beach and dune deposits mantling the uplifted landscape. The township of Kaikōura itself is located on a rocky peninsula consisting of uplifted Quaternary marine terraces underlain by Cretaceous to Paleogene sedimentary rocks (Chandra, 1968).

2.4 Ground shaking

At least 21 faults ruptured on and offshore during the Kaikōura earthquake. The ruptures began on The Humps Fault near Waiau and continued north-eastwards for ~180 km (Stirling *et al.*, 2017). Ground shaking was strongest in the epicentral region near Culverden, and to the northeast between Kekerengu and Seddon (Figure 3). Peak ground accelerations >1 g were recorded in the area around Ward. The observed distribution of strong ground shaking is possibly due to the southwest-to-northeast earthquake rupture sequence directed towards this part of the South Island (Kaiser *et al.*, 2017). The ground shaking attenuated rapidly towards the south, with minimal shaking south of Amberley (57 km south of epicentre), but moderate shaking affected areas as far north as Wellington (200 km northeast of the epicentre) across Cook Strait (Bradley *et al.*, 2017).

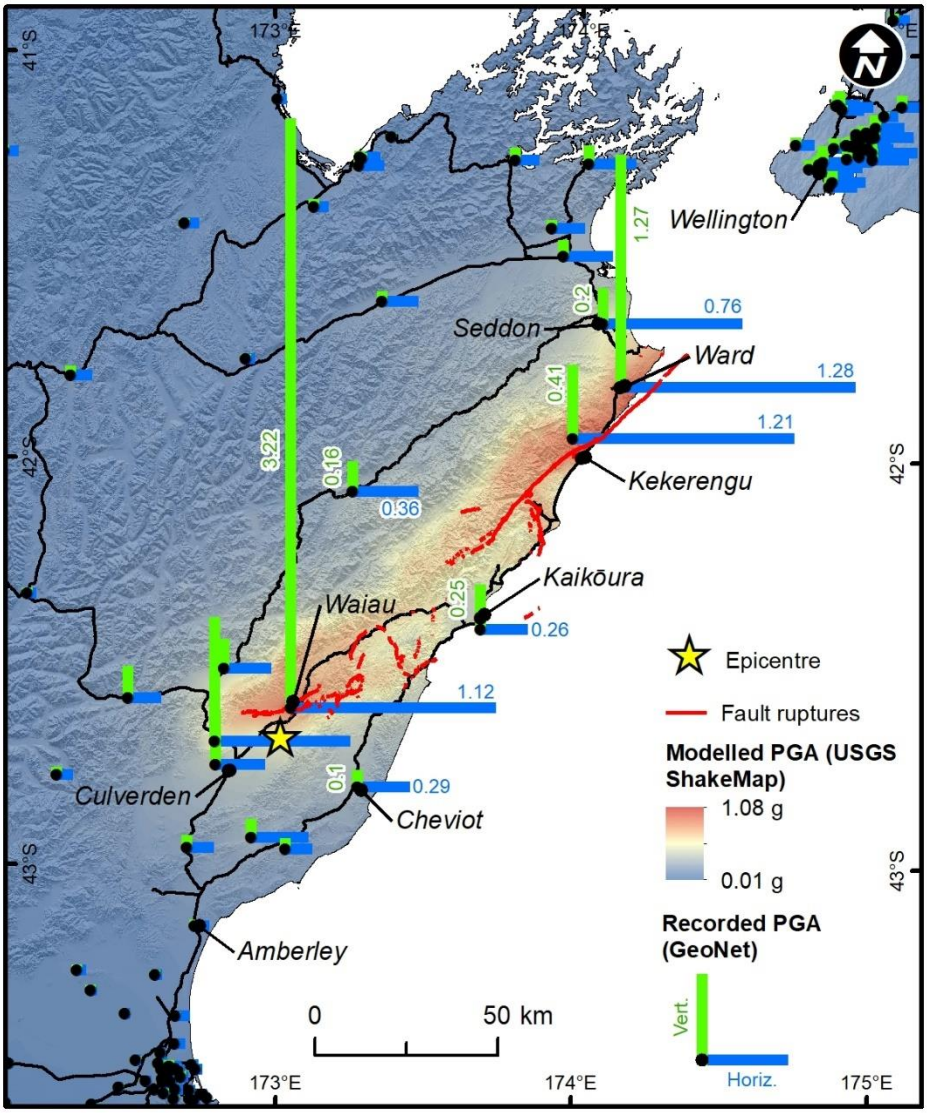

Figure 3: Ground shaking in the Kaikōura earthquake

3 Methods

3.1 Data sources

A series of surveys, investigations and data processing has been carried out since the 2016 earthquake to inform the emergency response, recovery and research stages. The types of data used in this study and their sources are listed in Table 1.

Table 1: Data sources

Phase	Data types	Sources
(1) Pre-earthquake	• Retaining wall assets	Waka Kotahi, KiwiRail, WSP
(2) Immediate post-earthquake emergency response	• Reconnaissance photos • Inspection reports • Slip clearance records	WSP, Waka Kotahi, KiwiRail, University of Canterbury
(3) Earthquake recovery	• Site investigation data • UAV and LiDAR terrain data • Rock fall records • Geotechnical design reports • Construction records	North Canterbury Transport Infrastructure Recovery Alliance (NCTIR)
(4) Post-earthquake EILD research programme	• LiDAR terrain data • Landslide inventory mapping • Ground motion records	GNS Science, GeoNet, WSP, University of Canterbury

3.2 Landslide inventory mapping

The locations of slope failures along transportation corridors in the 2016 Kaikōura earthquake-affected area have been mapped based on field mapping, immediate post-event reconnaissance photos, aerial orthophotos and LiDAR terrain data. The mapping is described in Mason and Brabhaharan (2023a). A total of 2,383 earthquake-induced slope failures have been mapped along transport routes from the Waipara River valley in north Canterbury to Picton in the Marlborough Sounds, a distance of c. 280 km (Figure 1). The mapped features consist of failures of geotechnical slope assets such as cut slopes, fill embankments and retaining walls, as well as landslides on modified or natural hillslopes along the road and rail corridors. Failure mechanisms have been characterised using landslide classification schemes (Glastonbury and Fell, 2000, 2010; Hungr *et al.*, 2014; Keefer, 1984) and fill slope deformation mechanisms described in previous large earthquakes (Rogers, 1992; Stewart *et al.*, 2001; Stewart *et al.*, 2004).

3.3 Classification of damage impacts

The direct damage impacts of the slope failures have been classified using 'performance states' (Brabhaharan *et al.*, 2006) to assess the resilience of transport infrastructure. The 'availability state', which defines the level of access after the earthquake (representing the reduced level of service), and the 'outage state', which represents the duration of reduced access at a given availability state have been assessed for each slope failure in the inventory. Capturing the damage impacts and linking these to the types of failures enables the identification of the key slope failure modes of engineering importance. The results of the damage impacts classification are described in Brabhaharan *et al.* (2017) and Mason and Brabhaharan (2023c). Specific damage impacts at the selected study sites are described for each site in the following sections.

3.4 Site selection

A long list of failure sites was drawn from the inventory of slope failures, consisting of illustrative examples of the various failure modes observed in the earthquake as well as sites where significant damage occurred to the road and rail corridors. From this long list, key sites were selected for further investigation and analysis, to identify the geological and geotechnical properties of the slope failures in more detail. The chosen study sites were selected to capture particular failure mechanisms and damage impacts of engineering significance, for these to be assessed in detail. The sites are summarised in Table 2, and the locations of the sites are shown in Figure 4.

Table 2: Study area summary

Site		Geology	Failure type	Location[1]	Coordinates[2]
Rock slopes	Awatere Valley	Mesozoic greywacke	Combined wedge and joint step-path slide	Awatere Valley Road RP-AVR3/7520	1658890 E 5365870 N
	Kahutara Bridge	Mesozoic greywacke	Planar slide	SH1S-RP-163/4300	1648356 W 5301718 N
	Okiwi Bay	Mesozoic greywacke	Wedge slide	SH1S-RP-118/9200 MNL 216.6 km	1670621 E 5325173 N
Fill/soil slopes	Hawkswood to Ferniehurst	Fill overlying Quaternary fan gravel and Neogene siltstone	Translational/semi-rotational slide	SH1S-RP-195/10450	1626057 E 5278327 N
	Hundalee Forest	Fill overlying Neogene siltstone	Translation / spread	SH1S-RP-185/2590	1636433 E 5289208 N
	The Sandpit	Late Quaternary aeolian sand	Translational slide	SH1S-RP-118/1800 MNL 223.95 km	1674806 E 5330458 N

[1] SH1S = State Highway 1; RP = Route Position; MNL = Main North Line railway

[2] Coordinates of the approximate centre of the study site, in NZTM projection

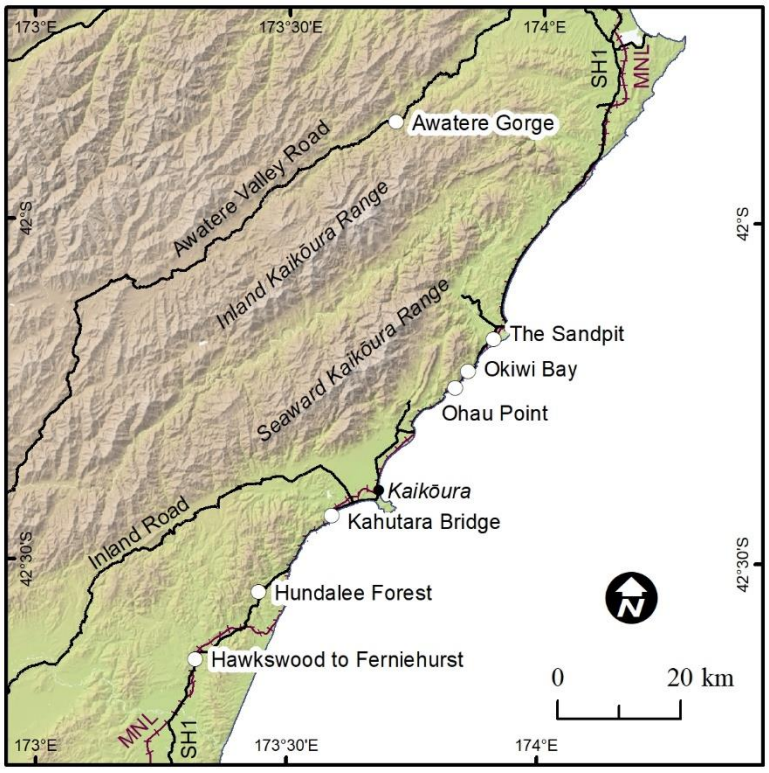

Figure 4: Study site locations

3.5 Site investigations and testing

Available results of intrusive investigations, surface mapping and surveys were collated for the shortlisted study sites. These were used to derive engineering geology models for each site, which form the basis for the analyses. The types of investigations are summarised below.

3.5.1 Ground investigations

Intrusive geotechnical investigations were conducted at selected slopes to observe the properties of the soil and bedrock materials, determine the thickness and properties of fill materials, collect samples for laboratory testing, observe groundwater conditions, and monitor any ongoing slope deformation. The ground investigations consisted of:

- Rotary cored boreholes, with downhole geophysical surveys of rock mass conditions using acoustic and optical televiewer and full waveform sonic logging,
- Surface geophysical surveys using multi-channel analysis of surface waves (MASW),
- Static cone penetration tests (CPTu),
- Test pits, and
- Scala penetrometer tests.

The ground investigations are summarised in Table 3. The locations of the site investigations at each site are provided in Mason and Brabhaharan (2023b).

Table 3: Site investigation summary

Site	Boreholes			CPTu[2]	Test pit/ WS[3]	Scala	MASW[4]
	No.	Depth	Logging[1]				
Awatere Gorge (Mason and Brabhaharan, 2023b)	1	49.9 m	ATV/OTV, FWS	-	-	-	-
Kahutara Bridge (Geotechnics, 2017c)	6	10.3 m-14 m	-	-	-	-	-
Okiwi Bay (Mason and Brabhaharan, 2023b; NCTIR, 2018d, 2018e; SouthernGeophysical, 2018)	6	9 m - 90 m	ATV/OTV, FWS	-	-	-	2
Hawkswood to Ferniehurst (Mason and Brabhaharan, 2023b)	1	25.9m	-	-	-	-	-
Hundalee Forest (Geotechnics, 2017a, 2017b; Mason and Brabhaharan, 2023b)	3	9.45m-15.4m	-	1	-	-	-
The Sandpit (NCTIR, 2019)	13	20.14m-25.9m	-	11	11	19	3

[1] ATV = acoustic televiewer; OTV = optical televiewer; FWS = full waveform sonic logging

[2] Static cone penetration test

[3] Window sampler

[4] Multi-channel analysis of surface waves

3.5.2 Mapping

Engineering geological and geomorphological mapping of each study site was also carried out as part of the site investigation. Soil and rock materials were observed and described using the NZ Geomechanics Society guidelines (NZGS, 2005). Desktop mapping of geomorphic features in GIS using pre- and post-earthquake aerial photography and LiDAR terrain data was used to supplement the field mapping.

3.5.3 Rock slope surveys

Selected rock slopes were surveyed using an Unmanned Aerial Vehicle (UAV), Terrestrial Laser Scanner (TLS), or LiDAR scanner, to generate point clouds and 3D ground surface models. The orientations of planar rock surfaces have been extracted from the point clouds using Coltop-3D software (Jaboyedoff *et al.*, 2007) and the Facets and Compass plugins for CloudCompare software (Dewez *et al.*, 2016; Thiele *et al.*, 2017) for structural geological analysis of the slopes.

3.5.4 Coseismic displacement measurement

Horizontal coseismic slope displacements were derived using Digital Image Correlation (DIC). DIC is an image processing technique that evaluates the internal misalignment of two images using a moving template window to measure displacements perpendicular to the line of sight for the imagery (Bickel *et al.*, 2018). Horizontal tectonic displacement at a study site is accounted for within the DIC algorithm through co-registration of the images during pre-processing. Displacements of selected features on the slopes were also manually measured in GIS using pre- and post-earthquake imagery, to help choose the appropriate window size for the DIC analyses as well as to validate the outputs. The DIC- and GIS-based displacements were supplemented by field measurement of tension crack apertures in both the horizontal and vertical directions at selected sites.

3.5.5 Laboratory testing

Laboratory testing was carried out to characterise the particle size distribution, water content, shear strength and plasticity of the fill materials, to help develop the numerical models. The shear strength was assessed by consolidated undrained triaxial testing of push tube samples retrieved from the boreholes at Hundalee Forest and Homestead Creek. Unconfined compression strength testing was attempted on core samples from BH101 at the University of Canterbury rock mechanics laboratory; due to the presence of many closely spaced incipient joints, suitable intact test specimens could not be prepared which consequently limited the reliability of the test results. The results of the UCS tests are provided in Mason and Brabhaharan (2023b).

3.6 Engineering geological models and numerical analysis of slope stability

Geotechnical modelling and analysis of the failures was carried out to understand and learn from the failure mechanisms and consequences of failure to infrastructure. The objective of the analyses was to identify the mechanisms of slope failures so these can be related to the observed impacts. This involved:

1. Developing engineering geological models of the slopes using the results of the site investigations and laboratory testing.
2. Calibration of the ground models by back-analysis using limit equilibrium slope stability analysis.
3. Assessing the earthquake performance of the slopes using commonly used methods of analysis in engineering practice, including kinematic, pseudostatic limit equilibrium and permanent-displacement analysis.

The engineering geological models for the selected sites are described in Sections 4 and 5. The methods and results of the slope stability analysis are described in Appendix A.

4 Rock slope sites

4.1 Awatere Gorge

The Awatere Gorge landslide is located in the Awatere Valley on the northern flanks of the inland Kaikōura ranges in southern Marlborough (Figure 2). The Awatere Valley is oriented southwest to northeast, parallel to the Awatere Fault, which last ruptured in 1848 in the M_w 7.4-7.7 Marlborough earthquake (Mason and Little, 2006). The land along the valley is used for pastoral farming, and access to the stations along the valley is provided by Awatere Valley Road, a low volume unsealed rural road. The majority of the road through the Awatere Valley was not significantly impacted by coseismic landslides in the Kaikōura earthquake, apart from a series of rock slides along the Awatere River in Gladstone Downs Station. The largest of these landslides is described here.

4.1.1 Geology and geomorphology

The landslide occurred on a steep northwest-facing hillslope above the Awatere River (Figure 5). The hillslopes are underlain by Mesozoic Pahau terrane greywacke. The hillslope has slope angles of 40˚ to 60˚ and ranges in elevation from 350 m at river level to 520 m at the ridge crest at the landslide head scarp. The Awatere River lies in a narrow gorge at the toe of the slope, with the road formed by cutting a bench into the hillslope and using the cut material to create a sidling fill embankment on the downhill side. The road is at approximately 410 m elevation at the landslide site.

Figure 5: Awatere Gorge landslide, Awatere Valley.

The geomorphology of the site observed from pre-earthquake aerial photography suggests previous landslides have occurred on this slope, likely to be a combination of retrogressive slope failures in response to ongoing river incision at the toe of the hillslope possibly in conjunction with earthquake-induced landsliding during the 1848 earthquake on the nearby Awatere Fault. The 2016 earthquake-induced landslide occurred in the head scarp area of this pre-existing landslide feature. The upper and middle parts of the slope failed, with debris mantling the slope down to river level and burying the road bench (Figure 6). The head scarp of the landslide is located at the top of a 20 m high sub-vertical rock bluff situated 110 m above road level.

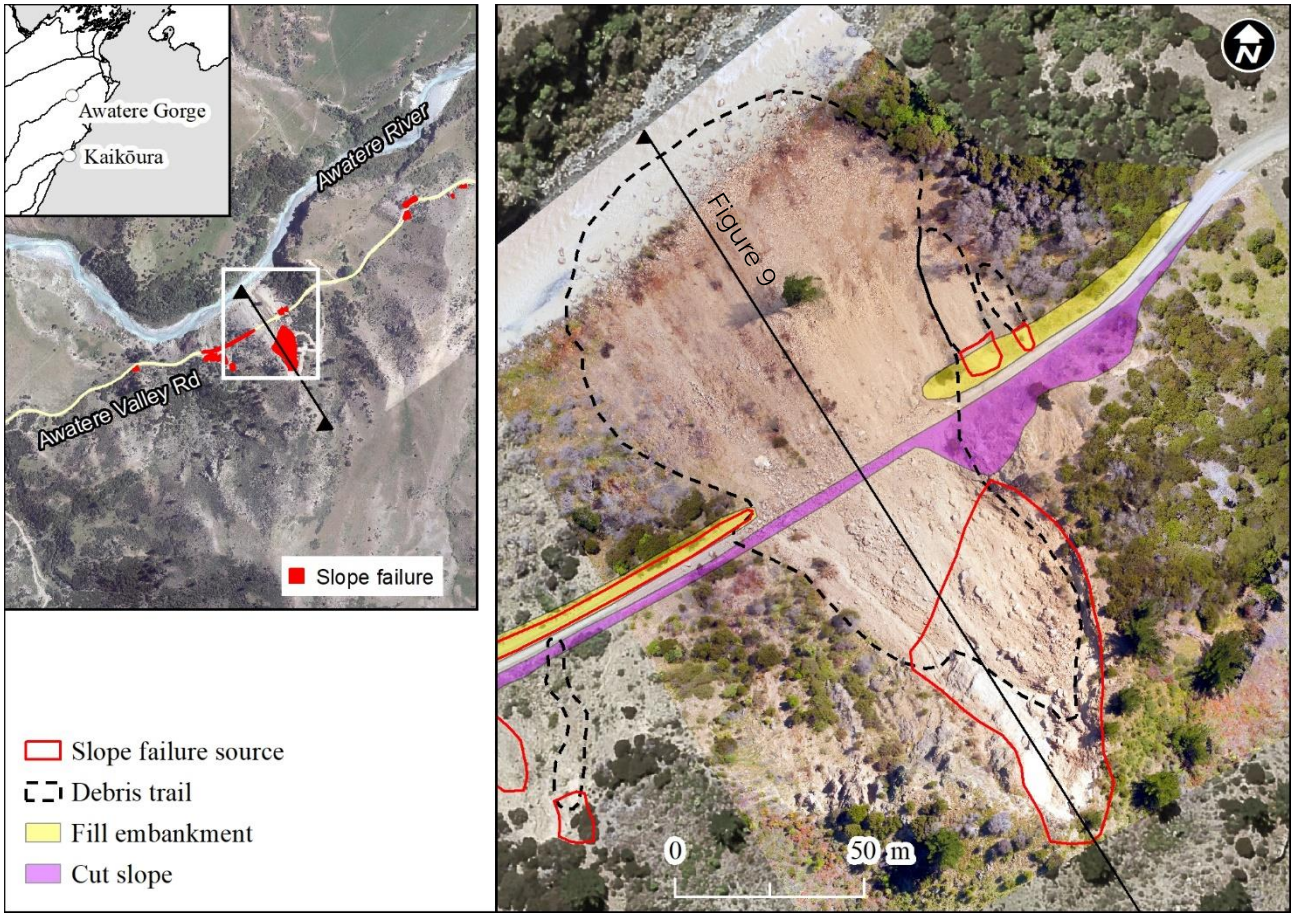

Figure 6: Site plan, Awatere Gorge landslide

4.1.2 Geotechnical slope assets

The road was formed by cutting into the slope on the uphill side of the road and filling over the slope on the downhill side. This cutting is likely to have been formed in the 1870s and 1880s when the Awatere Valley Road was constructed by the Public Works Department (Hall, 1881). Roads formed at this time were built by hand using horse packs and horse-drawn carts (McIntyre, 2007), and will have been realigned and widened since then to accommodate cars and then trucks, resulting in modifications to the angle, height and extent of the cutting.

There is a continuous cut slope above the road on the southeastern side for a length of approximately 300 m through the site. The cut ranges in height from <2 m to 30 m and has average slope angles of 50˚ to 60˚. Other than minor spalling of loose rock, the section of cut slope adjacent to the rock slide did not suffer slope failure in the 2016 earthquake, and the rock slide occurred above the cut slope (Figure 6).

There are two main fill bodies along this section of the road; these are inferred to be approximately 5 m thick. The exact thickness of fill was not able to be determined as no terrain data was available prior to the earthquake and the fill slope was not able to be differentiated from the natural hillslope using available aerial photography. Translational slide failures occurred in the fill body on the downhill side of the road to the northeast of the rock slide, as well as tension cracking and displacement along the crest of the fill slope to the west (Figure 6).

4.1.3 Site investigations

Site investigations at the site consisted of engineering geology mapping, survey of the site by UAV in November 2016 and February 2021, and drilling of a rotary cored borehole on the bench above the head scarp of the landslide in August 2020. The borehole was drilled to 49.9 m depth, with

downhole geophysical logging of the rock mass using acoustic televiewer, optical televiewer and full waveform sonic tools (Mason and Brabhaharan, 2023b).

4.1.4 *Rock mass conditions*

Bedrock is exposed over the full height of the landslide and in the cut slope at road level. The rock mass consists of slightly to moderately weathered, weak to strong, thinly to moderately thickly bedded sandstone and siltstone. Bedding generally dips steeply towards the west, however mapping of bedding attitudes exposed in the cut slopes and landslide head scarp shows a complex pattern of folding and shearing (Figure 7). The rock mass observed at the site is often intensely fractured and dilated with multiple joint sets. The principal rock defects identified from surface mapping, UAV surveys and downhole televiewer logging are summarised in Table 4 and shown in Figure 8.

Figure 7: Folded and sheared bedding exposed in the road cuts on Awatere Valley Road.

Table 4: Rock defect characteristics, Awatere Gorge landslide

Defect ID and type		Dip (°)	Dip direction	Persistence (m)	Spacing (m)	Surface roughness
JS1	Joints – planar slide surfaces	37 – 54	320 (280 – 026)	1 – 10+	0.05 – 0.8	Undulating to stepped, smooth
JS2	Joints – steps	42 – 88	330 (273 – 026)	0.8 – 3.5	0.02 – 0.4	Stepped, rough to smooth
JS3	Bedding / sheared zone	44 – 82	290 (259 – 013)	3 – 15+	0.01 – 0.5	Undulating, smooth
JS4	Joints – western wedge sliding surface	59	029	0.8 – 12	0.2 – 0.8	Undulating, smooth
JS5	Joints – eastern wedge sliding surface	62	309	1 – 10	0.02 – 0.3	Undulating, smooth

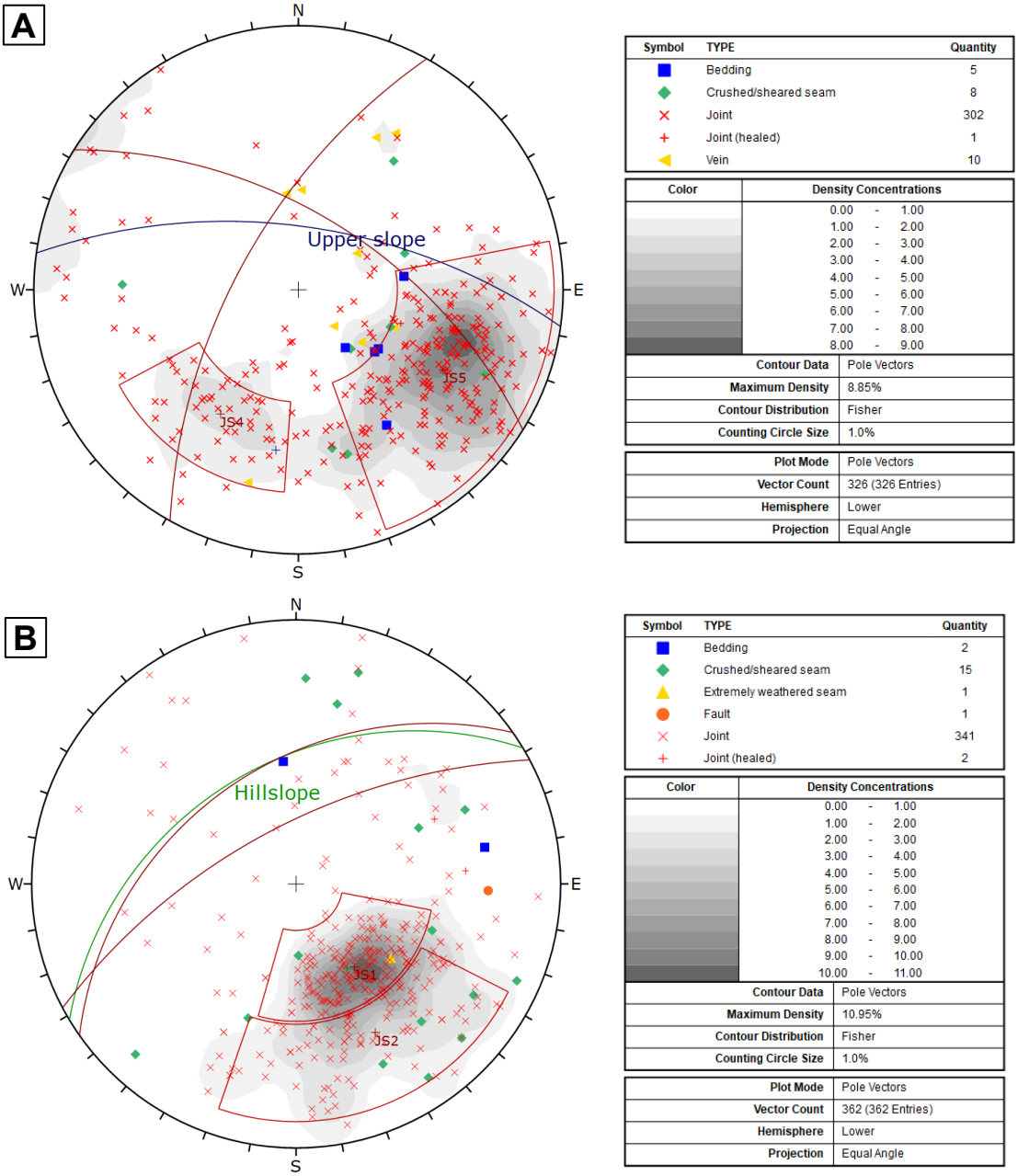

Figure 8: Discontinuities measured in (A) the wedge failure in the upper part of the slope (N=326), and (B) the step-path slide in the middle part of the slope (N=362).

4.1.5 Kaikōura earthquake-induced landslide

Ground shaking

The closest strong motion station is at Kekerengu, 25 km to the southeast. The peak horizontal ground acceleration recorded at that site was 1.21 g (GeoNet, 2016). The estimated horizontal PGA at the Awatere Gorge site was between 0.41 g (using the ShakeMapNZ model) and 0.53 g (Bradley *et al.*, 2017).

Failure mechanism

The rock slope failure at the Awatere Gorge site consisted of a combination of wedge sliding in the topmost part of the slope, with joint step-path sliding immediately below the wedge slide (Figure 9). The joint step-path failure is inferred to have propagated along persistent joint surfaces dipping out of the slope at 37° to 54° (JS1), stepping down along short persistence joints (JS2) that dip steeply out of the slope at oblique angles to the more persistent joints (Figure 9C). The wedge

failure occurred along two persistent joint sets dipping 59˚/029 (JS4) and 62˚/309 (JS5), with a line of intersection plunging 50˚/352. The average orientation of this part of the hillslope before the earthquake was 63˚/008.

Coseismic displacements of the hillslopes around the landslide were investigated using DIC analysis and field mapping. No features indicative of incipient slope deformation (such as tension cracks, uphill-facing scarps, slope bulges or hummocky ground) were able to be identified. This suggests that displacement of the slope during the strong ground shaking resulted in brittle kinematic failure, with associated disintegration and avalanche-type runout of the failed rock mass.

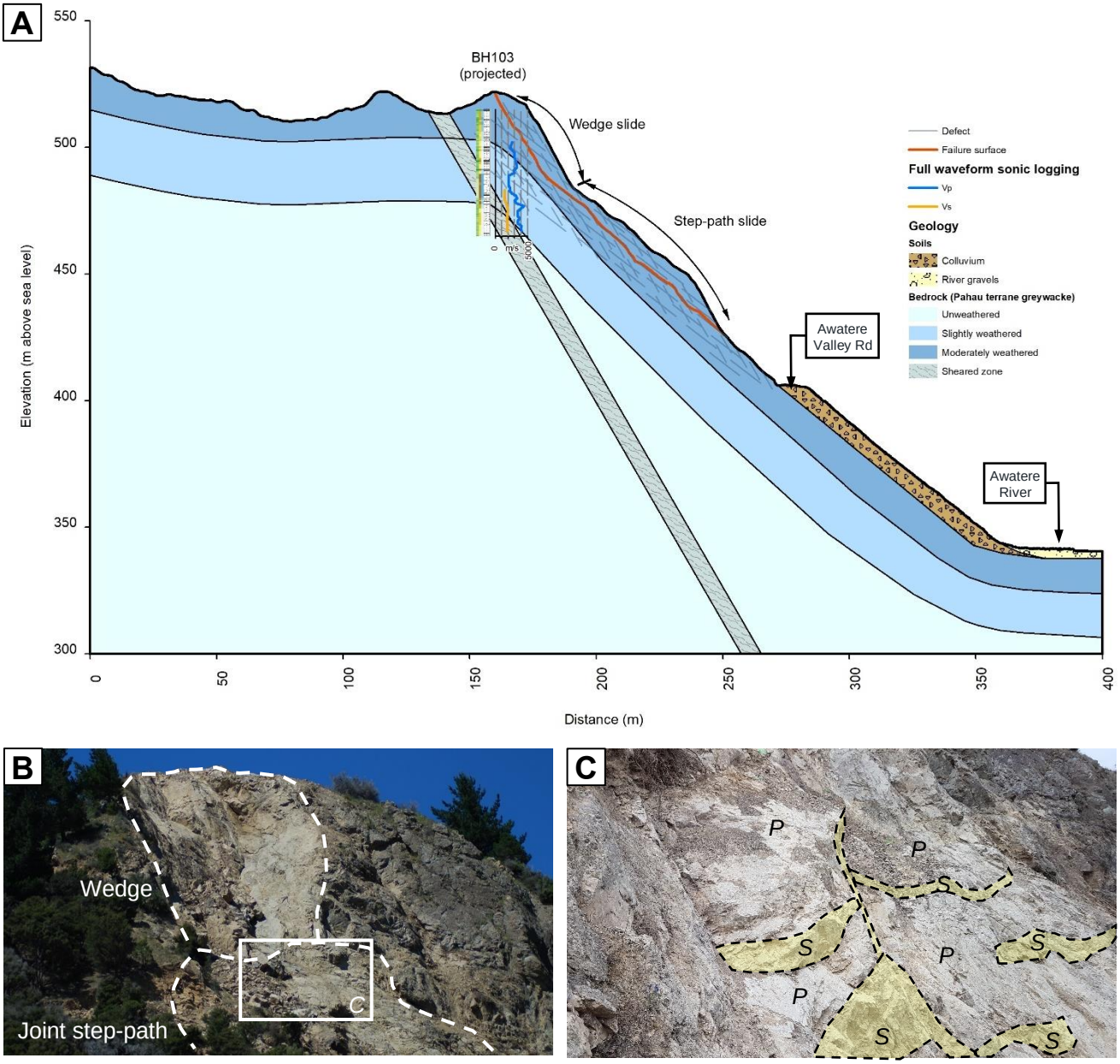

Figure 9: Ground model of the Awatere Gorge landslide
(A) Cross section through the landslide. (B) Wedge sliding failure occurred in the upper part of the slope, with joint step-path sliding in the less-steep part of the slope below. (C) Enlargement of the key joints forming the slide surface, showing outward-dipping slide planes (P) separated by short persistence, steeply dipping steps (S).

Damage and outage impacts

The damage caused by the landslide was blockage of the road by debris. The volume of debris was 14,000 m^3 ± 5,000 m^3, based on differencing of pre- and post-earthquake digital surface models. The response and recovery work at the site and the duration of the outage are summarised in Table 5 and described in detail below.

Table 5: Awatere Gorge road outage

Recovery activity	Date commenced	Date completed	Duration of outage from EQ
Reconnaissance and emergency works scoping	18 Nov 2016	21 Nov 2016	7 days
Helicopter sluicing and abseil scaling to remove loose/hazardous debris	28 Nov 2016	12 Jan 2017	8 weeks
Earthmoving to clear debris and re-open road	12 Dec 2016		

The strategy to reopen the road was formed during a reconnaissance inspection 4 days after the earthquake. The initial strategy was to form an access track onto the landslide near the top of the debris and to clear the debris by benching from the top down. This was attempted approximately 1 week after the earthquake but was soon abandoned due to unacceptable safety risks to the excavator operator.

After further reconnaissance and planning, a team of abseilers and helicopters was mobilised to remove the safety hazards posed by the loose debris in the upper slope by scaling, blasting and sluicing. This commenced approximately 2 weeks after the earthquake, with some limited earthmoving at road level during the scaling operation. The main period of earthmoving to clear the road bench began 4 weeks after the earthquake and was carried out using a remote-controlled excavator in conjunction with sluicing of the upper slope by helicopter and sluicing of the lower slope by high pressure hose.

The road was reopened on 12 January 2017 after a total outage of 8 weeks. The recovery work consisted entirely of earthworks to clear the road and restore access, and no slope stabilisation measures or rock fall barriers were constructed.

4.2 Kahutara Bridge Site

4.2.1 Location and failure overview

The site is located on SH1 on the south side of the Kahutara Bridge, 8 km southwest of Kaikōura. The Kaikōura earthquake triggered a translational landslide on the hillslope above the road (Figure 10A) as well as wedge and avalanche failures of bedrock on a cut slope above SH1 (Figure 10B).

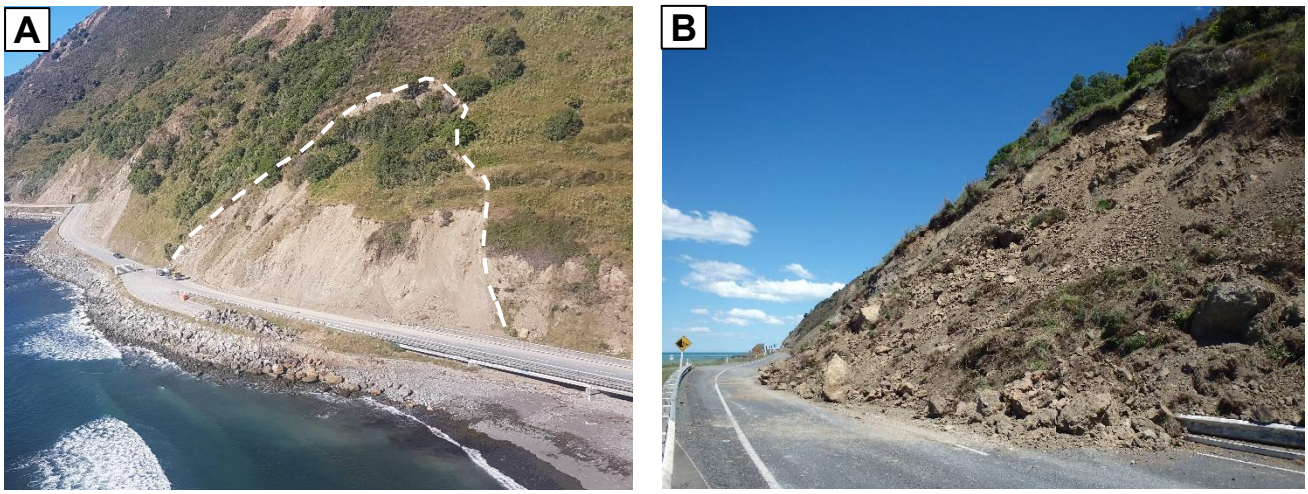

Figure 10: Kahutara Bridge Site landslide
(A) Incipient planar slide (dashed line) extending 55 m above road level (photo credit: J. Claridge); (B) Rock slides and avalanche from the cutting above SH1 (photo credit: J. Grindley).

4.2.2 Geology and geomorphology

The site consists of east-facing hillslopes at the northern end of a ridgeline running parallel to the coast. The hillslope is moderately steep, with slope angles between 30° and 38°, rising to the ridge crest 105 m above sea level. The hillslope is underlain by Pahau terrane greywacke, with a veneer of colluvium comprising coarse gravel, cobbles and boulders within a silt matrix. SH1 is situated on a bench at the base of the hill; the road platform is approximately 5 m above sea level and is underlain by fill, bedrock and beach/marine deposits. The MNL railway is situated within a tunnel through the hillslope, some 200 m west of the highway. Pre-earthquake LiDAR shaded relief maps and orthophotographs (Figure 11) do not show evidence of pre-existing landslide features at the site of the translational landslide. The cut slopes along the road show evidence for previous small scale failures such as wedge slides from the cuttings.

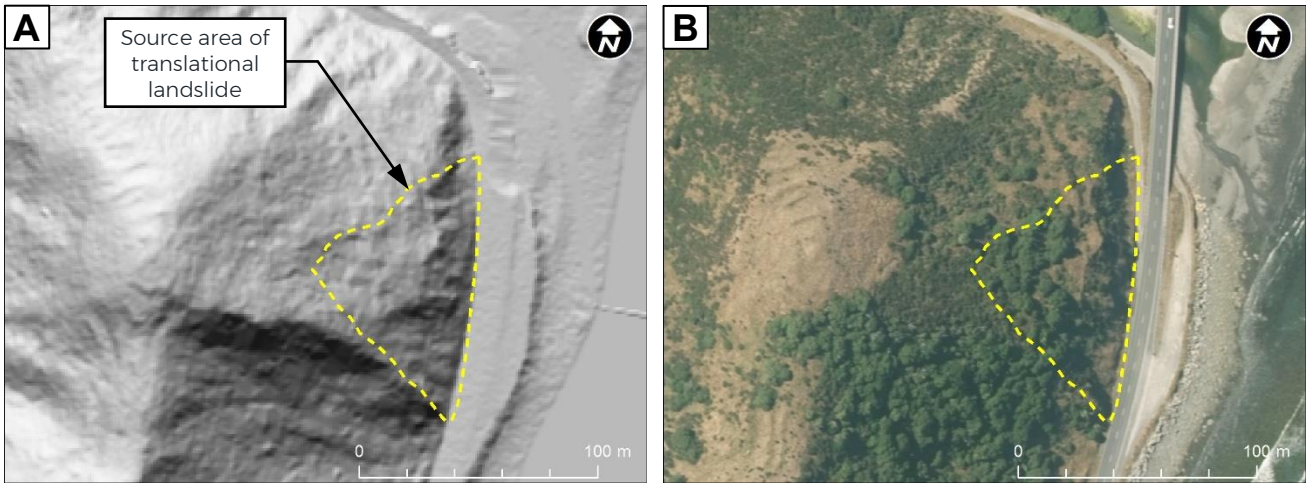

Figure 11: Pre-earthquake geomorphology of the Kahutara site.
(A) Hillshade relief map from 2012 LiDAR; (B) 2015 aerial photograph.

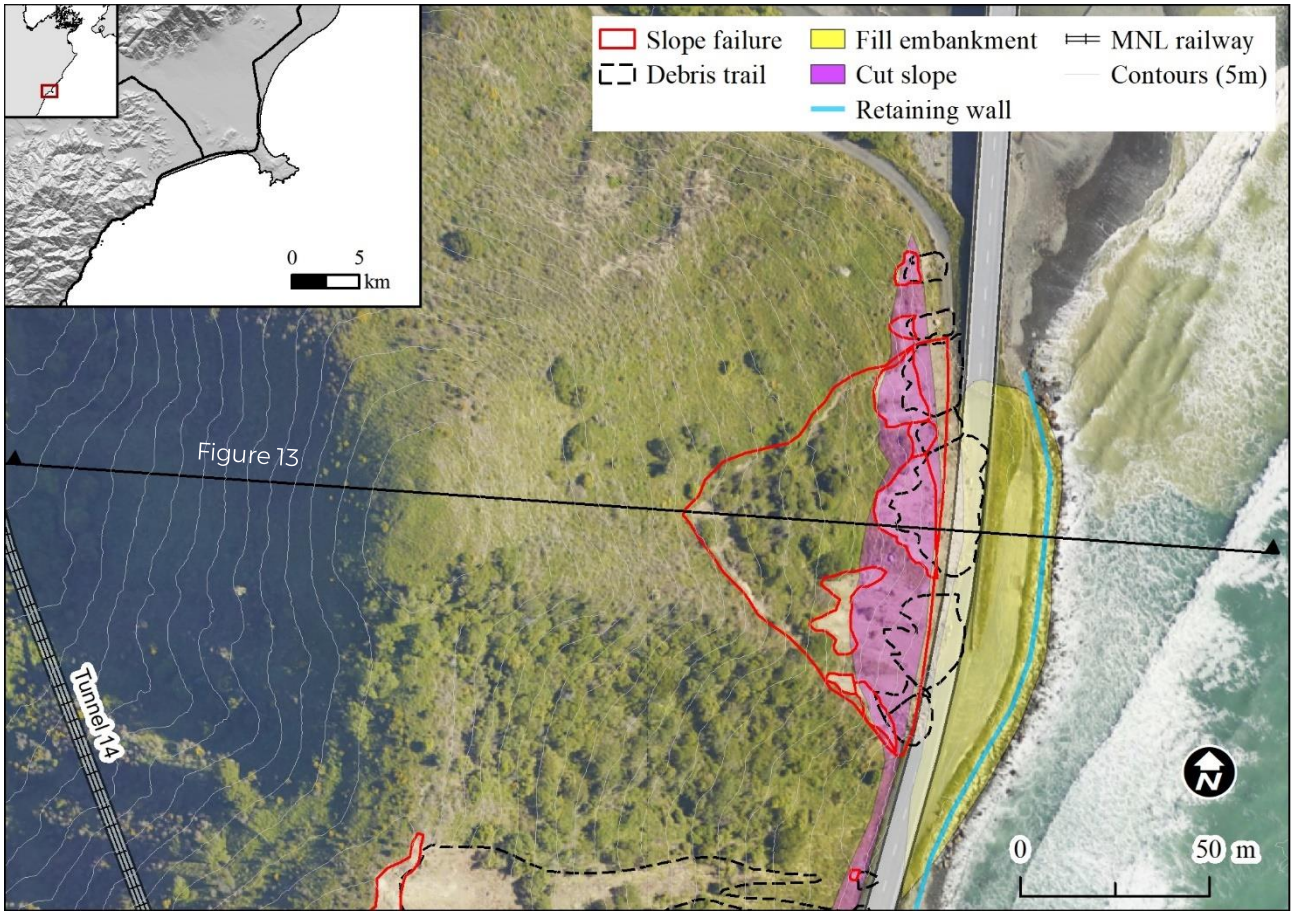

Figure 12: Kahutara Bridge site plan

4.2.3 Geotechnical assets

The structures and slope assets in the vicinity of the Kahutara Bridge landslide are summarised in Table 6.

Table 6: Slope assets at the Kahutara Bridge site

Asset type	Description
Cut slopes	The toe of the hillslopes appear to have been cut to form a platform for construction of the road. Prior to the earthquake the cut slopes were up to 25 m high with slope angles between 45° and 60°. The exact age of the cuts is not known; based on available historical information it is likely that the cut slopes for the road were formed during construction of the coastal section of the MNL railway in the 1930s (Topp, 1947).
Fill slopes	The road and southern approach to the Kahutara River Bridge are supported on fill embankments. The boreholes drilled at the toe of the landslide show the fill materials consist of fine to coarse gravel with a sand matrix. The fill is 0.8 m thick at the southern end of the site, increasing to 1.5 m thick at the northern end towards the southern abutment of the Kahutara Bridge.
Retention/scour protection	The base of the road embankment was armoured with rip rap to support the road embankment and prevent scour.
Tunnels	The railway lies within a tunnel through the hillslope (Tunnel 14). The tunnel itself was not damaged during the earthquake, however failures of the cut slopes at the northern portal blocked the rail line with debris.

4.2.4 Site investigations

Six boreholes were drilled at the site in the road shoulder adjacent to the hillslope in May and June 2017 (Geotechnics, 2017c). These boreholes were carried out external to this research project, however they were drilled to investigate the landslide site to help scope and design remedial measures and therefore provide useful information on the landslide for this research. Three of the boreholes were vertical (to depths of between 10.6 m and 13.2 m) and three were inclined at 45° below the base of the hillslope (to depths of between 10.3 m to 14 m). Inclinometer casing was installed in one of the vertical boreholes to allow monitoring of subsurface deformation at the base of the hillslope.

4.2.5 Rock mass conditions

Bedrock at the Kahutara Bridge site consists of moderately to highly weathered, weak to moderately strong, thinly to moderately thickly bedded sandstone and mudstone. Bedding dips out of the lower part of the hillslope at 30° towards the east, based on exposures in the slip scarp and in a wave-cut platform below the road located 100 m to the southeast of the site (Mason and Brabhaharan, 2023b). Mapping of bedding attitudes in exposures around the local site area suggests there are a series of plunging-upright and horizontal-inclined asymmetrical synclines and anticlines in the rock mass below the hill, with a range of fold axis orientations and trends. Bedding on the western side of the ridgeline was observed to be more tightly folded and contorted than on the eastern slopes (NCTIR, 2018f). The rock mass observed in outcrops around the landslide is highly fractured and dilated with multiple joint sets.

4.2.6 Kaikōura earthquake-induced landslide

Ground shaking

The closest strong motion recording station is in Kaikōura, approximately 20 km to the northeast. The peak horizontal ground acceleration recorded at the Kaikōura site was 0.26 g (GeoNet, 2016). The estimated horizontal PGA at the Kahutara site was between 0.3 g (ShakeMapNZ) and 0.57 g (Bradley *et al.*, 2017).

Failure mechanisms and coseismic displacements

The 2016 earthquake resulted in translation of a block of bedrock approximately 4,000 m^2 in area. Assessment of horizontal coseismic slope displacements was carried out by DIC and GIS-based measurement using pre- and post-earthquake aerial photos. Vertical displacements were assessed using pre- and post-earthquake LiDAR DEMs to give the total (i.e. 3D) coseismic slope displacements. The observed displacement patterns and structural geological mapping suggest the failure mechanism was planar sliding along bedding planes that dip approximately 30° towards the east in the lower part of the slope. This style of failure is classified as a coherent, planar rock block slide in the schemes of Keefer (1984), Glastonbury and Fell (2010) and Hungr *et al.* (2014). The displacement vectors are inclined parallel to the slope in the upper part of the landslide (Figure 13A), consistent with a translational failure surface dipping out of the slope at ~30°. Shallow wedge sliding and disaggregated avalanche-type failures also occurred on the over-steepened cut slope at the base of the hillslope, which blocked the state highway.

Displacements measured along a swath approximately 10 m wide along the cross section line are shown in Figure 13B. These show displacements of 0.3 m to 0.5 m (and locally up to 1.5 m) in the upper part of the hillslope, near the ridge crest. Discontinuous tension cracks were mapped in this part of the slope (Mason and Brabhaharan, 2023b), which suggests deformation of the top of the ridge consisted of localised fissuring of the surficial soils. Displacements increase significantly below the head scarp of the displaced landslide block, with a mean displacement of 4 m at the head scarp increasing to ~5.5 m (with a maximum of 7.6 m) at the crest of the cut slope. Beyond this point the slope displacements were unable to be resolved due to complete evacuative failure of the cut slope.

As the landslide is located in the lower half of the hillslope, where there would likely be less significant topographic amplification of ground shaking, displacement during the earthquake did not progress sufficiently for the displaced block to evacuate the failure area (*c.f.* the Okiwi Bay landslide, see Section 4.3). This may indicate the failure surface extended below the road and the landslide was buttressed by the road embankment and shore platform which prevented its transition to an avalanche. However, monitoring of an inclinometer casing installed within one of the vertical boreholes in the road showed <1 mm of displacement beneath road level compared to c. 1500 mm of displacement measured across ground surface extensometers at the landslide head scarp (NCTIR, 2018a), suggesting the failure surface daylighted from the hillslope above road level at the toe of the cut slope. The displacement vectors are inclined out of the slope in the lower part of the landslide, suggesting outwards translation of the landslide block on a failure surface that daylights at the toe of the slope (Figure 13). Exposures of slickensided bedding planes and bedding-parallel joints in the cut slope above the road during earthworks to remove debris also suggest the failure surface intersected the free face at the toe of the cut (NCTIR, 2018f).

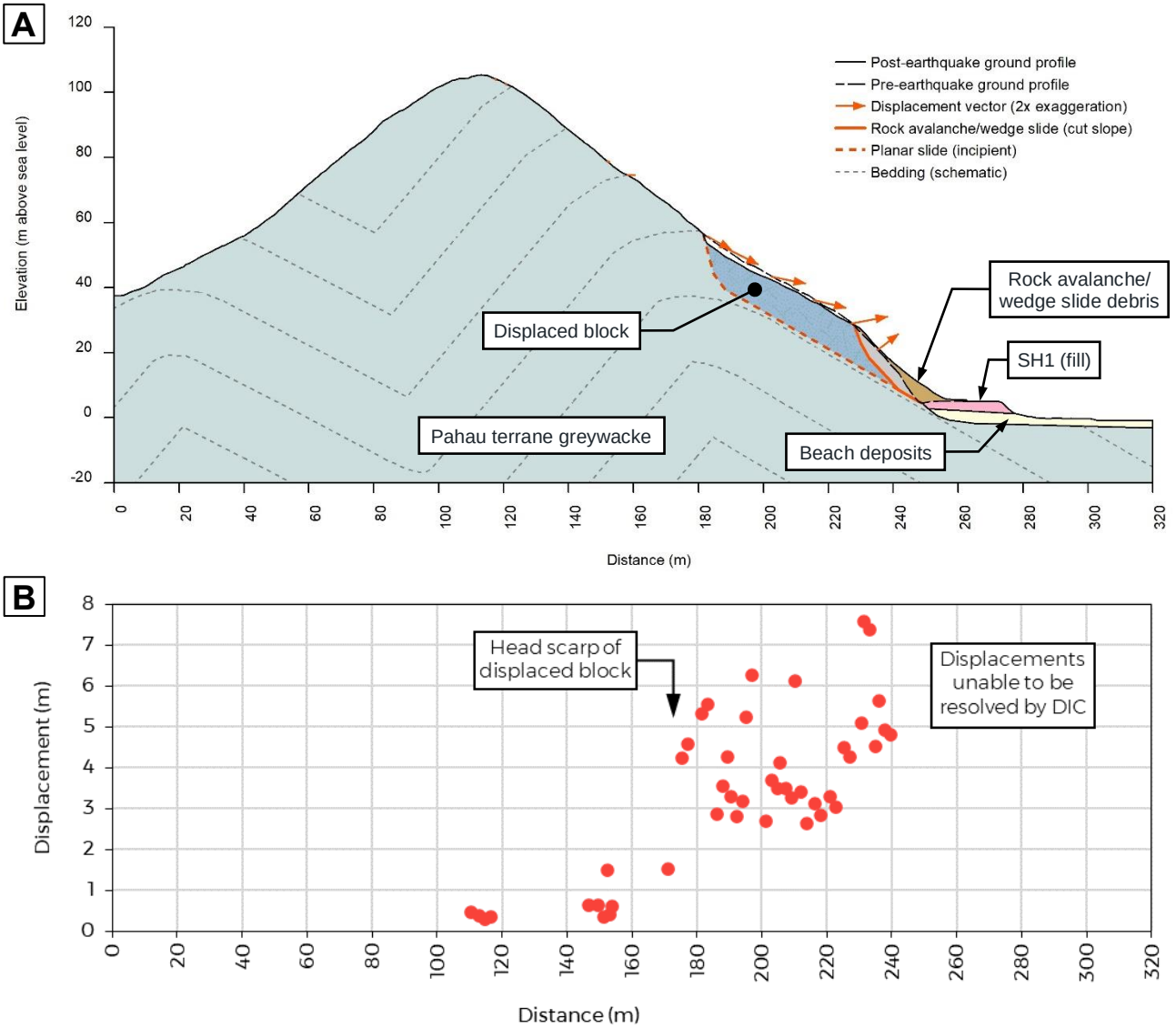

Figure 13: Ground model of the Kahutara Bridge site landslide
(A) Interpreted cross section. (B) Total (3D) displacements from DIC and manual feature tracking

Damage and outage impacts

The principal damage to the road infrastructure from the Kahutara Bridge site landslide was blockage of the road by debris from the shallow seated failures of the cut slope (Figure 10B). This debris lobe inundated both lanes of the state highway, blocking access along the corridor. The deep-seated landslide did not cause direct damage to the road in the earthquake or in the short-term recovery period. The recovery works and duration of the outage are described below and summarised in Table 7.

Table 7: Road outages at the Kahutara Bridge landslide during response and recovery phases

Recovery stage	Level of service	Date completed	Duration after EQ
Emergency response	Initial emergency access, single lane	16 Nov 2016	2 days
	Two lanes, temporary speed limit, daytime access for emergency vehicles and residents	End Nov 2016	2 weeks
Recovery	Two lanes, 24 hr access with temporary barrier	April 2018	17 months
	Optioneering and concept design	May 2018	18 months
	Detailed design	November 2018	2 years
	Construction of mitigation measures	TBC[1]	TBC[1]

[1] To be confirmed from NCTIR construction records

The initial emergency response phase concentrated on restoring vehicle access to Kaikōura along the coastal state highway corridor. At the Kahutara Bridge site, single lane access was able to be formed around the toe of the debris within two days of the earthquake. Two lane access was reinstated within two weeks with an earth bund to protect the road from rock fall. Further work carried out at the site prior to the December 2017 reopening of the SH1 corridor included drilling of sub-horizontal drain holes into the slope, temporary realignment of the road towards the sea, and installation of water-filled barriers at the toe of the slope (NCTIR, 2018a).

Permanent slope stabilisation and risk mitigation measures at the site were designed in 2018 and constructed in 2018-2019 to mitigate the risk to the road from rock fall and shallow debris slides. These consisted of rock anchors over the lower 4 m of the slope with a combination of shotcrete facing and pre-cast concrete panels. A proprietary rock fall fence was constructed above the concreted slope face to protect the road from rock falls from the weakened and dilated rock mass at the top of the cut slope (NCTIR, 2018a).

4.3 Okiwi Bay

4.3.1 Location and failure overview

Okiwi Bay is located approximately 25 km north of Kaikōura (Figure 2). The 2016 earthquake triggered extensive slope failures in the Okiwi Bay area, including a rock and debris slide from the coastal bluffs on the western side of the bay (Figure 14). This landslide was one of the principal slope failures along the coastal transport corridor (Justice *et al.*, 2018) and required lengthy mitigation work to clear the debris and construct rock fall protection structures.

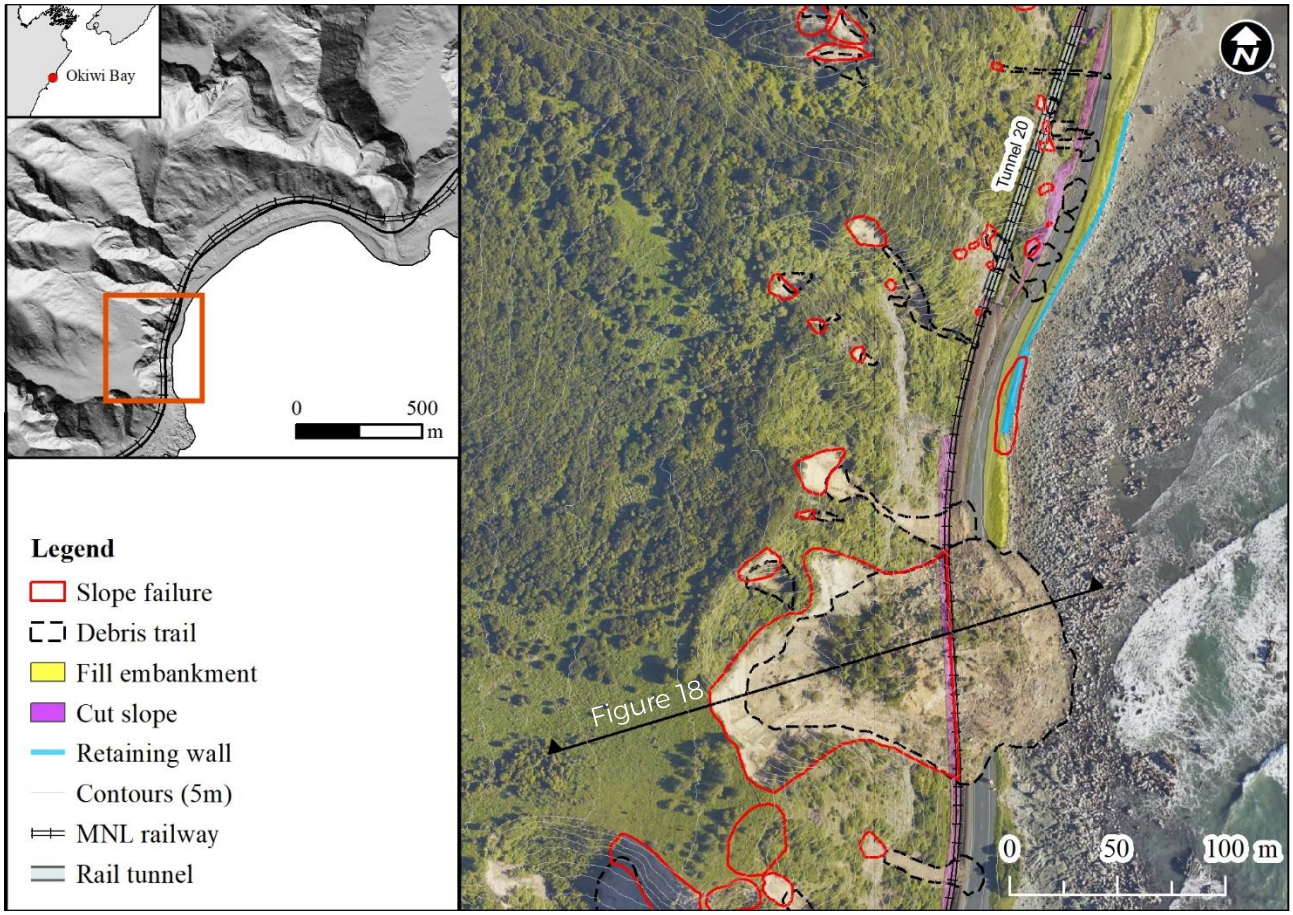

Figure 14: Okiwi Bay site plan

4.3.2 Geology and geomorphology

On the western side of the bay, late Pleistocene aggradational fan surfaces have been uplifted and eroded, forming a well-preserved terrace surface approximately 120 m above sea level (Figure 14). Very steep to vertical rock bluffs form the slope below the terrace surface, and SH1 and the MNL railway were constructed on an uplifted wave-cut platform at the base of the bluffs. Prior to the earthquake, the bluffs at the location of the landslide consisted of a central ridge with parallel, linear gullies on either side (Figure 15). Observations from pre-earthquake LiDAR and orthophotographs suggest these were pre-existing landslide features, with the gullies formed by previous wedge failures in the bedrock.

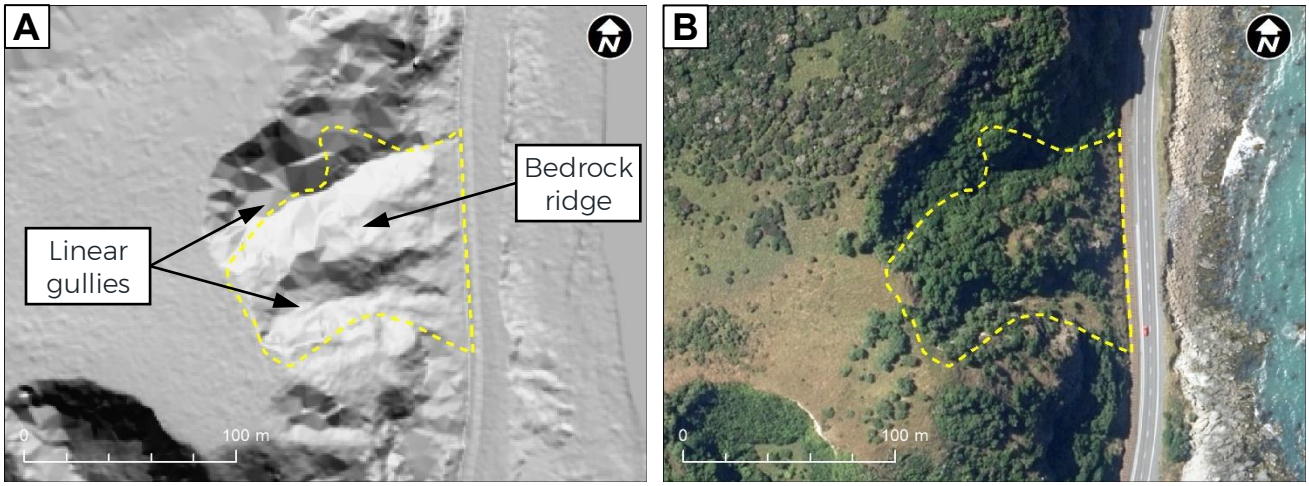

Figure 15: Pre-earthquake geomorphology of the Okiwi Bay site.
(A) Hillshade relief map from 2012 LiDAR; (B) 2015 aerial photograph. The dashed line indicates the extent of the 2016 landslide source area.

4.3.3 Geotechnical slope assets

The slope assets in the vicinity of the Okiwi Bay landslide are summarised in Table 8.

Table 8: Okiwi Bay slope assets

Asset type	Description
Cut slopes	The toe of the hillslope at the Okiwi Bay landslide was previously cut to create a bench for construction of the MNL railway. This cutting was up to 10 m high, and is presumed to date from the 1930s, when the section of the railway between Kaikōura and Waima was constructed (Topp, 1947).
Fill slopes	The state highway was constructed on a fill platform approximately 5 m thick. Boreholes were drilled along the road platform in 2018 show the fill materials consist of fine to coarse gravel with a matrix of sandy silt (Geotechnics, 2018a, 2018b).
Retaining walls	In the vicinity of the Okiwi Bay landslide the road platform was supported by 1 m to 2 m high gravity retaining walls (consisting of gabion baskets and concrete blocks), with a 3 m high rip rap revetment below the retaining walls to protect the slope below the walls from scour.

4.3.4 Site investigations

During the earthquake recovery six boreholes were drilled along the road platform below the landslide in February and November 2018 (Geotechnics, 2018a, 2018b). These boreholes were drilled to depths between 9 m and 11 m, to assess the ground conditions for rebuilding and realigning the road embankment. An additional borehole was drilled on the terrace above the landslide about 100 m above highway level, as part of this project in October 2020 (Mason and Brabhaharan, 2023b). This borehole was drilled to 90 m depth, with downhole geophysical surveys of the bedrock using acoustic televiewer and full waveform sonic logging.

4.3.5 Ground conditions

A representative engineering geological profile of the hillslope at the Okiwi Bay landslide is shown in Figure 18. Late Quaternary alluvial fan gravels underlie the terrace surface in the upper part of the slope. These gravels are approximately 35 m in thickness. The upper 25 m consists of well graded sandy gravel and cobbles with boulders and minor silt. Between 25 m and 30 m are interbedded layers of sandy gravel and gravelly silt. Immediately below the sandy gravels and gravelly silt layers is a layer of fine gravel and sand, that is dark bluish grey, wet, and weakly cemented. This unit is inferred to be a remnant of beach or shallow marine gravels that were deposited before the area was uplifted and the area transitioned to fluvial deposition.

Late Jurassic to Early Cretaceous greywacke bedrock of the Pahau terrane underlies the gravel sequences. The bedrock exposed in outcrop along the bluffs on the western side of Okiwi Bay consists of moderately weathered, grey to brown, thickly bedded, moderately strong to strong siltstone and sandstone. The rock materials recovered from the borehole behind the landslide head scarp consisted of slightly weathered to unweathered, dark grey, massive siltstone. Testing of unweathered core samples indicated a UCS of about 5 MPa (i.e. very weak to weak), with failure occurring along closely spaced incipient joints (Mason and Brabhaharan, 2023b). The characteristics of rock defects were observed from mapping the outcrops around the landslide site, geological logging of the borehole core, and from the downhole geophysical surveys. Bedding planes generally dip steeply (~70°) to the east, and are wavy or undulating and locally overturned. Major defects observed in the borehole are sheared, crushed and shattered zones (Figure 16). The orientation of these defects is generally towards the southeast, with dip angles between 25° and 78°. Joints show a much greater scatter in the dip angles and orientations (Figure 17).

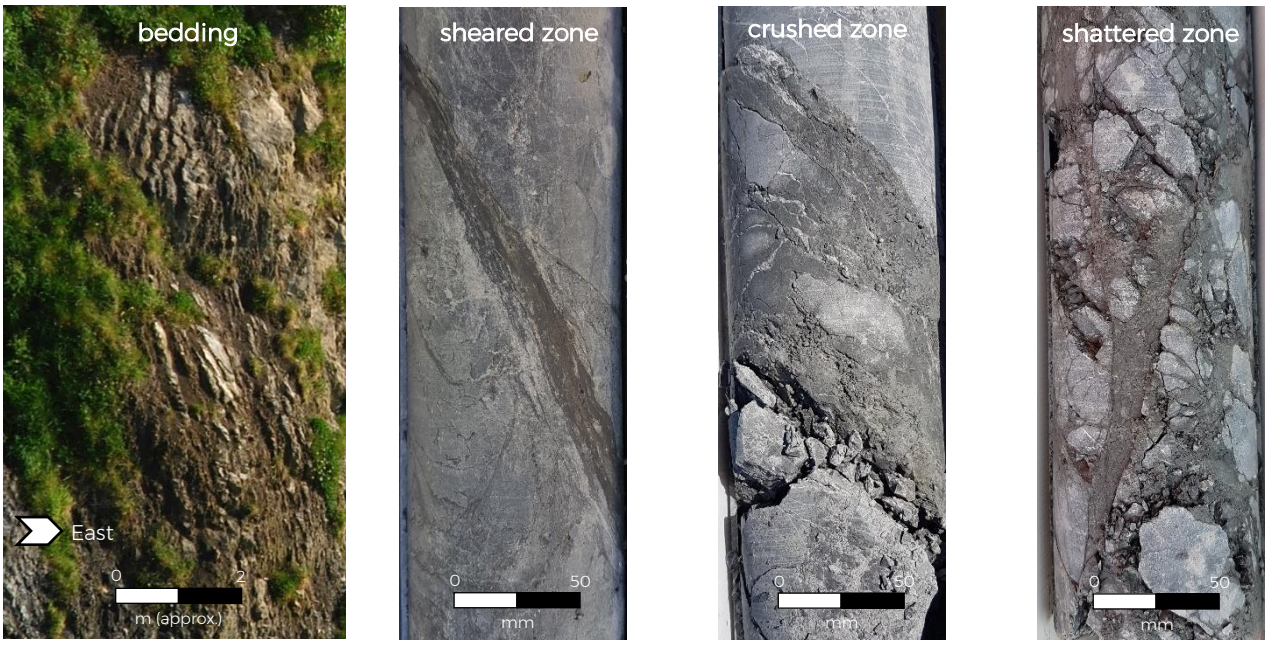

Figure 16: Examples of major defects observed at Okiwi Bay

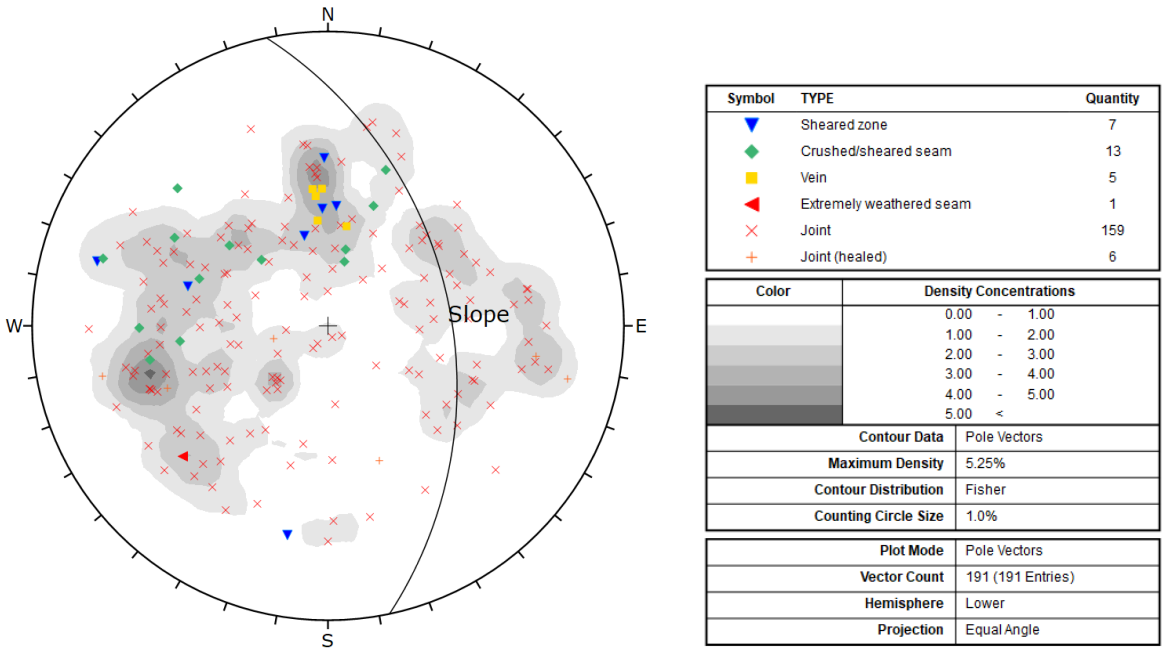

Figure 17: Defect orientations from ATV logging of BH101, Okiwi Bay

4.3.6 Kaikōura earthquake-induced landslide

Ground shaking

Okiwi Bay is approximately equidistant between the Kaikōura and Kekerengu strong motion recording stations. The recorded peak horizontal ground accelerations were 0.26 g at the Kaikōura site and 1.21 g at Kekerengu (GeoNet, 2016). The estimated horizontal PGA at the Okiwi Bay site was between 0.57 g (Bradley *et al.*, 2017) and 0.6 g (USGS ShakeMap).

Coseismic displacements

The 2016 earthquake resulted in translation of a block of bedrock approximately 10,000 m^2 in area. Estimation of coseismic slope displacements was carried out by GIS-based measurement using pre- and post-earthquake aerial photos and LiDAR DEMs. Both the crest and toe of the landslide displaced approximately 50 m horizontally, with vertical displacement of c. 55 m across the head scarp. No displacement or cracking of the slope above the head scarp was discernible from field mapping or review of post-earthquake aerial imagery.

Failure mechanism

The Okiwi Bay landslide was a compound slide, consisting of a rock wedge slide in the upper part of the rock slope and breakout through the rock mass in the lower part of the slope. The landslide mass remained largely intact during translation down the slope with minimal internal deformation. Wedge sliding occurred on intersecting continuous joints and sheared zones in the mudstone to either side of the central ridge. The failure surface was not exposed in the lower part of the slope by the earthworks to reopen the transport corridor. Based on the lack of distortion and rotation of the translated landslide block and the pattern of displacement of the railway lines, it is inferred to have daylighted at the base of the hillslope (Figure 19). The line of the wedge intersection plunges at 41°, which was too steep to daylight from the slope and therefore shear failure extended through the rock mass underneath the ridge, possibly along persistent sheared or crushed zones observed from the site investigations. Translation of the rock block undermined the overlying fan gravels, resulting in toppling/tensile failure extending through the gravels leaving a sub-vertical head scarp.

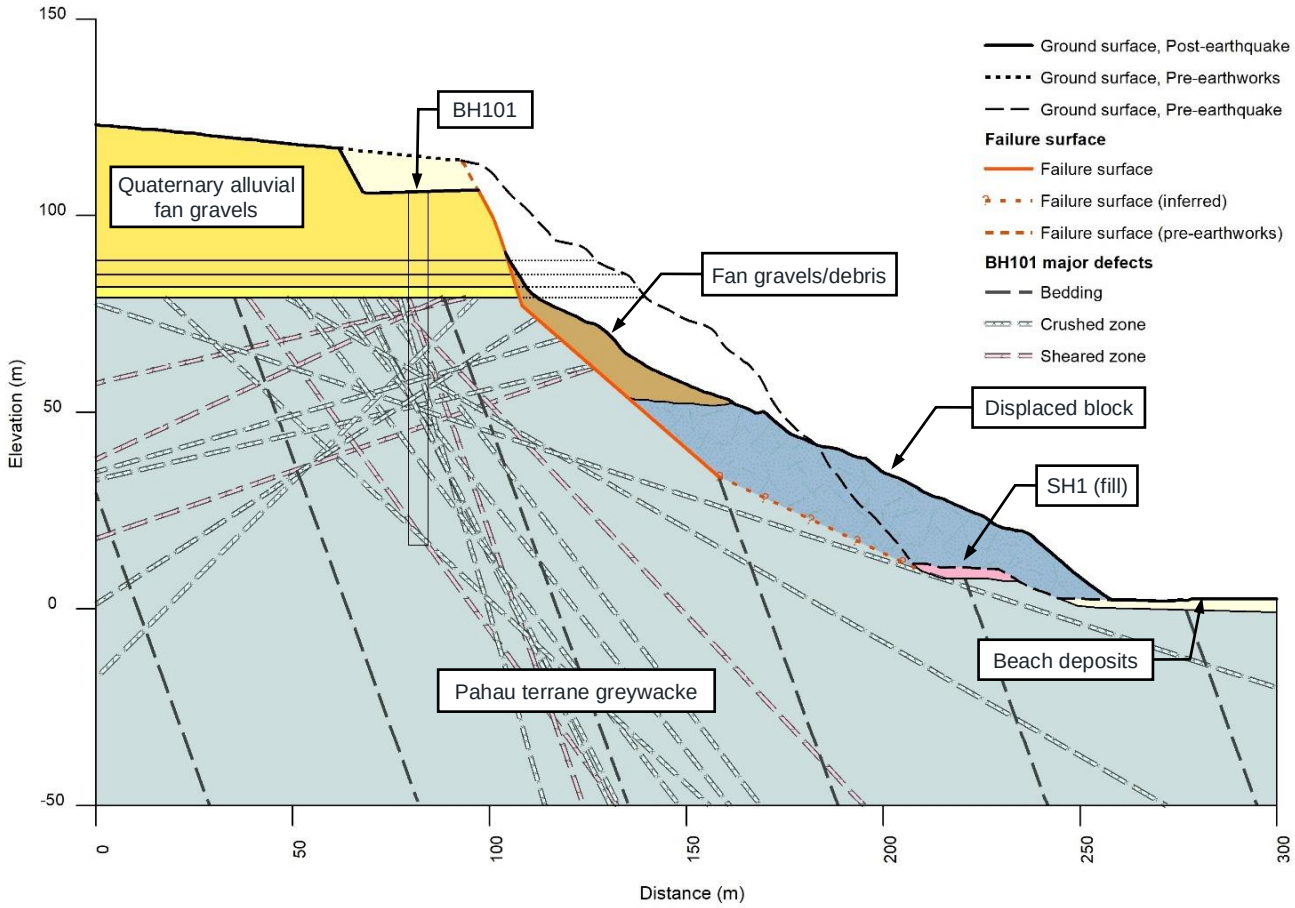

Figure 18: Ground model for the Okiwi Bay landslide

Damage impacts

The total volume of the landslide was approximately 100,000 m^3, with 50,000 m^3 of that volume lodged within the transport corridor, based on differencing of pre- and post-earthquake LiDAR DEMs. These estimates are *in situ* solid volumes, as minimal bulking of the landslide mass occurred as it displaced downslope. Earthworks volumes recorded by NCTIR show 130,000 m^3 of debris was removed (Figure 20). These volumes represent loose unconsolidated spoil removed by dump trucks, and also include additional material cut from the head scarp area (discussed below). In addition to the accumulation of debris, the impact of the sliding landslide mass caused extensive damage to the road pavement and rail structures, displacing the railway tracks by 40 m towards the sea (Figure 19) and causing severe distortion of the tracks to the north and south of the landslide.

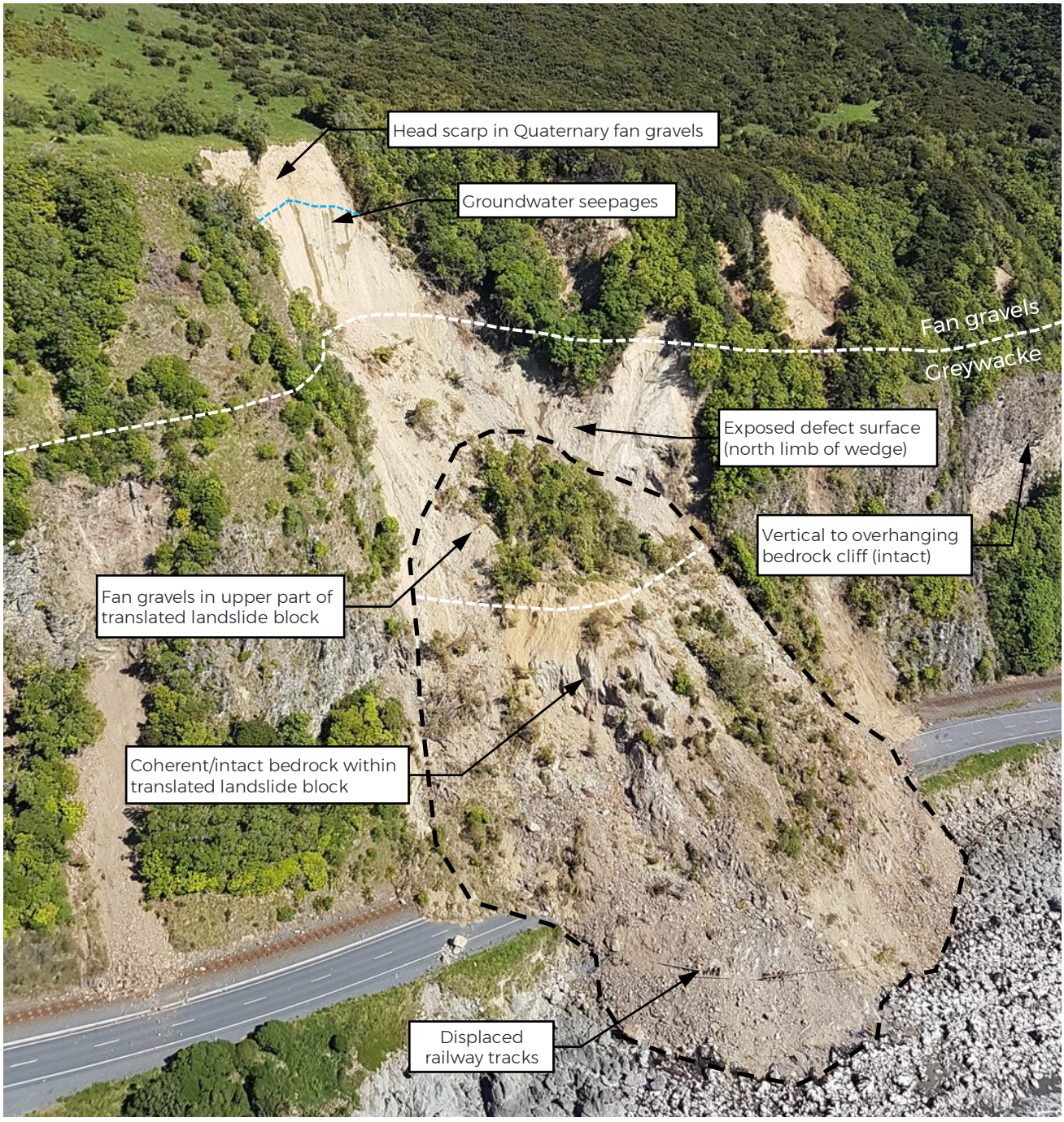

Figure 19: Okiwi Bay landslide

Outage and recovery

The response and recovery work at the Okiwi Bay site and the duration of the outage are summarised in Table 9 and described in detail below.

The transport corridor remained blocked and fully closed by the Okiwi Bay landslide until January 2017 (~6 weeks after the earthquake), when a 4WD access track was formed around the outside of the landslide debris to provide access past the slip for residents and construction personnel. Clearance of the landslide debris commenced in March 2017, 3.5 months after the earthquake (Figure 20).

This involved bulk earthworks to:

(a) Remove the debris that lodged within the transport corridor,

(b) Excavate material from the top of the landslide to lower the height of the head scarp and remove large boulders that posed a significant safety risk to construction personnel and public road users,
(c) Construct mid-slope catch benches for rock fall,
(d) Temporarily realign the rail line 7 m seawards, and
(e) Widen the access track to two lanes for earthworks plant (NCTIR, 2018d).

Table 9: Okiwi Bay road outages during response and recovery phases

Recovery stage	Level of service	Date completed	Duration after EQ
Emergency response	4WD access track, single lane	Early Jan 2017	6 weeks
	4WD access track, two lanes	March 2017	4 months
Recovery	MNL railway re-opened	September 2017	10 months
	SH1 open for public – two lanes, temporary speed limit, daytime access	December 2017	13 Months
	Two lanes, 24 hr access with temporary barrier	April 2018	17 months
	Optioneering and concept design	June 2018	21 months
	Detailed design	August 2018	21 months
	Construction of mitigation measures	September 2019	34 months

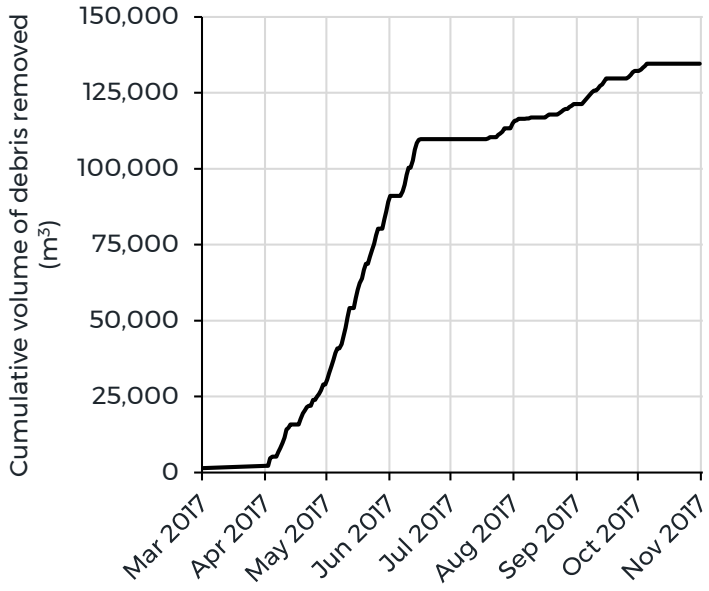

Figure 20: Progress of debris removal from the Okiwi Bay landslide (Source: NCTIR)

Removal of landslide debris from the base of the slope commenced in late March 2017. Debris removal was most intensive from April to June 2017, as shown in Figure 20. During July 2017, earthmoving ceased so the rail tracks could be re-laid. The railway line was reinstated in July 2017 and the line was reopened to freight trains in September 2017.

The access track around the toe of the landslide was realigned and progressively enhanced from July prior to re-opening of the SH1 corridor in December 2017, however earthworks and complete reinstatement of the road at the site were not completed until February 2018.

Risk mitigation work at the site continued after the reopening of the road and rail, with construction of engineered MSE bunds and rock fall fences along the base of the landslide and adjacent rock bluffs to protect the road and rail from rock fall, which was completed in September 2019.

4.4 Performance of rock slope stabilisation measures

Observations of the performance of slope stabilisation measures in previous earthquakes show measures such as rock bolts, anchors and shotcrete have been effective against earthquake induced landsliding in the 1999 Chi-Chi and 2008 Wenchuan earthquakes, whereas adjacent unsupported natural and cut slopes suffered widespread shallow landslides and rock falls (Khazai and Sitar, 2004; Zhang *et al.*, 2012). Prior to the 2016 earthquake there were only two slopes stabilised with rock bolts at Ohau Point and Okiwi Bay. Given the observations of performance of slope stabilisation measures in overseas earthquakes it is worthwhile examining the performance of these slopes. Unfortunately, the design records have not been able to be retrieved and the post-earthquake condition of the rock bolts was not investigated during the recovery works, so forensic examination of the actual performance of the bolts against their expected design performance could not be carried out. Therefore, only visual observations of the performance of the stabilised slopes have been made, and these are summarised below.

4.4.1 Ohau Point

Ohau Point is at the eastern end of Half Moon Bay, approximately 20 km northeast of Kaikōura (Figure 2). Prior to the earthquake, SH1 was situated on a 10 m wide bench approximately 20 m above sea level. The slope above the road is a 160 m high cliff exposing greywacke bedrock (Figure 21). The properties of the rock mass exposed in the Ohau Point cliff vary considerably, from slightly weathered blocky sandstone at the base of the cliff to highly weathered, intensely fractured and dilated sandstone and mudstone in the upper third of the cliff. Failures of the rock slope at this site consisted of extensive coalescing rock and debris avalanches originating at the top of the cliff, and defect-controlled wedge and toppling failures originating in the middle parts of the cliff. Based on volume differencing between pre- and post-earthquake LiDAR surveys, the cumulated volume of debris from the coseismic landslides is estimated to be 150,000 ±30,000 m^3.

An area of rock bolting and mesh was installed on the slope in 2007, covering 750 m^2 of the lower part of the cliff. The rock bolts consisted of 3 m long, 32 mm diameter 500 MPa bars grouted into 55 mm diameter drillholes. The rock bolts were positioned in a grid pattern with 3 m to 4 m spacing. The mesh consisted of Tecco rock fall mesh constructed by Geobrugg (C. Parkes, pers. comm., 2022). The area of rock bolting on the north face of the cliff is shown in Figure 21. The rock bolts did not fail in the earthquake, however limited failures occurred between the bolts, either as disaggregated failure of loose rock on the slope surface, or combined toppling and sliding along a stepped-planar failure surface of outward-dipping joints. The disaggregated failures were of sufficiently small volume that they were readily contained by the mesh facing; the deeper joint-controlled failure of blocks of rock between the bolts ruptured the mesh at the northern end of the stabilised section of slope (Figure 21). Dilation of outward-dipping defects and minor displacement of the rock block occurred in the area adjacent to this failure.

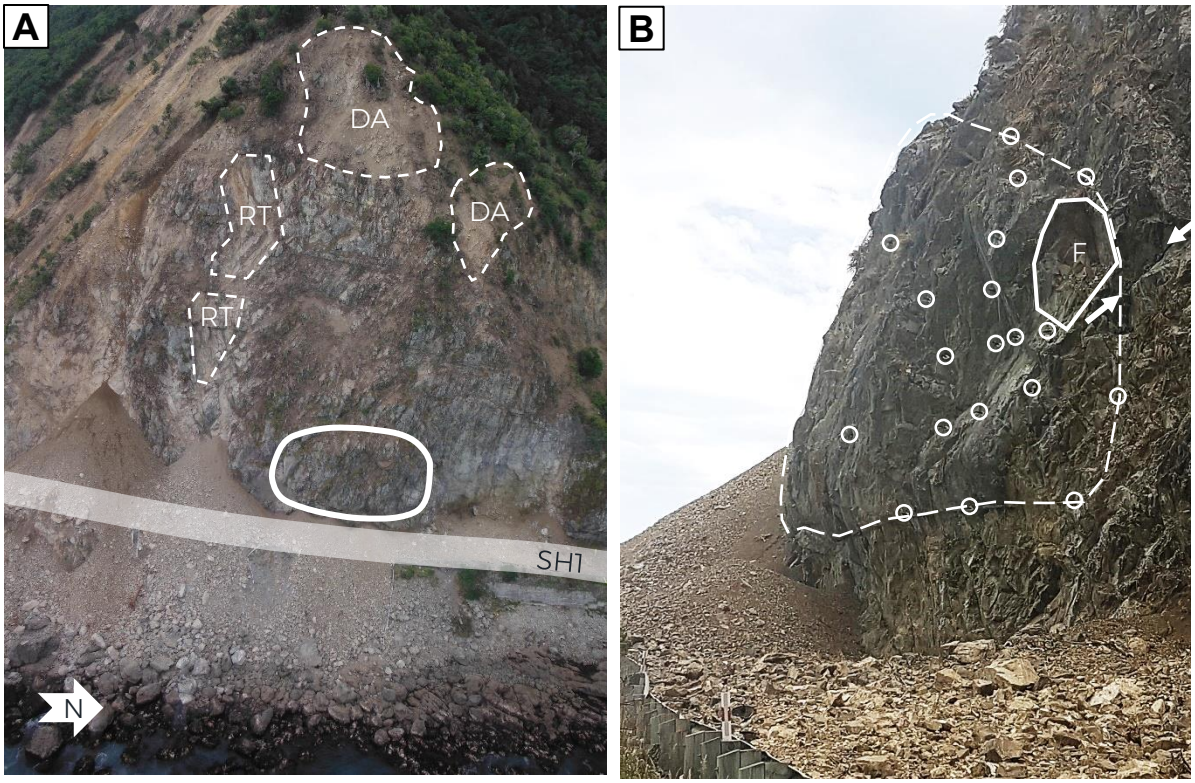

Figure 21: Slope failures on the northeastern cliff face above SH1 at Ohau Point.
(A) Debris avalanches (DA) and rock topples (RT) were triggered in the middle and upper parts of the slope, inundating the road bench with debris. The area circled in the lower slope is the approximate area of slope stabilisation.
(B) The northern end of the area of rock bolts (circled) and mesh in the lower part of the slope. Failure (F) of a small section of the rock face occurred by combined toppling and sliding on a stepped-planar failure surface of outward-dipping joints at the lateral margin of the meshed area. In the adjacent part of the slope (between the arrows), dilation of joints and displacement of the joint-bounded block occurred but did not transition to failure (photo credit: J. Grindley).

4.4.2 Okiwi Bay

Approximately 180 m to the north of the Okiwi Bay landslide described in Section 4.3, SH1 is situated on a bench with a section of cut slope above the road. This section of SH1 was realigned in 2005-2006 to straighten curves and involved cutting into the rock slope on the western side of the road. Localised areas of rock bolting and mesh were constructed on the cut slope during the realignment work to retain unstable wedges of rock in the upper parts of the cutting. The rock bolts were less than 10 m long and spaced in a diagonal grid pattern with 1.5 m to 2 m horizontal and 1.5 m vertical spacing. The mesh consisted of Tecco rock fall mesh manufactured by Geobrugg (T. McMorran, pers. comm., 2022). Approximately 140 m^2 (12%) of the slope was treated (Figure 22A).

Failure of the unsupported parts of that slope consisted of wedge failures along intersecting joints at the top of the cut slope. Within the areas of mesh and rock bolts, deformation of the rock slope consisted of incipient displacement of rock wedges between the bolts, failure of small wedges of rock and minor spalling of loose debris from the face. Where this occurred, the mesh retained the failed rock, with only fine gravel-sized debris passing through or beneath the mesh. The unmeshed parts of the slope generated larger volumes of debris from wedge failures, with the resulting rock fall inundating both lanes of the state highway.

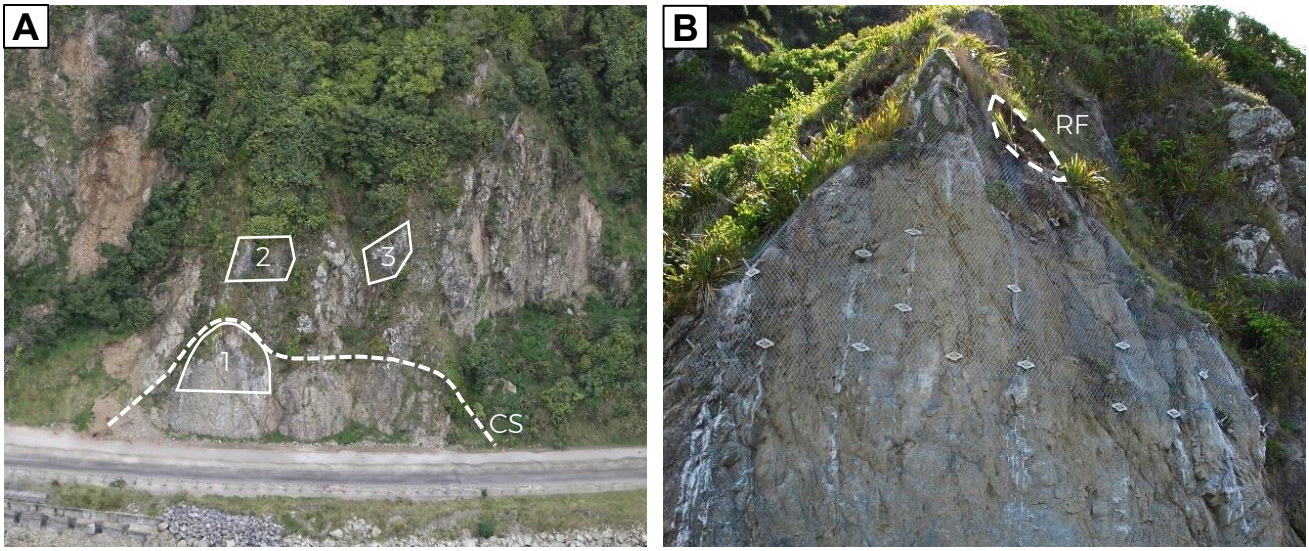

Figure 22: Cut slope and rock bolting areas north of the Okiwi Bay landslide. (A) Areas of rock bolts and mesh (numbered 1-3) on the bluff above SH1 on the western side of Okiwi Bay. The extent of the cut slope (CS) is shown by the dashed line. (B) Rock bolts and mesh in area 1 on the cut slope with no observed deformation at the surface following the 2016 earthquake. A minor rock fall (RF) occurred from the slope above the top of the mesh.

4.4.3 Summary

Areas of rock bolts and mesh performed well where failure of the rock slope consisted of small-scale kinematic failures (wedges or topples) or disaggregation of dilated and weakened rock on the slope surface. The rock bolted areas are unlikely to have retained larger scale mechanisms, as evidenced by the partial failure of the mesh at Ohau Point where deeper-seated blocks of rock displaced or failed.

5 Fill slope sites

5.1 Hawkswood to Ferniehurst

The Hawkswood Deviation and the Siberia-Ferniehurst Realignment are two adjacent sections of SH1 approximately 18 km north of Cheviot in north Canterbury (Figure 23). These realignments of the state highway were constructed in 1999-2001 to improve a winding and sub-standard section of the highway (Koorey, 2009). This involved cutting and filling across a series of alluvial terraces, ridges and gullies. The fill slopes along this section of SH1 suffered extensive damage in the 2016 Kaikoura earthquake.

5.1.1 Geology and geomorphology

The geomorphology of the Hawkswood area consists of a series of alluvial terraces and linear ridges that have been incised by northwest-flowing streams (Figure 23). The terrace surfaces and ridge crests are flat (generally less than 5°), the side slopes of the ridges are moderately sloping (10° to <30°), and the incised gully slopes along the streams are steep to very steep (generally 40° to 60° and locally up to 80°).

The geology of the site is dominated by Quaternary alluvium, with Holocene river gravel and sand deposits underlying the low-lying terrace to the northeast of Chilly Stream, and Pleistocene alluvial fan gravels and sand underlying the elevated terraces in the central part of the realignment. The Quaternary deposits are underlain by Pliocene siltstone of the Greta Formation (Rattenbury *et al.*, 2006).

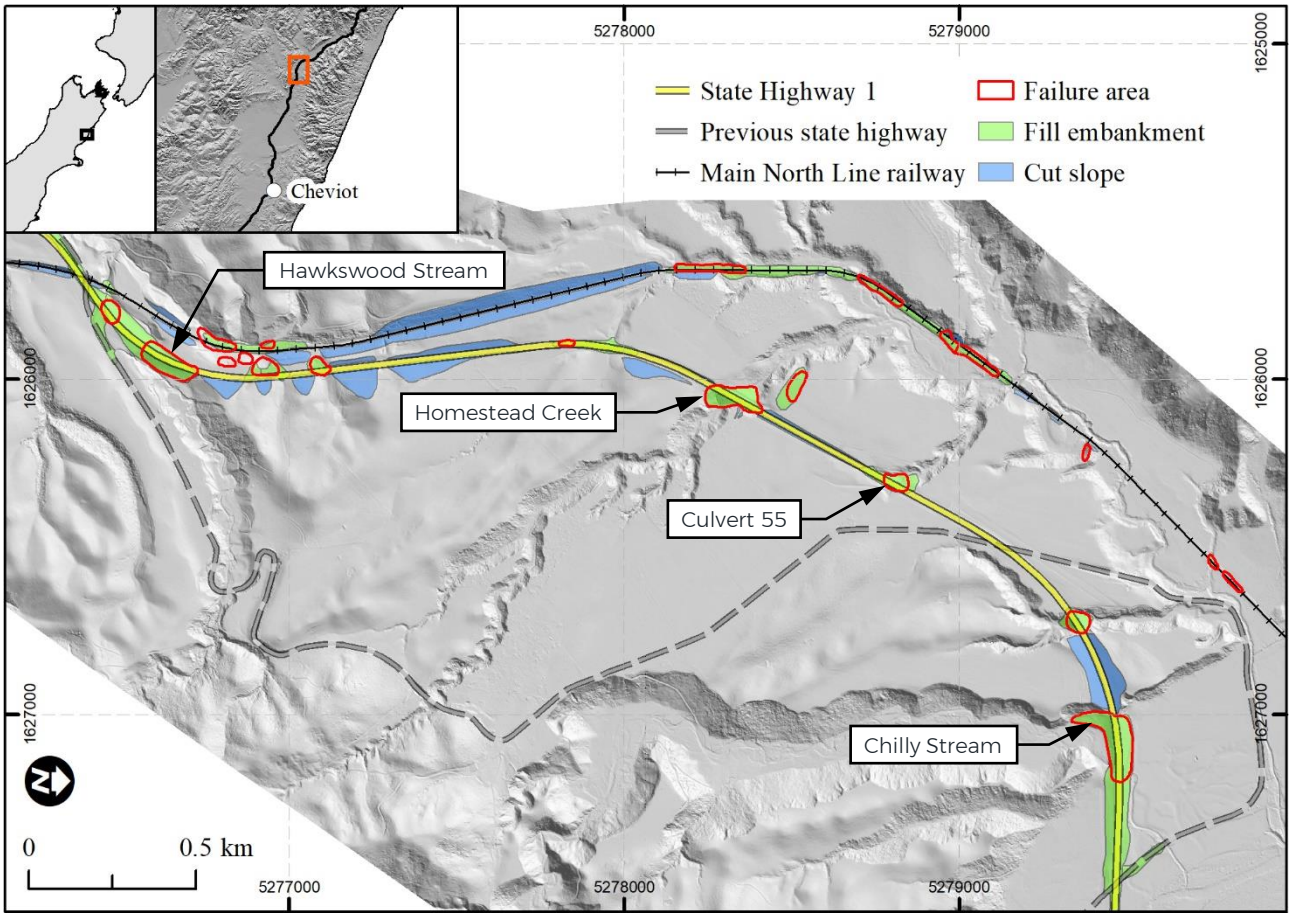

Figure 23: Hillshade relief map of the SH1 Hawkswood to Ferniehurst realignment, with key embankment failure sites highlighted

5.1.2 Geotechnical slope assets

The slope assets between Hawkswood and Ferniehurst are summarised in Table 10.

Table 10: Hawkswood to Ferniehurst slope assets

Asset type	Description
Cut slopes	Realignment of the state highway consisted of cutting into the ridges and alluvial terrace surfaces and using the cut material to build fill embankments across the gullies. A total of 15 cut slopes were formed, between 2 m and 23 m in height. The cuts were formed at slope angles of 18° (3H:1V), so the land could be returned to the landowner for grazing (Cook and Spriggs, 1998), thereby reducing the land requirement for the state highway corridor.
Fill slopes	A total of 15 fill slopes were formed, from 2 m to 22 m high. The fill embankments were designed for a maximum batter angle of 26° (2H:1V). Examination of LiDAR terrain data shows the sidling and embankment fills were formed with overall slope angles between 16° and 28°.

5.1.3 Site investigations

Previous investigations at the site consisted of test pits and machine auger boreholes. These were carried out between 1990 and 1998 to inform the geotechnical design of the road realignment (Cook and Spriggs, 1998). The logs from these investigations were not available for this study, however these were reviewed by Cook and Spriggs (1998) who provide a summary of the ground conditions in the local area.

A rotary cored borehole was drilled to 25.9 m depth at the Homestead Creek embankment in September 2020 as part of this research project (Mason and Brabhaharan, 2023b).

5.1.4 Ground conditions

The ground conditions along the Hawkswood to Ferniehurst alignment have been summarised based on the historical and recent site investigations as follows:

- The terrace surfaces are underlain by recent aeolian materials, consisting of topsoil, fine sand and silt to ~3 to 4 m depth.
- The gullies are underlain by young alluvial deposits, which consist of soft silt and loose sand overlying loose sandy gravel.
- Fan gravels underlie the aeolian and stream deposits, and consist of dense sandy and silty gravel.
- Neogene Greta Formation siltstone underlies the fan gravels, and consists of very weak to weak, massive siltstone.

5.1.5 Kaikōura earthquake-induced slope failures

The Kaikōura earthquake triggered a number of slope failures along the Hawkswood to Ferniehurst realignment, with nearly every fill body showing signs of deformation including settlement and rotational sliding. In particular, significant damage to fill embankments at Homestead Creek and Culvert 55 resulted in closure of the state highway for ~3 months while the damaged sections of road were excavated and rebuilt.

Ground shaking

The closest strong motion stations are at Cheviot, 18 km to the south, and Waiau, 21 km to the west. The recorded horizontal PGAs were 0.29 g at Cheviot and 1.12 g at Waiau (GeoNet, 2016). Modelled peak ground accelerations in the Hawkswood to Ferniehurst area were between 0.23 g (Bradley *et al.*, 2017) and 0.48 g (USGS ShakeMap).

Failure mechanisms and damage impacts

Nearly all of the fill embankments experienced some form of damage in the earthquake, while none of the cut slopes were affected. Damage of the fills ranged from localised and minor cracking of the pavement at the margins of the fill bodies to extensive settlement and slumping. Frequent but minor cracking of the road surface occurred throughout the site, particularly at the boundaries of the fill bodies (i.e. at the interface between the fill materials and natural soils) and near the crests of the fill slopes. The pavement cracking was also accompanied by settlement of the road surface, which is presumed to be in response to densification of the underlying fill due to ground shaking. Development of wider and deeper tension cracks occurred where the fill bodies were thicker and the batter slopes were steeper. The most severe damage occurred to the fill embankments at Hawkswood Stream, Homestead Creek, Culvert 55 and Chilly Creek, which are shown in Figure 24 and described below.

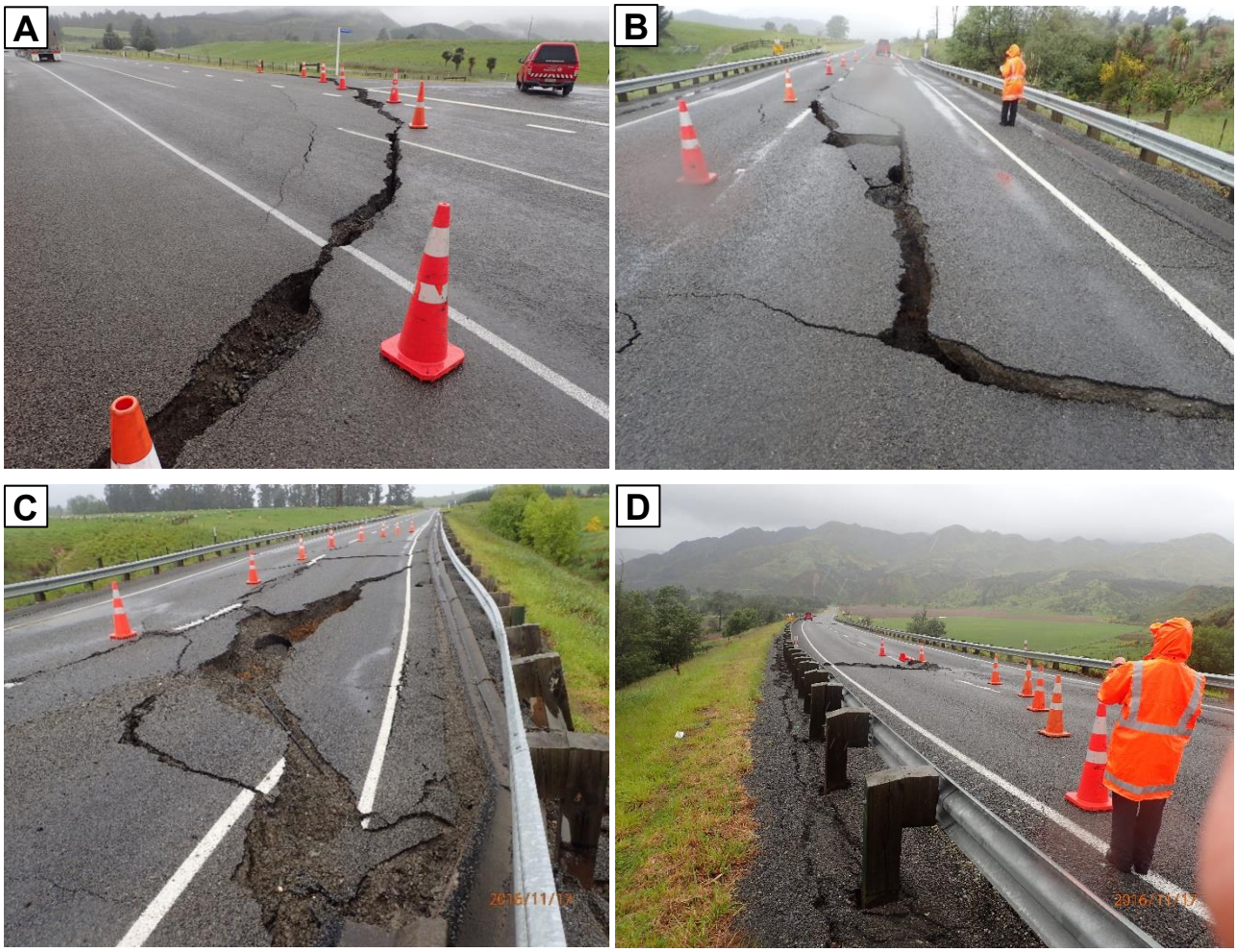

Figure 24: Damage to fill embankments on the Hawkswood to Ferniehurst section of SH1. (A) Hawkswood Stream; (B) Homestead Creek; (C) Culvert 55; (D) Chilly Stream. Photo credits: C. Parkes.

The damage to the Hawkswood Stream embankment potentially experienced densification of the fill materials, which caused settlement of the road surface, slumping at the crest of the fill slope, severe tension cracking at the interface between the fill and native ground (Figure 24A), and distortion of a corrugated steel culvert conveying the stream beneath the embankment. At Homestead Creek, the damage consisted of widespread cracking and slumping of the embankment, with the southbound lane inaccessible due to severe cracking with up to 0.5 m vertical separation of the road pavement across the tension cracks (Figure 24B). Culvert 55 was the most severely damaged embankment (Figure 24C), as described below. Less severe damage occurred to the embankment at Chilly Stream, including settlement and persistent tension cracking along the crest of the fill slope and through the middle of the road (Figure 24D).

Culvert 55 failure mechanism and coseismic displacements

A translational to semi-rotational slump formed on the northwestern side of the fill slope at Culvert 55. The damaged embankment was excavated following the earthquake, and replaced with reinforced fill. During the excavation works, several areas of groundwater seepage at high levels within the fill were observed (Figure 25), and the concrete pipe was found to be completely blocked with silt and debris from the farm pond above, resulting in the groundwater table sitting several metres above the level of the culvert.

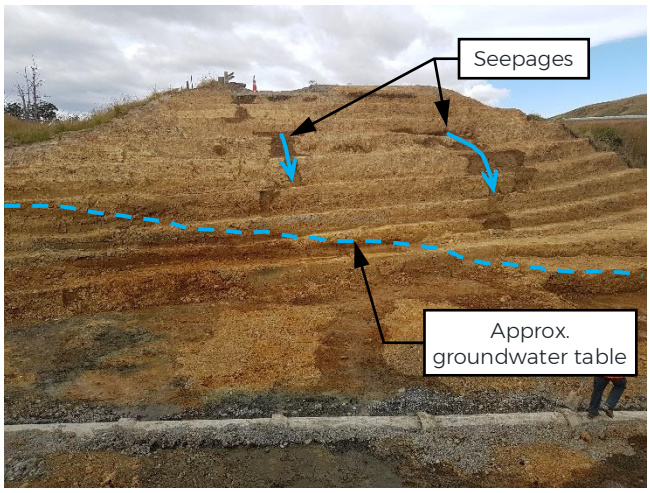

Figure 25: Post-earthquake excavation of the embankment at Culvert 55

The failed mass displaced 5.8 m downslope, with a ~1 m high scarp forming in the northbound lane, and extensive cracking and settlement throughout the remainder of the fill body; Figure 26A). The mean displacement of the road surface was c. 0.5 m, with a sharp increase across the head scarp of the main part of the failure near the crest of the fill slope. The displacement of the landslide also caused separation of the concrete pipe sections of the culvert within the embankment. Slope displacements were measured in GIS by identifying displaced ground surface features in pre- and post-earthquake aerial photos, supplemented by field-based measurement of horizontal and vertical offsets of the road surface across tension cracks. The measured displacements along the cross section are shown in Figure 26B.

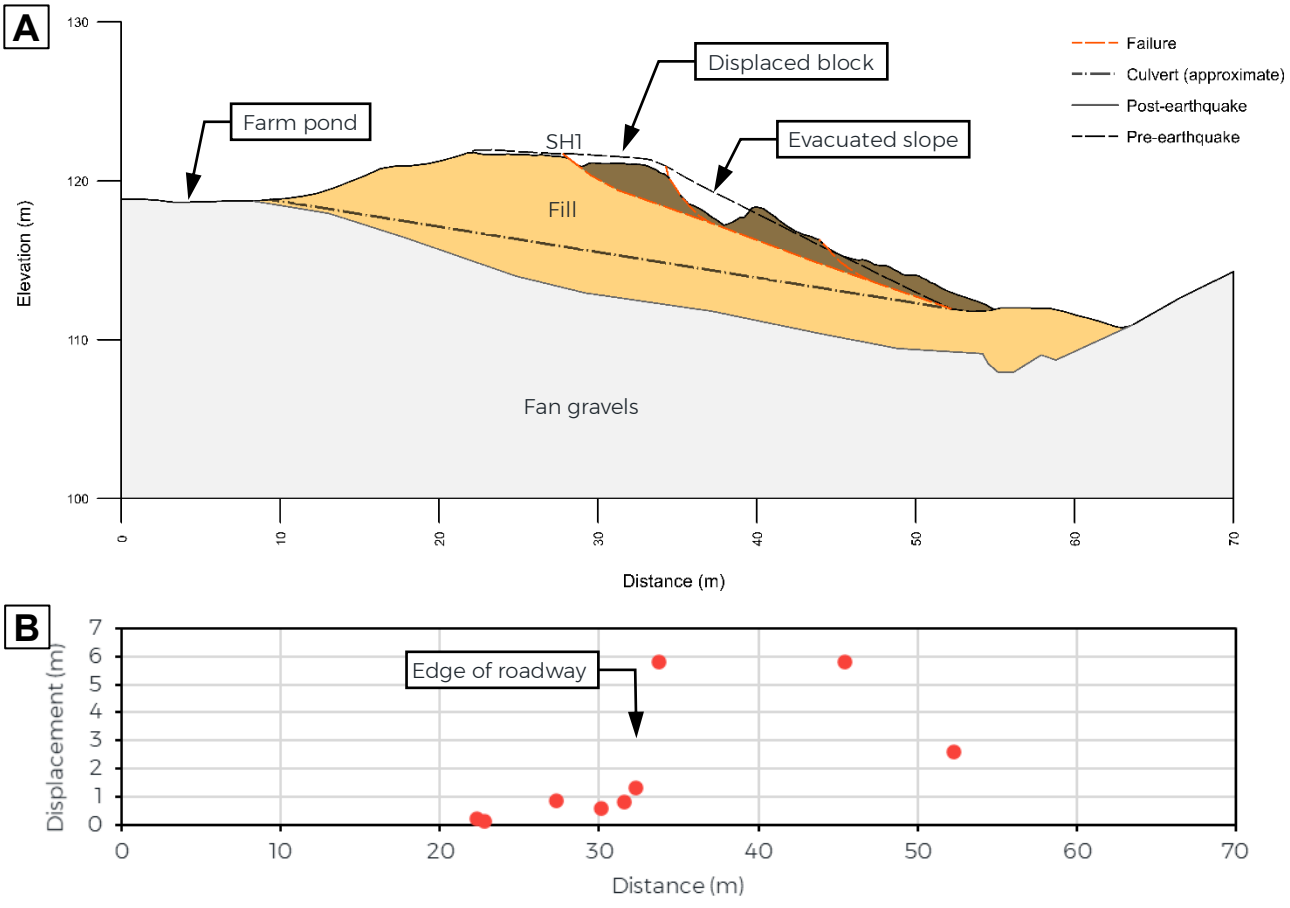

Figure 26: (A) Cross section and (B) displacement profile through the Culvert 55 embankment

Outage and recovery

Damage to the majority of the embankments consisted of cracking and settlement of the road surface, which were repaired by trenching the cracks and backfilling with compacted aggregate, stripping the surface and re-levelling the embankment with granular fill as required, and re-laying the road pavement. The majority of these repairs were undertaken within the first 3 weeks after the earthquake, however the whole section of the road remained closed for access until February 2017 due to the extensive repairs required to excavate the embankment at Culvert 55, re-lay the culvert and rebuild the embankment. Traffic was diverted along Hawkswood Road (the former route of SH1) during the earthworks at Culvert 55.

5.2 Hundalee Forest

South of Kaikōura, SH1 passes through the Hundalee Hills between Oaro and Ferniehurst. The Hundalee Hills are typically steep and deeply incised, and consequently the road alignment through the hills is often narrow and winding and constructed on sidling fill slopes. The Kaikōura earthquake triggered a number of fill slope failures in this area, particularly along the c. 1 km long Hundalee Forest section, which is located approximately 25 km southwest of Kaikōura (Figure 27).

5.2.1 Geology and geomorphology

At the Hundalee Forest site, the state highway follows a stream valley, and the road is situated between 3 m and 9 m above stream level on the eastern side of the valley. On the eastern side of the road, moderately steep hillslopes rise at average angles of 30° to 40° to a ridgeline 50 m above road level. The hillslopes commonly show evidence of recent and historic landsliding, with arcuate head scarps and undulating hummocky ground below the scarp features (Figure 27). The geology of the site area consists of Pliocene siltstone of the Greta Formation, with Holocene alluvium infilling the base of the valley (Rattenbury *et al.*, 2006).

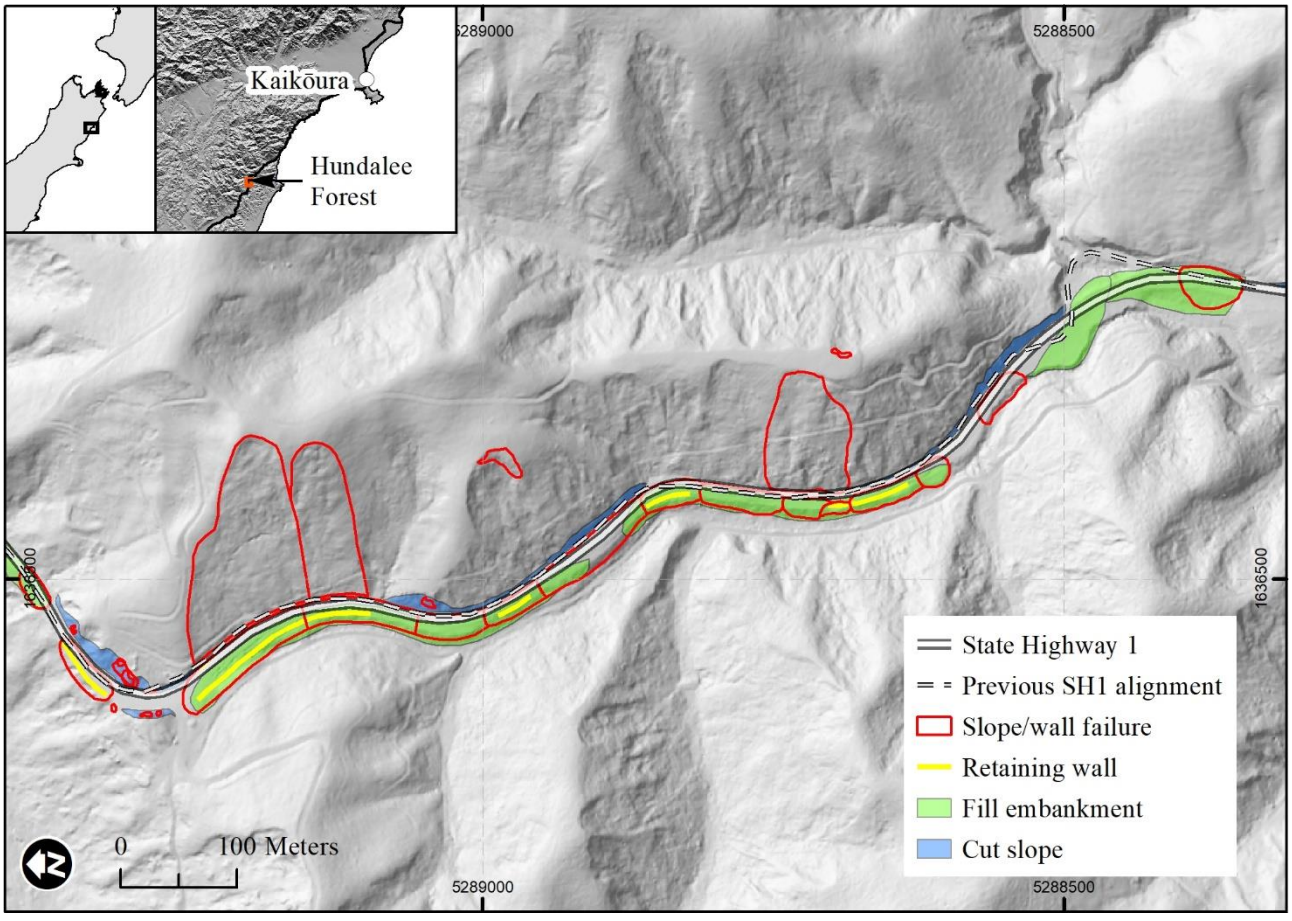

Figure 27: Hundalee Forest site plan

5.2.2 Geotechnical slope assets

Realignment works were carried out on the Hundalee Forest section of SH1 in 2010, to improve safety by easing corners, widening the carriageway, and installing guard rails. The realignment was designed to minimise cutting into the uphill slopes, to avoid reactivating existing landslides, and consequently the majority of the work involved construction of fill slopes and retaining walls on the downhill (western) side of the road (Parkes, 2010).

There were two cut slopes in the site area after the realignment work, totalling 500 m in length. The cuts were formed at slope angles between 40° and 55° and are up to 10 m high. Counterfort drains with sub-horizontal drainage pipes were installed into the slope above the road in areas of pre-existing instability to relieve groundwater pressures (Parkes, 2010).

The outside half of the road is supported on sidling fill embankments 3 m to 5 m thick along approximately 800 m of this section of SH1. The construction practices at the time of the initial formation of the road corridor are not well documented for this area, however anecdotal evidence from construction of the arterial roads and the trunk railways in the South Island in the late 19th and early 20th centuries point to a non-engineered fill where the road construction was achieved by side-casting fill over the edge of the pre-existing slope with little benching of the foundation and no mechanical compaction of the fill material (ArchivesNZ, 2022; Merrifield, 1973). Fill slopes constructed or extended for the realignment work in 2010 were formed by stripping vegetation and topsoil, benching the slope and placing the fill material in compacted layers. Excess or unsuitable material cut from the uphill side of the road was placed in a fill disposal area, infilling the gully at the northern end of the realignment (Parkes, 2010). Sections of unreinforced gabion walls 1 to 3 m high, and totalling 330 m in length, were also constructed to support the road embankment and guard rails. Design records are currently not available, however it is considered unlikely that earthquake loads were included in the design of the walls (NCTIR, 2018b).

5.2.3 Site investigations

During the earthquake recovery, two boreholes were drilled and one CPT was carried out along the road in this section of SH1 (Geotechnics, 2017a, 2017b). The boreholes were drilled to depths between 9 m and 11 m, to assess the ground conditions for repairing the damaged embankments and retaining walls. An additional borehole was drilled to 15.4 m depth in the gully below the road at the northern end of the Hundalee Forest site in September 2020 as part of this research (Mason and Brabhaharan, 2023b).

5.2.4 Ground conditions

The ground conditions along the Hundalee Forest section of SH1 have been summarised based on the historical and recent site investigations as follows:

- The road is constructed along a sidling fill embankment; the fill materials consist of silty and sandy gravel, and are up to 5 m thick.
- The hillslopes are underlain by variable thicknesses of recent colluvium, consisting of silt and gravel mixtures derived from weathering and erosion of the underlying siltstone bedrock. These deposits increase in thickness from <1 m at the ridge crest to ~2 to 3 m towards the base of the hillslopes and within gullies in the bedrock surface.
- The stream valley alongside the road is underlain by young alluvial deposits, which consist of soft silt and loose sand.
- Neogene Greta Formation siltstone underlies the recent deposits, and consists of very weak to weak, massive siltstone.

5.2.5 Kaikōura earthquake-induced slope failures

Ground shaking

The closest strong motion recording station is in Kaikōura, approximately 20 km to the northeast. The peak horizontal ground acceleration recorded at the Kaikōura site was 0.26 g (GeoNet, 2016). The peak ground accelerations in the Hundalee Forest area were estimated to be between 0.22 g (ShakeMapNZ) and 0.5 g (USGS ShakeMap).

Failure mechanisms and damage impacts

Deformation and displacement of the hillslopes above the road occurred throughout this section of the road, with frequent tension cracking within the pre-existing landslide features and some minor slumps from the head scarp areas near the ridgeline. However, the deformation of the uphill slopes did not impact the road.

There was widespread cracking and displacement of the fill slopes along the 1 km length of this site. Damage of the fills ranged from minor surficial cracking of the pavement to extensive slump and spread failures of the slopes. The most severe deformation extended across the full width of the road (Figure 28), whereas the minor to moderate cracking and deformation typically extended to the centre of the road, where the interface between the fill and in situ natural soils is likely to be located.

The gabion walls also suffered extensive damage, with frequent overturning failures and a number of instances of translation observed of single basket-high walls. Pavement cracking and loss of shoulder support to the carriageway occurred along the length of the damaged walls, with the loss of one lane adjacent to walls with the most displacement, often where the pavement seal extended over the top of the gabion baskets.

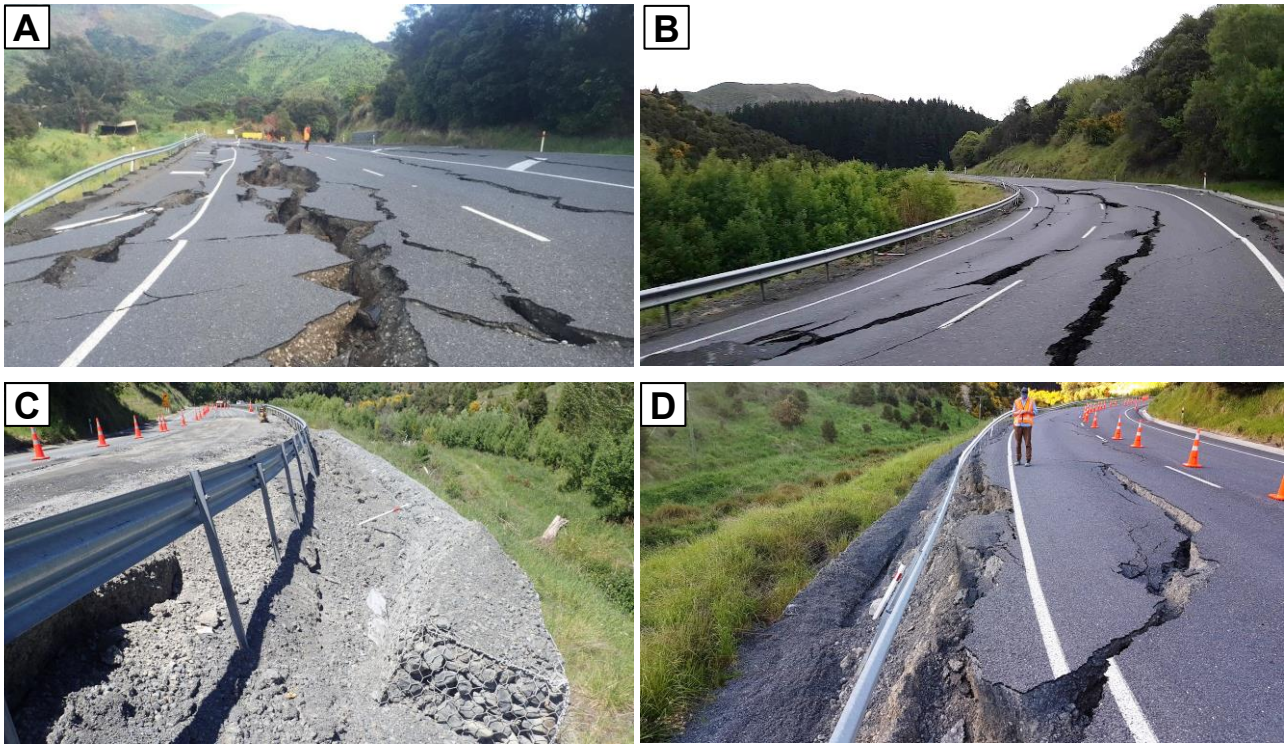

Figure 28: Major damage to slope assets along the Hundalee Forest section of SH1. (A) Translational failure of a gabion wall and spreading of the road embankment at RP 185/2.65 (photo credit: stuff.co.nz). (B) Displacement of a gabion wall and the road embankment at RP 185/3.05 (photo credit: D. Coll). (C) Overturning failure of an unreinforced gabion wall (photo credit: M. Broughton). (D) Translational failure of a gabion wall and slumping of the road embankment (photo credit: K. Jadrnicek).

Outage and recovery

Immediately following the earthquake, the road was reduced to a single lane, with some sections passable only by 4WD vehicles with difficulty due to wide cracking with significant vertical offset of the road surface (Figure 28). Access for emergency vehicles was able to be re-established quickly, by stripping the asphalt surfacing and infilling the cracks with aggregate. Repair of the minor to moderate severity cracking and settlement of the road surface consisted of trenching the cracks and backfilling with compacted aggregate, stripping the surface and re-levelling the embankment with granular fill as required, and re-laying the road pavement. Repairs to the more severely damaged embankments and gabion walls included excavation of the damaged section to a stable platform, and replacement with compacted geogrid-reinforced fill, with the gabion baskets tied to the geogrids as shown by NCTIR (2018b).

5.3 The Sandpit

The 'Sandpit' site is located on SH1 and the MNL approximately 1.5 km south of Clarence River. The 2016 earthquake caused extensive damage to the road and rail corridors at this site from fill embankment deformation, failure of retaining walls and slumping of cut slopes.

5.3.1 Geology and geomorphology

This site consists of southeast-facing slopes between a coastal plain and an elevated alluvial terrace surface (Figure 29). The state highway has been formed on a bench excavated into the middle part of the slope, and the Main North Line railway lies on the flats at the base of the slope. The geology of the local area is mapped as weak Neogene siltstone of the Waima Formation overlain by Quaternary alluvial gravel and aeolian sand deposits (Rattenbury *et al.*, 2006). Exposures of soil materials show the near-surface geology consists of loose to medium dense aeolian sand. Alluvial gravels were observed outcropping at the crest of a ridge to the west of the site, approximately 120 m above road level.

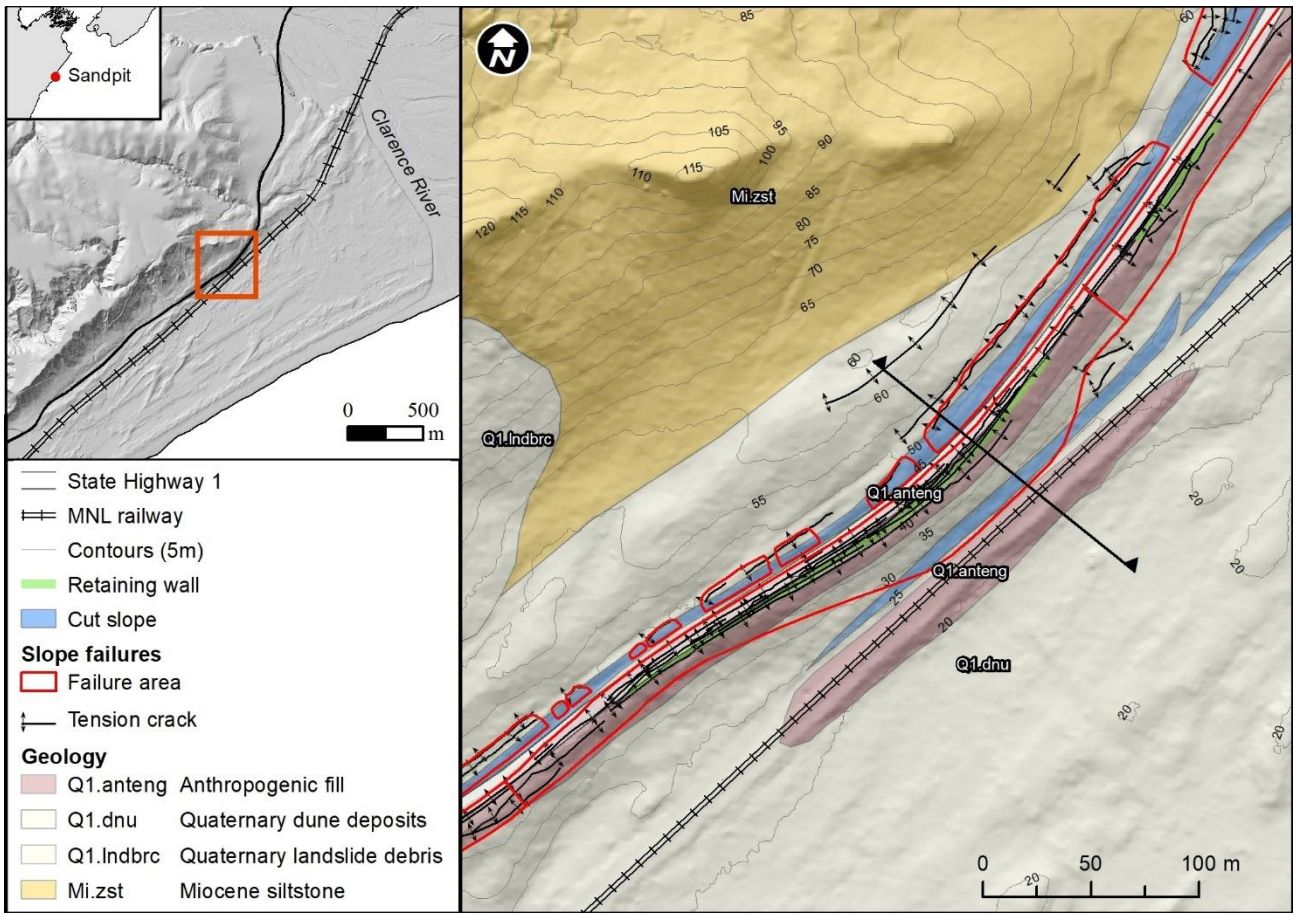

Figure 29: The Sandpit site plan

5.3.2 Geotechnical slope assets

The bench for the state highway has been formed by cutting into the uphill slope on the western (northbound) side of the road and forming a sidling embankment on the eastern (downhill) side beneath the southbound carriageway. The road has also been realigned several times since its construction. In particular, a significant realignment of the bends at the northern end of the site in the 1990s required retreat of the road into the uphill/western slope, with consequential expansion of the cut slopes on that side of the road and construction of a new fill embankment across the stream gully to the north (Figure 30). Exposures in the slip scarps beneath the road surface show that dune sand cut from the uphill side was used as fill material in the embankments. Road maintenance records from before the earthquake show there was an underslip at the site, although no records of the lateral and vertical extent of the underslip are available (NCTIR, 2018c). Review of available aerial and Google Streetview imagery show the gabion walls were constructed in 2008-2009.

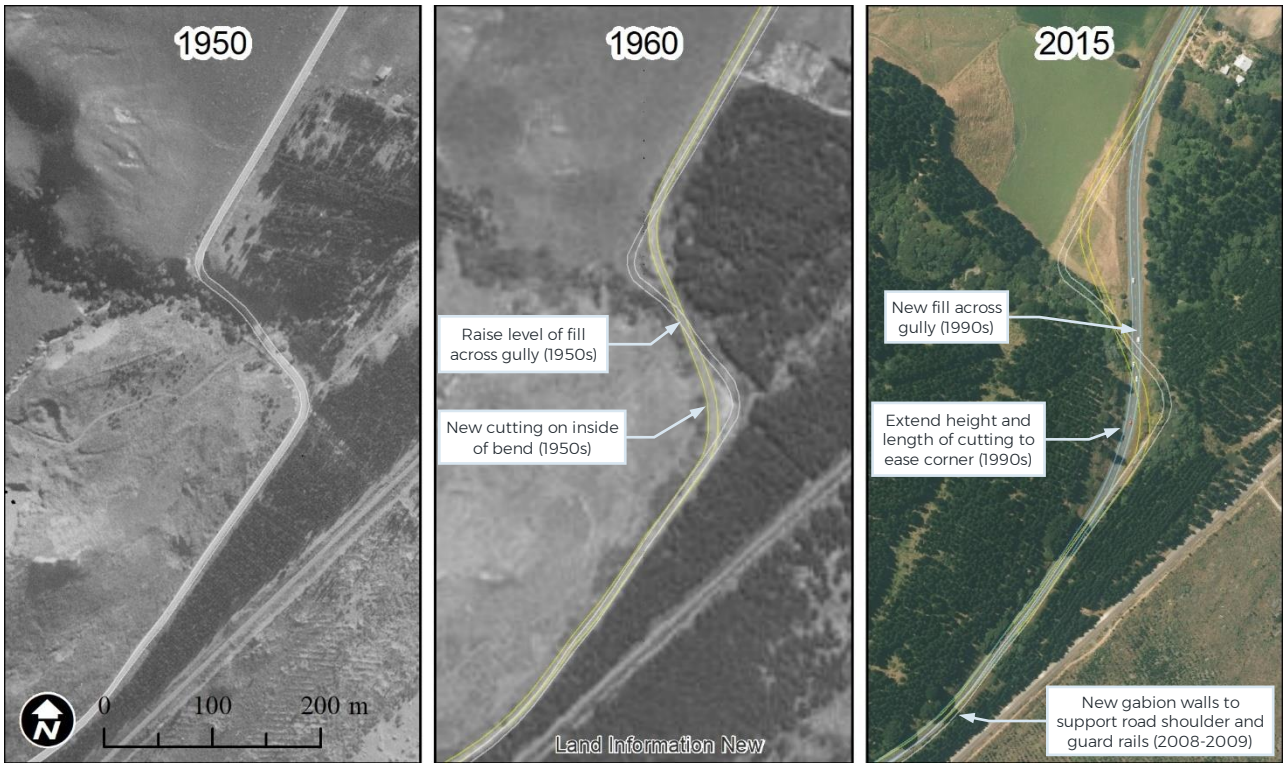

Figure 30: Realignments of SH1 at the Sandpit

5.3.3 Site investigations

During the earthquake recovery an extensive programme of site investigations was carried out in the road and rail corridors. The investigations were carried out in stages, in March-April 2017, November 2017, January 2018, July 2018 and March 2019. The investigations consisted of 13 boreholes, 11 static cone penetration tests, 11 test pits, 3 window sampler boreholes, 16 scala penetration tests, and 3 MASW survey lines (NCTIR, 2019). The boreholes were drilled to depths between 20.14 m and 25.9 m, to assess the ground conditions for design of the replacement retaining walls and road embankment, as well as to assess the stability of the whole slope for assessing the risk of future landslides to the road and rail corridor.

5.3.4 Ground conditions

The site investigations on the state highway bench and the hillslope above the road encountered a thick sequence of aeolian sand deposits, very loose to loose at the ground surface and increasing in relative density to medium dense or dense at 10 m depth below ground level. Very dense alluvial gravels were encountered below the sands at approximately 20 m below ground level.

The investigations at the base of the slope encountered a thinner dune sand sequence, which was interbedded with intermittent layers of loose silt and silty sand. The dense gravels underlying the sand deposits were encountered at approximately 5 m to 10 m below ground level.

A representative engineering geological profile of the hillslope at the Sandpit site is shown in Figure 32.

5.3.5 Kaikōura earthquake-induced landslide

Ground shaking

The closest strong motion station is at Kekerengu, 25 km to the north. The peak horizontal ground acceleration recorded at that site was 1.21 g (GeoNet, 2016). The estimated horizontal PGA at the Sandpit site in the 2016 earthquake was between 0.57 g (Bradley *et al.*, 2017) and 0.78 g (ShakeMapNZ).

Coseismic displacements

The strong ground shaking triggered a series of fill embankment and cut slope failures along the 700 m long section of SH1 through the site. Assessment of coseismic slope displacements was carried out by DIC and GIS-based measurement using pre- and post-earthquake aerial photos (shown in Figure 31). Representative displacements are shown on the cross section profile (Figure 32A), and displacements measured along a swath approximately 20 m either side of the cross section line are shown in Figure 32B. These show the magnitude of displacements are consistent from the upper slope to the lower slope (generally between 3.3 m and 6.6 m, with a mean displacement of 4.8 m). The maximum displacements (between 7 m and 7.8 m) occurred along the margins of the road corridor, with outward displacement of the toe of the cut slope above the road and downslope displacement of the gabion wall and fill embankment below the road.

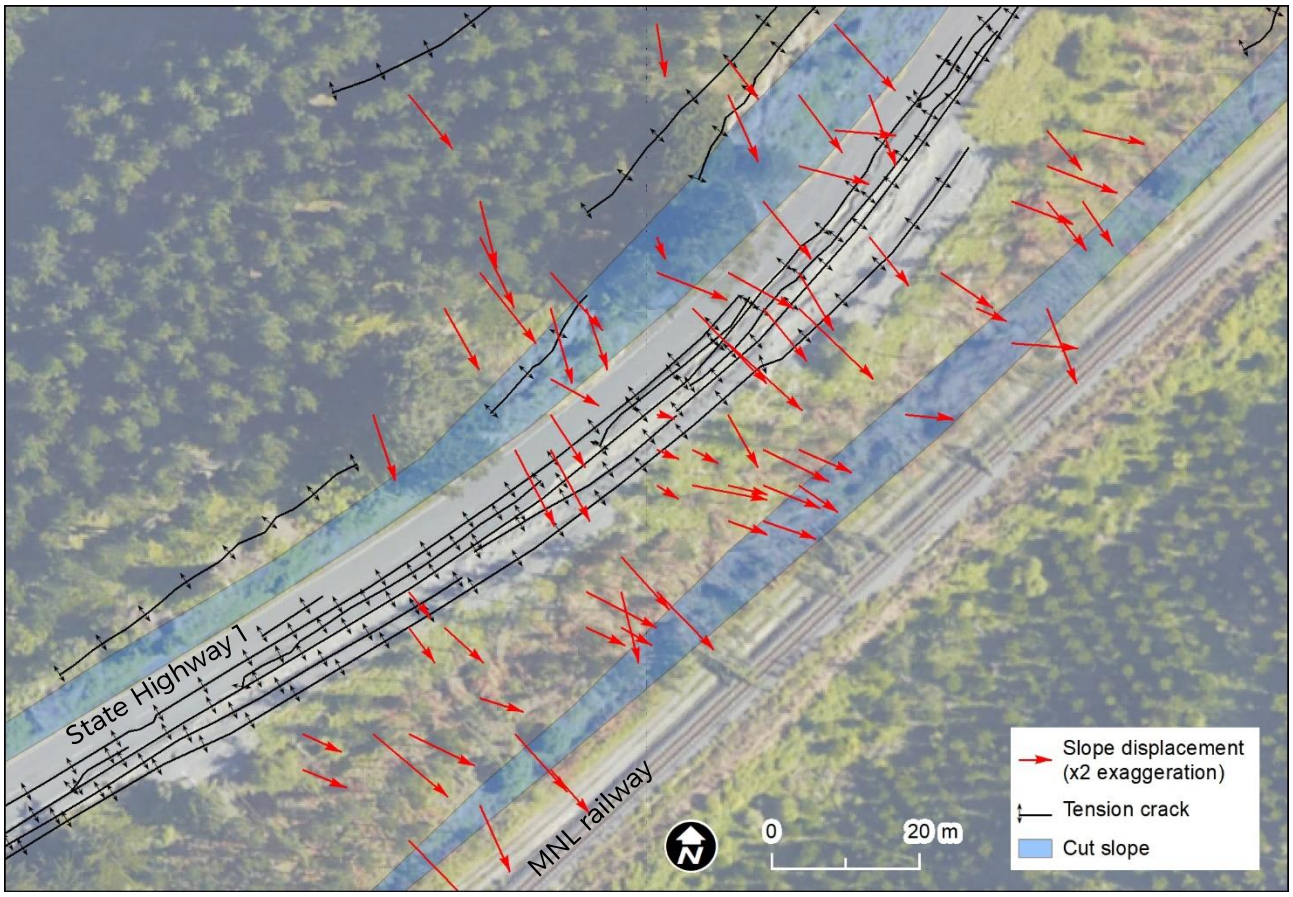

Figure 31: Slope displacements at The Sandpit from DIC analysis, field mapping and GIS-based feature tracking

Failure mechanisms

The principal failure mechanisms were translational sliding of the fill embankment and natural slope below the road and translational sliding of the over-steepened cut slope above the road (Figure 32). Typical failures are shown in Figure 33.

The failure of the slope below the road consisted of translational or semi-rotational displacement along a slip surface extending from the approximate centre of the road to the toe of the slope (daylighting at or near the level of the railway) and inferred to lie at c. 5 m depth in the centre of the slope. Displacement at the top of the head scarp was around 1.5 m to 2 m at an angle of 55° below horizontal. The gabion walls and the crest of the fill slope displaced about 7 m downslope at angles of 30° to 45°, and the lower parts of the slope displaced between 3.5 m and 5.5 m at ~15°.

The failure of the cut slope above the road was a translational sliding failure, with a 3.5 m deep failure surface dipping at 30°. The landslide mass consists of two parts: the frontal part, consisting of the slope from road level to ~5 m behind the crest of the cut slope, and the rear part, extending to ~13 m behind the crest of the cut slope. The failure surface behind the cut slope is approximately circular in shape, shallowing from 60° at the head scarp to intersect the main failure surface (30°) at the toe of the cut slope. The rear part of the landslide displaced towards the road between 0.5 m and 1.5 m at an angle of 30° to 40° (steepening closer to the road). Deformation of the rear part of the landslide manifested as tension cracks and tilted trees.

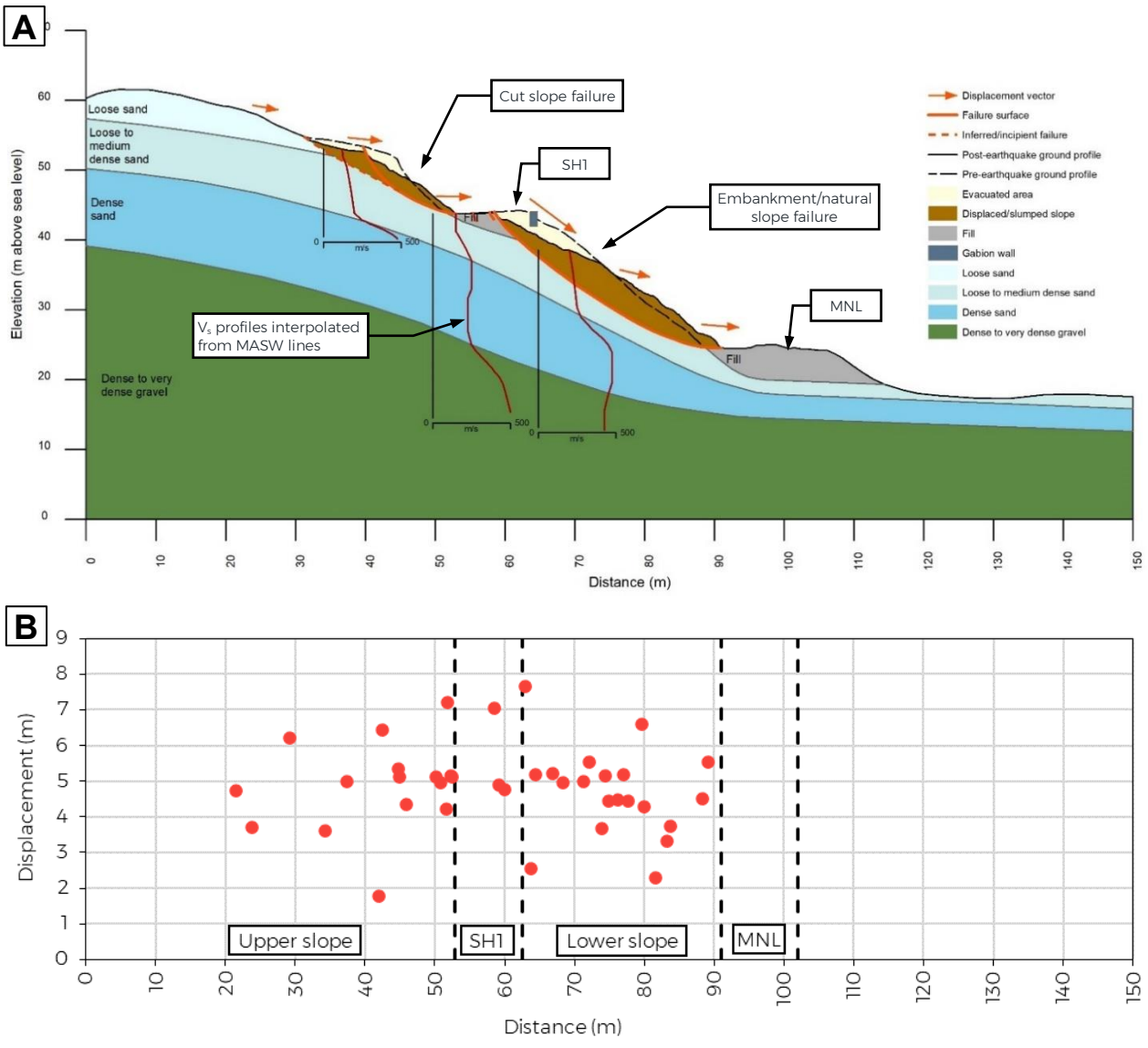

Figure 32: (A) Engineering geological profile of failures (B) slope displacements at Sandpit site

Figure 33: Damage to geotechnical slope assets at the Sandpit
(A) Translational failure of the road embankment and unreinforced gabion retaining wall (RW).
(B) Damage to the gabion wall (photo credit: E. Boam).
(C) Slumping of the cut slope above the road (photo credit: E. Boam).
(D) Displacement of gabion wall causing settlement and cracking to the middle of the road.

Damage and outage impacts

The damage impacts from this slope failure consisted of moderate to severe cracking along the 700 m length of the state highway through the site, with total loss of the southbound (eastern) lane along a length of approximately 150 m where the gabion retaining wall failed (Figure 33A). No available bypass routes were available, and because of the significant coseismic down slope displacements of the underslip (>7 m) and the disturbed ground and very loose debris on both sides of the remaining lane, a temporary second lane could not be formed easily and safely. Consequently, the state highway remained single lane under stop-go traffic control and a temporary speed limit past this site until the recovery works were completed in December 2017.

Recovery

The principal requirement of Waka Kotahi for the repair of this section of SH1 was to restore the full road width to its pre-earthquake level of service by December 2017 (Kendal-Riches, 2018). Permanent long-term solutions to meet Waka Kotahi Bridge Manual requirements were considered but were not pursued because these would take longer to design and construct, and could not be achieved by the road reopening deadline. Consequently the preferred solution consisted of an anchored gabion wall that was designed as a short term temporary structure (with a design life of the order of 2 to 5 years) and a reduced level of seismic loading because of the short design life (Kendal-Riches, 2018). We understand that long term options to realign the road to the west onto the hillslope above the existing road have been investigated and are under consideration by Waka Kotahi NZ Transport Agency.

6 Performance of retaining walls

Retaining wall structures which were tied back with geogrid reinforcement or ground anchors included gabion basket walls and timber pole walls up to 5 m retained height. Deformation of these structures consisted of minor displacement and rotation, causing subsidence of the fill materials behind the wall and consequential settlement-induced cracking of the road surface (Figure 34). The effects of the deformation of the walls on the availability of the road was generally minor; the tension cracks in the pavement were generally able to be traversed by 4WD vehicles and were infilled with aggregate or re-sealed with asphalt early on in the emergency response phase after the earthquake to allow access.

Gravity retaining structures included gabion basket walls and crib walls ranging in height from 1 m to 3 m height. These structures tended to perform poorly, with frequent overturning failures and a number of instances of translation observed of single basket-high walls. This was particularly common along the Hundalee Forest section of SH1. Pavement cracking and loss of shoulder support to the carriageway typically occurred at walls which exhibited this type of failure, with more severe damage to the wall or underslips resulting in loss of one lane (Figure 34).

Figure 34: Examples of damage to retaining walls.

(A) Tied-back timber pole wall with little deformation observed (photo credit: M. Broughton).

(B) Deformation of a recently-engineered soldier pile wall with minor cracking in the road pavement behind the wall (photo credit: M. Broughton).

(C) Translation of an unreinforced crib wall, with loss of access in the near lane and deformation (cracking and settlement) extending to the far lane (photo credit: K. Jadrnicek).

(D) Translation of an unreinforced gabion wall, with complete loss of the shoulder but only minor damage to the live lane (photo credit: M. Broughton).

(E) Overturning of an unreinforced gabion wall, with extensive pavement damage causing closure of one lane (photo credit: M. Broughton).

(F) Deformation (bulging) and displacement of a crib wall supporting a bridge abutment, with settlement and vertical displacement of the road surface (photo credit: C. Parkes).

7 Conclusions

The November 2016 M7.8 Kaikōura earthquake caused widespread damage and severe disruption to the road and rail networks from coseismic landslides and embankment failures. The damage caused by cut and fill slope failures highlights the need to consider the key mechanisms driving slope failure in response to strong ground shaking and the consequences of failure in a resilience-based approach to slope design. The landslides caused by the earthquake have been mapped, and the performance of selected cut and fill slope failures has been assessed. The salient points from this stage of the Kaikōura EILD research are as follows:

- Assessment of rock slope failures identified combinations of kinematic failure mechanisms including structurally-controlled slides and joint-controlled step-path slides in rock where limited displacements led to evacuative failure, due to the brittle nature of the rock mass.
- Many of the failures in rock slopes originated at the top of the slope, or where there were changes in the slope angle, potentially representing the weaker weathered and dilated rock mass as well as likely topographical amplification.
- Understanding the rock mass and defects and earthquake induced failure mechanisms, together with consideration of kinematic failure mechanisms and stepped or en echelon failures are fundamental to assess and design for earthquake performance of cut slopes.
- The significant runout of landslide debris resulting from these brittle failure mechanisms caused significant damage impacts on the transport corridors and long outage times for earthmoving to clear debris and implementation of risk mitigation measures.
- Areas of rock slope stabilisation performed well to retain small scale kinematic failures (wedges or topples) or disaggregation of dilated and weakened rock on the slope surface. The rock bolts and mesh are less likely to perform where deeper seated or larger scale failure mechanisms develop.
- Extensive displacement and slumping of low height fill embankments occurred along the coastal transport corridor and on the Inland Route 70.
- Progressive thickening of the fills for road realignment without engineering design, a lack of geogrid reinforcement or subsoil drainage measures, lack of undercutting to remove topsoil or other weak surface materials before construction of the embankment and inclusion of potentially unsuitable cohesive soils within the fill materials all were contributing factors to the poor performance of these slopes.
- Decoupled slope stability and displacement assessment, resilience-based design and sound construction practices provide a basis for design to achieve resilience in the performance of fill embankments.
- The ductile displacement of the fill embankments generally meant displacement and cracking, rather than the brittle failure, disaggregation of rock masses and large runouts observed in the rock cut slopes.
- This commonly reduced the available road or lane width, but the overall consequence was relatively minor, as slow access for 4WD vehicles was still available along the roads and the damage was quickly reinstated by temporary repairs of the damaged sections.
- Low height, unreinforced gravity retaining walls had been added to some sections of these embankments, and these also performed poorly. Retaining wall structures which were tied back with geogrid reinforcement or ground anchors performed well with minimal deformation.

8 References

Ambraseys, N., and Menu, J. M. (1988). Earthquake-induced ground displacements. *Earthquake Engineering and Structural Dynamics, 16*, 985-1006.

Ambraseys, N., and Srbulov, M. (1995). Earthquake induced displacements of slopes. *Soil Dynamics and Earthquake Engineering, 14*, 59-71.

Archives New Zealand (2022). Public Works Department – maps and plans (series 22541). Retrieved from https://collections.archives.govt.nz. (Accessed 30/01/2022).

Bickel, V., Manconi, A., and Amann, F. (2018). Quantitative assessment of digital image correlation methods to detect and monitor surface displacements of large slope instabilities. *Remote Sensing, 10*(6). doi:10.3390/rs10060865

Brabhaharan, P., Wiles, L., and Freitag, S. (2006). Natural hazard risk management for road networks. Part III: Performance criteria. *Land Transport New Zealand Research Report 296*. Wellington, NZ: Opus International Consultants, 117 p.

Brabhaharan, P., Mason, D., and Callosa-Tarr, J. (2017). Resilience of state highways. Lessons from the 2016 Kaikōura earthquake for resilience studies. *Opus report no. GER2017-29*. Wellington, NZ: Opus International Consultants, 53 p.

Bradley, B. A., Razafindrakoto, H. N. T., and Polak, V. (2017). Ground-motion observations from the 14 November 2016 Mw 7.8 Kaikoura, New Zealand, earthquake and insights from broadband simulations. *Seismological Research Letters, 88*(3), 740-756. doi:10.1785/0220160225

Bray, J., and Travasarou, T. (2007). Simplified procedure for estimating earthquake-induced deviatoric slope displacements. *Journal of Geotechnical and Geoenvironmental Engineering, 133*(4), 381-392.

Brideau, M.-A., Massey, C., Carey, J., Kellett, R., Abbott, E., Monteith, F., and Kupec, J. (2021). Geomechanical characterisation and dynamic numerical modelling of two anthropogenic fill slopes. *Engineering Geology, 281*. doi:10.1016/j.enggeo.2020.105980

Chandra, S. (1968). Geomorphology of the Kaikoura area. Unpublished M.Sc. thesis, University of Canterbury, 208 p.

Cook, D., and Spriggs, D. (1998). SH1 Hawkswood realignment geotechnical assessment. *Project No. 69762/01*. Christchurch, NZ: Montgomery Watson NZ Ltd, 22 p.

Dewez, T. J. B., Girardeau-Montaut, D., Allanic, C., and Rohmer, J. (2016). Facets : A Cloudcompare plugin to extract geological planes from unstructured 3D point clouds. *ISPRS - International Archives of the Photogrammetry, Remote Sensing and Spatial Information Sciences, XLI-B5*, 799-804. doi:10.5194/isprsarchives-XLI-B5-799-2016

GeoNet (2016). M 7.8 Kaikōura earthquake. Retrieved from www.geonet.org.nz/earthquake/technical/2016p858000. (Accessed 31/01/2022).

GeoSlope. (2021a). Slope/W – GeoStudio 2021 R2.

GeoSlope. (2021b). Quake/W – GeoStudio 2021 R2.

Geotechnics (2017a). Site report – SH1 Hundalee, Canterbury – Piezocone penetration testing (CPTu). *NCTIR Report 200126-AA-GT-RP-0001*. Christchurch, NZ: North Canterbury Transport Infrastructure Recovery Alliance, 20 p.

Geotechnics (2017b). Hundalee boreholes, Kaikōura – Site report. *NCTIR Report 200126-AA-GT-RP-0002*. Christchurch, NZ: North Canterbury Transport Infrastructure Recovery Alliance, 40 p.

Geotechnics (2017c). Site report – SR1-SR4 borehole geotechnical investigations. *NCTIR Report 200015-AA-GT-RP-0002*. Christchurch, NZ: North Canterbury Transport Infrastructure Recovery Alliance, 37 p.

Geotechnics (2018a). Okiwi Bay realignment geotechnical investigation, Kaikōura – Site report. *NCTIR Report 400006-AA-GT-RP-0001*. Christchurch, NZ: North Canterbury Transport Infrastructure Recovery Alliance, 17 p.

Geotechnics (2018b). Shared path: Geotechnical borehole investigation, Kaikōura – Site report. *NCTIR Report 300305-AA-GT-RP-0002*. Christchurch, NZ: North Canterbury Transport Infrastructure Recovery Alliance, 17 p.

Glastonbury, J., and Fell, R. (2000). Report on the analysis of "rapid" natural rock slope failures. *School of Civil and Environmental Engineering Report No. R-390*. Sydney, Australia: University of New South Wales, 301 p.

Glastonbury, J., and Fell, R. (2010). Geotechnical characteristics of large rapid rock slides. *Canadian Geotechnical Journal, 47*(1), 116-132. doi:10.1139/t09-080

Hall, J. (1881). Public Works Statement, by the acting Minister for Public Works, the Hon. John Hall, Tuesday 9th August, 1881. *Appendix to the Journals of the House of Representatives, 1881 Session I, D-01*. 142 p.

Horspool, N., Chadwick, M., Ristau, J., Salichon, J., and Gerstenberger, M. (2015). ShakeMapNZ: Informing post-event decision making. Paper presented at the New Zealand Society for Earthquake Engineering Annual Conference, Rotorua, NZ. 369-376 p.

Hungr, O., Leroueil, S., and Picarelli, L. (2014). The Varnes classification of landslide types, an update. *Landslides, 11*(2), 167-194. doi:10.1007/s10346-013-0436-y

Ishibashi, I., and Zhang, X. (1993). Unified dynamic shear moduli and damping ratios of sand and clay. *Soils and Foundations, 33*(1), 182-191. doi:10.3208/sandf1972.33.182

Jaboyedoff, M., Metzger, R., Oppikofer, T., Couture, R., Derron, M., Locat, J., and Turmel, D. (2007). New insight techniques to analyze rock-slope relief using DEM and 3D-imaging cloud points. In E. Eberhardt, D. Stead, & T. Morrison (Eds.), *Rock Mechanics: Meeting Society's Challenges and Demands* (pp. 61-68).

Jibson, R. W. (2007). Regression models for estimating coseismic landslide displacement. *Engineering Geology, 91*(2-4), 209-218. doi:10.1016/j.enggeo.2007.01.013

Justice, R., Saul, G., and Mason, D. (2018). Kaikōura earthquake slope hazards - risk mitigation and network resilience. *NZ Geomechanics News, 96,* 26-37.

Kaiser, A., Balfour, N., Fry, B., Holden, C., Litchfield, N., Gerstenberger, M., . . . Gledhill, K. (2017). The 2016 Kaikōura, New Zealand, Earthquake: Preliminary Seismological Report. *Seismological Research Letters, 88*(3), 727-739. doi:10.1785/0220170018

Keefer, D. (1984). Landslides caused by earthquakes. *Geological Society of America Bulletin, 95*, 406-421.

Kendal-Riches, L. (2018). The design of ground anchors and soil nails in the repair of State Highway 1. *NZ Geomechanics News, 96,* 70-81.

Khazai, B., and Sitar, N. (2004). Evaluation of factors controlling earthquake-induced landslides caused by Chi-Chi earthquake and comparison with the Northridge and Loma Prieta events. *Engineering Geology, 71*(1-2), 79-95. doi:10.1016/s0013-7952(03)00127-3

Koorey, G. (2009). Incorporating safety into rural highway design. Unpublished Ph.D. thesis, University of Canterbury, Christchurch, NZ. 275 p.

Makdisi, F., and Seed, H. B. (1978). Simplified procedure for estimating dam and embankment earthquake-induced deformations. *Journal of Geotechnical Engineering Division American Society of Civil Engineers, 104*(GT7), 849-867.

Mason, D., and Little, T. A. (2006). Refined slip distribution and moment magnitude of the 1848 Marlborough earthquake, Awatere Fault, New Zealand. *New Zealand Journal of Geology and Geophysics, 49*, 375-382.

Mason, D., and Brabhaharan, P. (2023a). Kaikōura Earthquake-Induced Landscape Dynamics Research – Theme 6 – Stage 1 – Landslide inventory report. *WSP report no. GER 2023/12*. Wellington, NZ: WSP, 18 p.

Mason, D., and Brabhaharan, P. (2023b). Kaikōura Earthquake-Induced Landscape Dynamics Research – Theme 6 – Stage 2 – Site investigation report. *WSP report no. GER 2023/13*. Wellington, NZ: WSP, 202 p.

Mason, D., and Brabhaharan, P. (2023c). Kaikōura Earthquake-Induced Landscape Dynamics Research – Theme 6 – Stage 4 – Recommendations for earthquake resilient design of earthworks slopes (In preparation). *WSP report no. GER 2023/15*. Wellington, NZ: WSPp.

Massey, C., Abbott, E., McSaveney, M., Petley, D., and Richards, L. (2016). Earthquake-induced displacement is insignificant in the reactivated Utiku landslide, New Zealand. Paper presented at the Landslides and Engineered Slopes. Experience, Theory and Practice: Proceedings of the 12th International Symposium on Landslides, Rome, Italy. 31-52 p.

Massey, C., Della Pasqua, F., Holden, C., Kaiser, A., Richards, L., Wartman, J., . . . Janku, L. (2017). Rock slope response to strong earthquake shaking. *Landslides, 14*(1), 249-268. doi:10.1007/s10346-016-0684-8

Massey, C., Townsend, D., Rathje, E., Allstadt, K. E., Lukovic, B., Kaneko, Y., . . . Villeneuve, M. (2018). Landslides triggered by the 14 November 2016 Mw 7.8 Kaikōura Earthquake, New Zealand. *Bulletin of the Seismological Society of America, 108*(3B), 1630-1648. doi:10.1785/0120170305

Massey, C., Townsend, D., Lukovic, B., Morgenstern, R., Jones, K., Rosser, B., and de Vilder, S. (2020). Landslides triggered by the Mw7.8 14 November 2016 Kaikōura earthquake: an update. *Landslides, 17*(10), 2401-2408. doi:10.1007/s10346-020-01439-x

McIntyre, R. (2007). *Historic heritage of high-country pastoralism: South Island up to 1948*. Wellington, NZ: Department of Conservation, 174 p.

Merrifield, A. (1973). Of stone, steel and skill. In G. Troup (Ed.), *Steel Roads of New Zealand – An Illustrated Survey* (pp. 109-125). Wellington, NZ: A.H. and A.W. Reed Limited.

NCTIR (2018a). Detailed design report – Kahutara South sites 1 to 4. Slip SR1-2. *NCTIR Report 200015-DD-GT-RP-0001*. Christchurch, NZ: North Canterbury Transport Infrastructure Recovery Alliance, 180 p.

NCTIR (2018b). Detailed design report – Hundalees structures. *NCTIR Report 200073-DD-RW-RP-0001*. Christchurch, NZ: North Canterbury Transport Infrastructure Recovery Alliance, 604 p.

NCTIR (2018c). Detailed design report – NZTA – Sandpit slip – Waipapa retaining wall and roading. *NCTIR Report 200074-DD-GE-RP-0001*. Christchurch, NZ: North Canterbury Transport Infrastructure Recovery Alliance, 494 p.

NCTIR (2018d). Detailed design report – Kaikōura North slip NRP8 and NS24. *NCTIR Report 200009-DD-GT-RP-0001*. Christchurch, NZ: North Canterbury Transport Infrastructure Recovery Alliance, 150 p.

NCTIR (2018e). Detailed design report – Okiwi Bay – slope resilience improvement. *NCTIR Report 200248-DD-GT-RP-0001*. Christchurch, NZ: North Canterbury Transport Infrastructure Recovery Alliance, 231 p.

NCTIR (2018f). Engineering geological assessment – Kahutara South landslide complex. *NCTIR Report 200298-GE-GT-RP-0028*. Christchurch, NZ: North Canterbury Transport Infrastructure Recovery Alliance, 90 p.

NCTIR (2019). Geotechnical investigation factual report – Sandpit road realignment. *NCTIR Report 200270-AA-GT-RP-0003*. Christchurch, NZ: North Canterbury Transport Infrastructure Recovery Alliance, 366 p.

Newmark, N. (1965). Effects of earthquakes on dams and embankments. *Geotechnique, 15*, 139-160. doi:https://doi.org/10.1680/geot.1965.15.2.139

NZGS (2005). Field Description of Soil and Rock; Guideline for the Field Classification and Description of Soil and Rock for Engineering Purposes. New Zealand Geotechnical Society Inc, 38 p.

NZTA (2022). Bridge manual (third edition, amendment 4). *Manual no. SP/M/022*. Wellington, NZ: Waka Kotahi NZ Transport Agency, 374 p.

Parkes, C. (2010). Okarahia Downs shape correction RP185/2.5-3.42: Geotechnical appraisal. *Opus report ref. CG10/143*. Christchurch, NZ: Opus International Consultants Ltd, 11 p.

Rattenbury, M., Townsend, D., and Johnston, M. (2006). Geology of the Kaikoura area. *Institute of Geological and Nuclear Sciences 1:250 000 geological map 13*. Lower Hutt, NZ: GNS Science, 1 sheet + 70 p.

Rizzitano, S., Cascone, E., and Biondi, G. (2014). Coupling of topographic and stratigraphic effects on seismic response of slopes through 2D linear and equivalent linear analyses. *Soil Dynamics and Earthquake Engineering, 67*, 66-84. doi:10.1016/j.soildyn.2014.09.003

Rocscience. (2021). SWedge v.7.

Rocscience. (2022). Slide2.

Rogers, J. D. (1992). Seismic response of highway embankments. *Transportation Research Record, 1343*, 52-62.

Rollins, K., Evans, M., Diehl, N., and Daily, W. (1998). Shear modulus and damping relationships for gravels. *Journal of Geotechnical and Geoenvironmental Engineering, 124*(5), 396-405.

Rollins, K. M., Singh, M., and Roy, J. (2020). Simplified equations for shear-modulus degradation and damping of gravels. *Journal of Geotechnical and Geoenvironmental Engineering, 146*(9). doi:10.1061/(asce)gt.1943-5606.0002300

Schnabel, P., Seed, H. B., and Lysmer, J. (1972). Modification of seismograph records for effects of local soil conditions. *Bulletin of the Seismological Society of America, 62*(6), 1649-1664.

Seed, H. B., and Idriss, I. M. (1970). Soil moduli and damping factors for dynamic response analysis. *Report No. EERC 70-10*. Berkeley, CA: University of California Berkeley, 48 p.

Seed, H. B., Wang, R., Idriss, I. M., and Tokimatsu, K. (1986). Moduli and damping factors for dynamic analyses of cohesionless soils. *Journal of Geotechnical Engineering, 112*(11), 1016-1032.

SouthernGeophysical (2018). MASW investigation: Site 8, Kaikōura. Christchurch, NZ: Southern Geophysical Ltd, 8 p.

Stewart, J., Bray, J., McMahon, D., Smith, P., and Kropp, A. (2001). Seismic performance of hillside fills. *Journal of Geotechnical and Geoenvironmental Engineering, 127*(11), 905-919.

Stewart, J., Smith, P., Whang, D., and Bray, J. (2004). Seismic compression of two compacted earth fills shaken by the 1994 Northridge earthquake. *Journal of Geotechnical and Geoenvironmental Engineering, 130*(5), 461-476.

Stewart, S. (2007). Rock mass strength and deformability of unweathered closely jointed New Zealand greywacke. Unpublished Ph.D. thesis, University of Canterbury, Christchurch, NZ. 472 p.

Stirling, M. W., Litchfield, N., Villamor, P., Van Dissen, R., Nicol, A., Pettinga, J. R., . . . Zinke, R. (2017). The Mw 7.8 2016 Kaikōura earthquake: Surface fault rupture and seismic hazard context. *Bulletin of the New Zealand Society for Earthquake Engineering, 50*(2), 73-84.

Thiele, S. T., Grose, L., Samsu, A., Micklethwaite, S., Vollgger, S. A., and Cruden, A. R. (2017). Rapid, semi-automatic fracture and contact mapping for point clouds, images and geophysical data. *Solid Earth, 8*(6), 1241-1253. doi:10.5194/se-8-1241-2017

Topp, E. (1947). The contribution of railways to the settlement and development of the South Island of New Zealand. Unpublished M.A. (Hons) thesis, University of New Zealand, Christchurch, NZ. 90 p.

Townsend, D. (2001). Neogene evolution of the Pacific - Australia plate boundary zone in NE Marlborough, South Island, New Zealand. Unpublished Ph.D. thesis, Victoria University of Wellington, Wellington, NZ. 255 p.

USGS (2022). M 7.8 - 53 km NNE of Amberley, New Zealand. Retrieved from https://earthquake.usgs.gov/earthquakes/eventpage/us1000778i/shakemap/pga. (Accessed 14/10/2022).

Zhang, J., Qu, H., Liao, Y., and Ma, Y. (2012). Seismic damage of earth structures of road engineering in the 2008 Wenchuan earthquake. *Environmental Earth Sciences, 65*(4), 987-993. doi:10.1007/s12665-011-1519-5

Appendix A: Slope analyses

Introduction

Geotechnical slope stability analysis of selected sites was carried out to understand and learn from the failure mechanisms and consequences of slope failure to infrastructure. The objective of the analyses was to identify the mechanisms of slope failures so these can be related to the observed impacts. This involved:

1 Developing engineering geological models of the slopes using the results of the site investigations and laboratory testing and any other available geotechnical information such as published geological mapping, the New Zealand Geotechnical Database, and unpublished in-house reports and site investigation data (the engineering geological models are described in Sections 4 and 5).

2 Calibration of the engineering geological models by back-analysis of the slope failures using limit equilibrium slope stability analysis.

3 Assessing the earthquake performance of the slopes using commonly used methods of analysis in engineering practice, including kinematic, pseudostatic limit equilibrium, and permanent-displacement analysis, to compare the predicted failure surfaces and slope performance with the actual observed damage.

Methods

Limit equilibrium back analysis

Back analyses of the selected landslides were carried out along representative topographic and engineering geological model profiles (shown in Sections 4 and 5) using the limit equilibrium software Slope/W (GeoSlope, 2021a) and Slide2 (Rocscience, 2022), as well as SWedge (Rocscience, 2021) for the Awatere Gorge and Okiwi Bay landslides.

Material parameters for the limit equilibrium analysis are given in Table 11. These were derived using the results from the site investigations, laboratory testing and relevant published parameters from the literature review.

The slopes were assessed using the pre-earthquake ground profiles from LiDAR-derived digital elevation models and photogrammetry-derived digital surface models. Circular and fully specified non-circular failure surfaces were used in the analyses, to capture the overall failure surfaces observed in the Kaikōura earthquake. The Morgenstern-Price solution was used, with a half-sine function for the side forces on the slices. The pseudostatic factor of safety for the Kaikōura earthquake was calculated using peak ground accelerations (PGA) from the ShakeMapNZ (Horspool *et al.*, 2015), Bradley *et al.* (2017) and USGS ShakeMap (USGS, 2022) models.

Permanent displacement analysis

For the selected sites, numerical analysis was conducted to assess the seismic response of the slopes and the magnitude of earthquake-induced permanent displacements. The objective was to compare the observed failure surfaces and displacements with those predicted using analysis techniques commonly used in engineering practice.

The displacements were assessed using a methodology similar to that of Massey et al. (2016; 2017) and Brideau et al. (2021), which is a simplified method based on the decoupled seismic slope deformation method of Makdisi and Seed (1978). This is a modified version of the Newmark (1965) sliding block method that accounts for the dynamic response of the sliding mass. The analyses were conducted as follows:

1 In situ static stresses were first assessed using the two-dimensional finite element software Quake/W (GeoSlope, 2021b), and the factor of safety was calculated for each potential sliding surface based on the static stresses using Slope/W.

2 A dynamic site-response assessment was carried out using Quake/W to conduct an equivalent linear analysis of the dynamic loading. Acceleration time histories from the Cheviot (CECS), Kaikōura (KIKS), Kekerengu (KEKS) and Ward (WDFS) strong motion recording stations (GeoNet, 2016) were used in the analysis, using accelerations at 0.02s sampling intervals scaled to produce a free-field acceleration consistent with the modelled PGA at each site from the USGS ShakeMap, ShakeMapNZ, and Bradley et al. (2017) models. The average acceleration time history, averaged along the base of the slide surface of a potential sliding mass, is calculated to capture the cumulative effect of the nonuniform acceleration profile (horizontal and vertical) acting on the slide mass.

3 The average acceleration time history was double integrated in Slope/W, using the Newmark (1965) rigid sliding-block method, to estimate the permanent displacement along each slide surface. Circular and fully specified non-circular failure surfaces were used, consistent with the limit equilibrium analyses.

For the model mesh setup, the lateral boundaries were positioned away from the region of interest to ensure that reflected waves were sufficiently damped and did not adversely affect the model results. The model height was varied for each site to ensure that the results were not significantly affected by wave reflection and amplification/de-amplification caused by the model thickness below the slope toe. Mesh elements were varied from 1 m to 2 m (height and width) in the area of interest and up to 5 m (height and width) away from the area of interest at the model boundaries, to avoid artificial filtering of the high-frequency component of the input seismic motion during the propagation process (Rizzitano *et al.*, 2014).

For the static and dynamic assessment, no vertical or horizontal motions relative to the input motions were allowed at the mesh nodes forming the bottom of each model. To prevent model-edge effects from affecting the results, the mesh nodes forming the lateral boundaries were allowed to move only in the vertical direction for the static assessments, and only in the horizontal direction for the dynamic assessments.

Equivalent linear soil behaviour models were used in the analyses, with the ranges of geotechnical material parameters shown in Table 11. Strain-dependent material damping ratio and G/Gmax reduction factors for the fill, sandy soils, gravelly soils and bedrock materials were derived from Ishibashi and Zhang (1993), Rollins *et al.* (1998); (2020), Schnabel *et al.* (1972), Seed and Idriss (1970), and Seed *et al.* (1986).

For comparison, permanent slope displacements were also assessed using the methods described by Ambraseys and Menu (1988), Ambraseys and Srbulov (1995), Jibson (2007) and Bray and Travasarou (2007), as specified in the Bridge Manual (NZTA, 2022).

Permanent displacement analyses were carried out for each of the slopes considered for completeness. However, it should be noted that the permanent displacement analyses assume that the strength of the ground is not degrading with ground shaking. Rock slopes are expected to behave in a brittle manner, with rapid degradation of strength with displacement due to the degradation of the rock mass. Therefore, the results are not expected to represent the true behaviour of the brittle rock slopes.

Table 11: Material properties for the soil and rock masses adopted for the slope stability analyses

Geological unit	Material type		Unit weight (kN/m^3)	Cohesion (kPa)	Friction (°)	Shear modulus (MPa)	Poisson's ratio
Anthropogenic fill	Silty gravel		20	5	32	200	0.4
Late Quaternary aeolian and alluvial deposits	Root zone		17	30	35	25	0.2
	Loose sand		17	0	35	25	0.25
	Medium dense sand		18	0	38	28	0.25
	Dense sand		19	0	42	50	0.33
	Dense gravel		19	0	46	90	0.33
Pleistocene fan gravels	Silty gravels		19	10	40	200	0.4
Greta Formation	Siltstone		21	30	30	2,000	0.35
Pahau Terrane greywacke	Sandstone	Sheared zone	24	25	26	2,000	0..2
		HW-CW	24	140	28	2,000-5,500	0.25
		MW	25	300	29	5,700	0.25
		SW	26	360	32	6,000	0.3
		UW	26	480	37	9,000	0.35
	Siltstone	MW-HW	26	260	25	2,000-4,000	0.3
		UW-SW	26	380	32	4,000-8,000	0.3

Rock defects used in the SWedge analysis were assumed to have cohesion of 0.02-0.1 MPa and friction angles of 30°-40°

Results

The results of the slope analyses are summarised in Table 12. The salient points from the engineering geological models and slope analysis at each site are described in the subsequent sections.

Table 12: Slope analysis results

Site	Failure mode	Static FoS	Kaikōura earthquake PGA[1] (g)	Pseudo-static FoS	Yield acceleration (g)	Newmark displacement (mm)	
						Decoupled[2]	Semi-empirical[3]
Awatere Gorge	Combined wedge and step-path slide	1.36	0.41 ShakeMapNZ	0.82	0.26	**200** (150-700)	10-150
			0.53 Bradley	0.74			
			0.34 USGS	0.89			
	Wedge slide (SWedge)	1.52	0.41 ShakeMapNZ	0.82	0.28	-	-
			0.53 Bradley	0.69			
			0.34 USGS	0.91			
Kahutara Bridge	Block slide	1.51	0.30 ShakeMapNZ	0.90	0.21	**550** (180-1,140)	10-340
			0.57 Bradley	0.73			
			0.48 USGS	0.80			
Okiwi Bay	Block slide	1.45	0.58 ShakeMapNZ 0.57 Bradley 0.60 USGS	0.66-0.68	0.25	**675** (675-1,540)	90-250
	Wedge slide (SWedge)	2.52		0.66-0.69	0.34	-	-
Culvert 55	Translational slide	1.34	0.28 ShakeMapNZ	0.79	0.14	**170** (50-230)	30-390
			0.24 Bradley	0.84			
			0.42 USGS	0.65			
The Sandpit	Translational slide	1.15	0.78 ShakeMapNZ	0.35	0.1	**90** (0-1,580)	520-1,700
			0.57 Bradley	0.46			
			0.70 USGS	0.39			

[1] Modelled peak ground acceleration, from ShakeMapNZ (Horspool *et al.*, 2015), Bradley *et al.* (2017), and USGS ShakeMap (USGS, 2022) models

[2] Newmark displacement modelled using decoupled Quake/W-Slope/W analysis (following the approach described in the previous section). Values in bold are for the approximated actual failure surface; values in parentheses represent the range of displacements estimated for the 50 slip surfaces with the lowest factor of safety.

[3] Displacements assessed using Ambraseys and Menu (1988), Ambraseys and Srbulov (1995), Jibson (2007) and Bray and Travasarou (2007) methods. The 84th percentile displacements are shown.

Awatere Gorge

- Field observations at this site suggest that displacement of the slope during the earthquake resulted in brittle kinematic failure, with strength loss and disintegration of the rock mass. It is not known what amount of strain the rock mass was able to accommodate before disintegrating and transitioning into a debris avalanche. Consequently, displacements estimated with a Newmark rigid sliding block approach for this brittle rock mass cannot be compared reliably to slope performance thresholds based on displacement amounts.

- Seismicity effects such as topographic amplification are likely to have contributed significantly to this landslide. The slope crest PGA simulated by the dynamic slope analysis was approximately 1.4x higher than the free field PGA, and significantly larger displacements were derived from the dynamic analysis relative to the semi-empirical methods. Directivity or wave trapping effects may also have had a significant influence on the landslide, as it occurred at the northern end of an elongated and sharp ridgeline that trends perpendicular to the fault ruptures on the eastern side of the Kaikōura ranges. However, there is insufficient data to enable analysis of these effects, and is beyond the scope of this assessment.

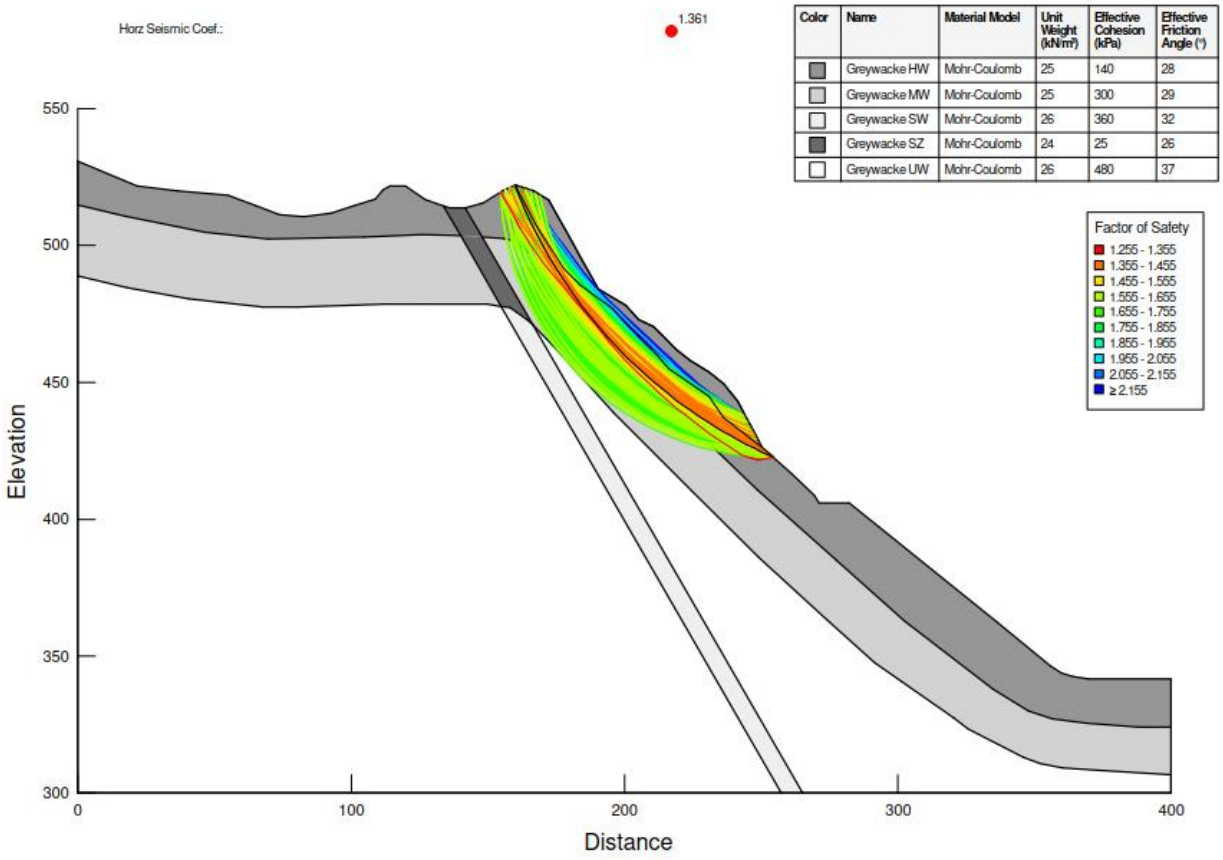

Awatere Gorge, static stability analysis

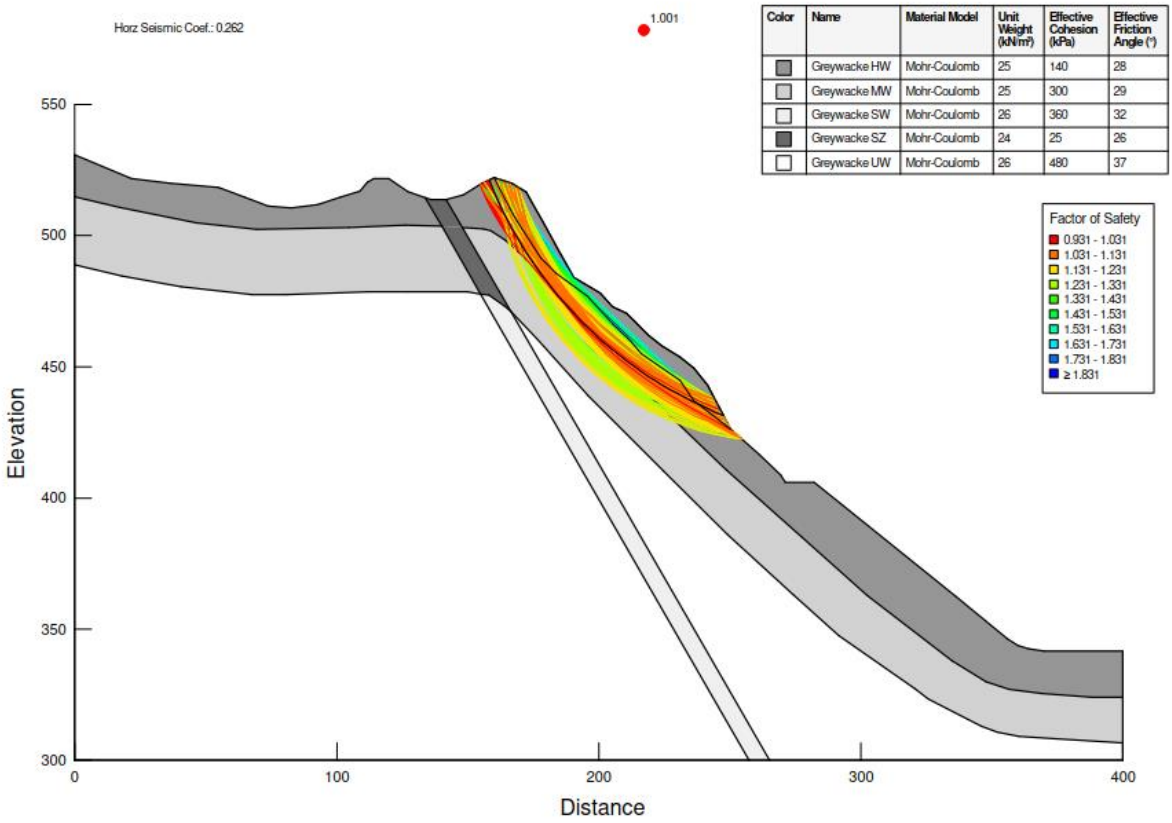

Awatere Gorge, seismic back-analysis (critical acceleration = 0.26g)

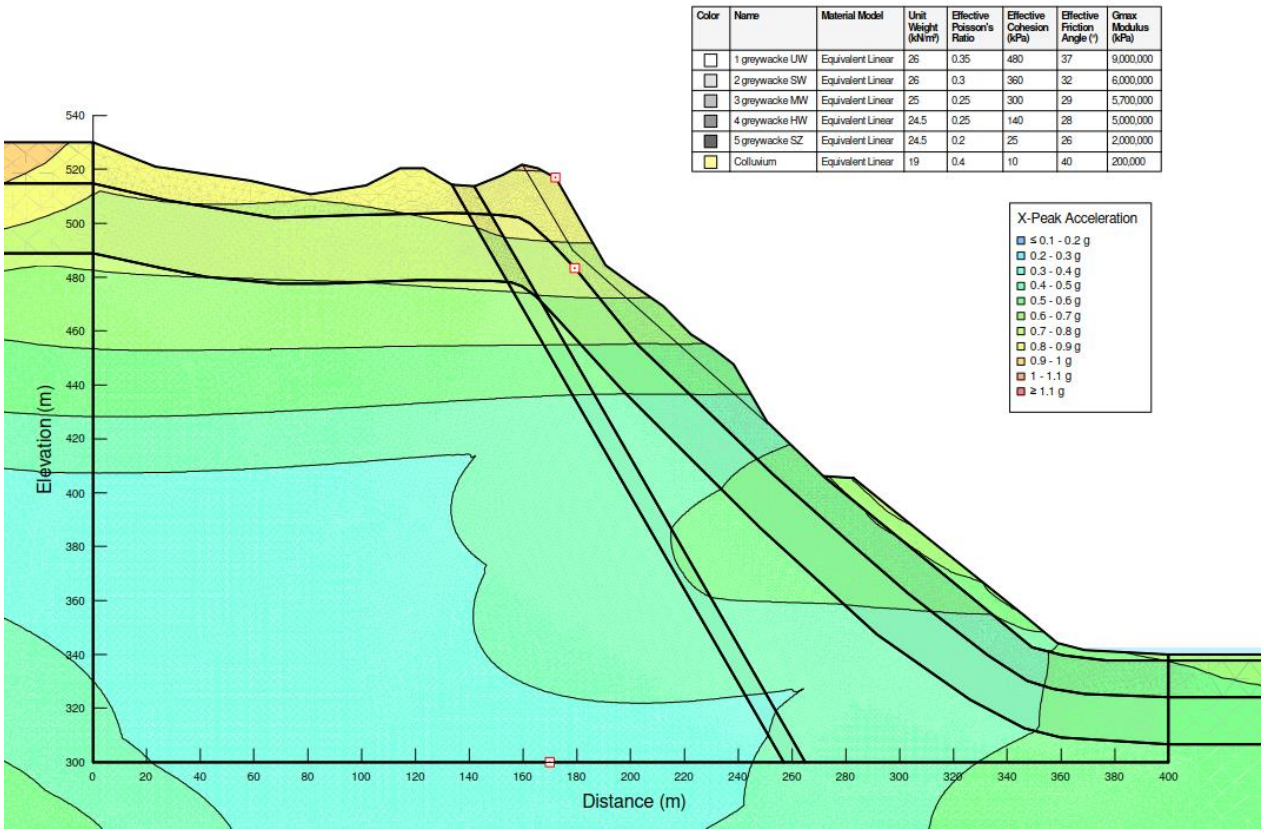

Awatere Gorge dynamic analysis, contours of peak horizontal acceleration

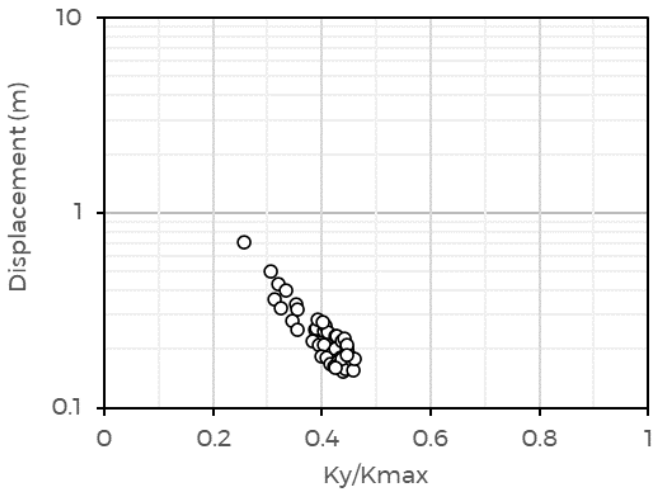

Awatere Gorge simulated Newmark ground displacements, shown as a function of the ratio of the yield acceleration (Ky) to the average acceleration of the landslide mass (Kmax) for the 50 slide surfaces with the lowest factors of safety.

Kahutara Bridge

- The Kahutara landslide was a structurally controlled translational slide that occurred in the lower half of the hillslope, in contrast to the majority of landslides along the coastal slopes in this area, which were disrupted soil and rock avalanches which occurred in the upper parts of the hillslopes. This highlights the importance of structural geology in influencing the location and extent of these deeper-seated landslides, as this failure occurred on bedding planes that are adversely oriented in the lower part of the slope but are inwardly-dipping in the upper part of the hill due to the complex folding and deformation of the greywacke rock mass.
- Larger displacements were modelled using the decoupled analysis than were calculated using semi-empirical methods. Significant variability in the modelled PGA between the Shakemap, Bradley and USGS models results in a wide range of predicted displacements using the semi-empirical methods.
- The actual displacements of the landslide mass are much larger (7.6 m) and indicates the reduction of strength along the sliding surface in brittle rock materials.
- Topographic amplification was significant in the response of the ridge to the earthquake shaking, with the Quake/W model showing amplification of the ridge crest PGA on the order of 1.1 to 1.7x the free field PGA.

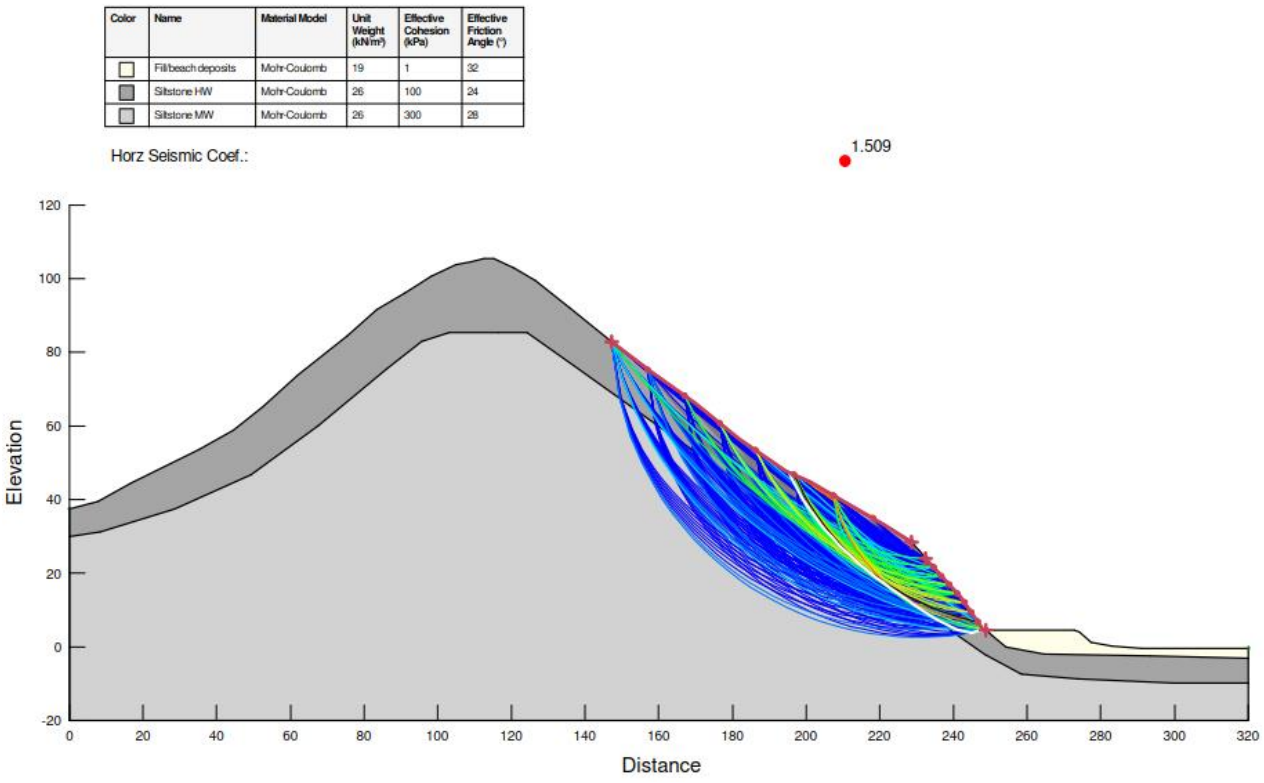

Kahutara Bridge static stability analysis

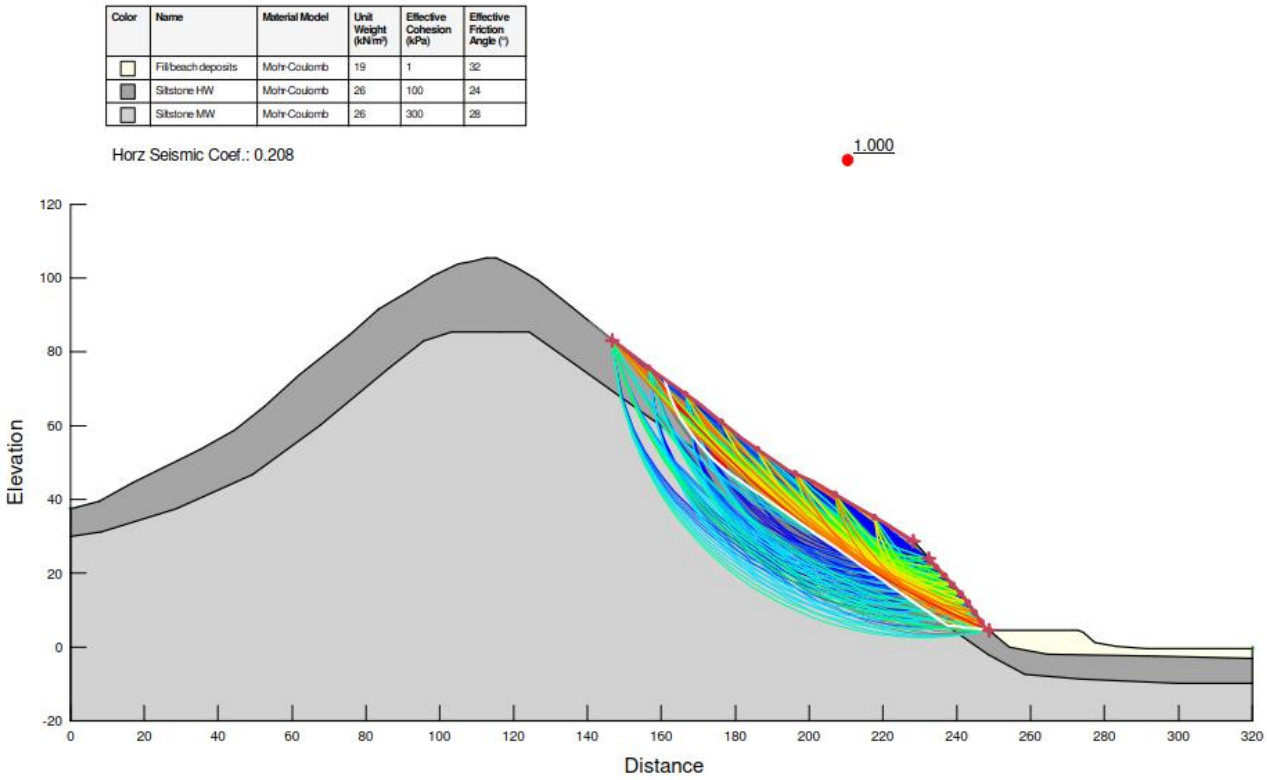

Kahutara Bridge seismic back-analysis (critical acceleration = 0.21 g)

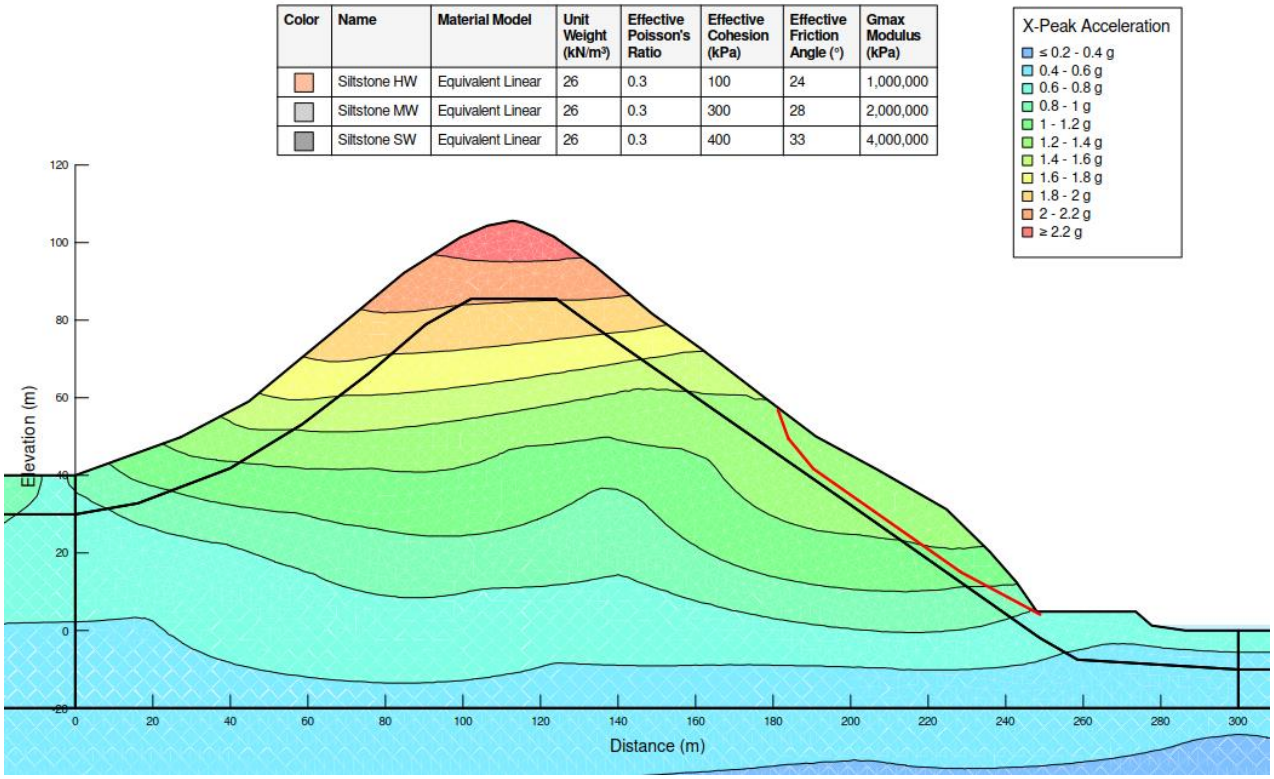

Kahutara Bridge dynamic analysis, contours of peak horizontal acceleration

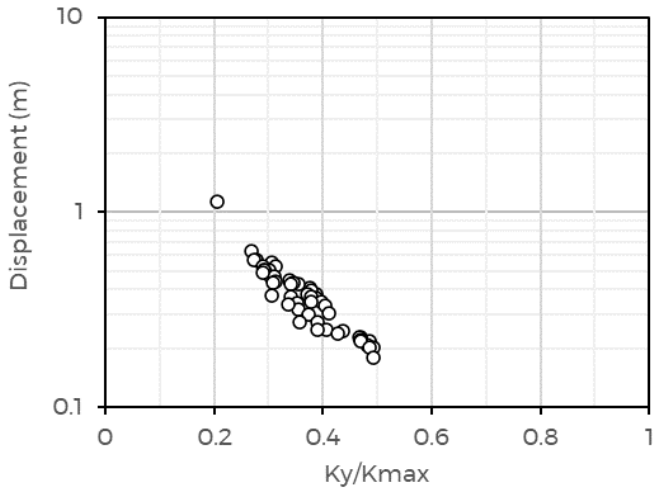

Kahutara Bridge simulated Newmark ground displacements, shown as a function of the ratio of the yield acceleration (Ky) to the average acceleration of the landslide mass (Kmax) for the 50 slide surfaces with the lowest factors of safety.

Okiwi Bay

- The Okiwi Bay landslide was a structurally controlled failure that extended over the full height of the slope. The sliding mass displaced approximately 50 m downslope and out over the shore platform, but remained largely intact.
- These large observed displacements were much larger than those calculated during either the decoupled analyses or the semi-empirical methods. This demonstrates why such displacement analyses cannot be reliably used in the analyses of slopes comprising brittle materials and brittle failure mechanisms.
- The combined effects of the steep, high terrace slope and the impedance contrast between the 30 m thick sequence of fan gravels and underlying greywacke bedrock resulted in large site amplification of ground shaking in the dynamic slope analysis, with the peak ground acceleration at the crest approximately 3.8x the free field acceleration. The contribution of topographic amplification to the overall site amplification has not been assessed here.

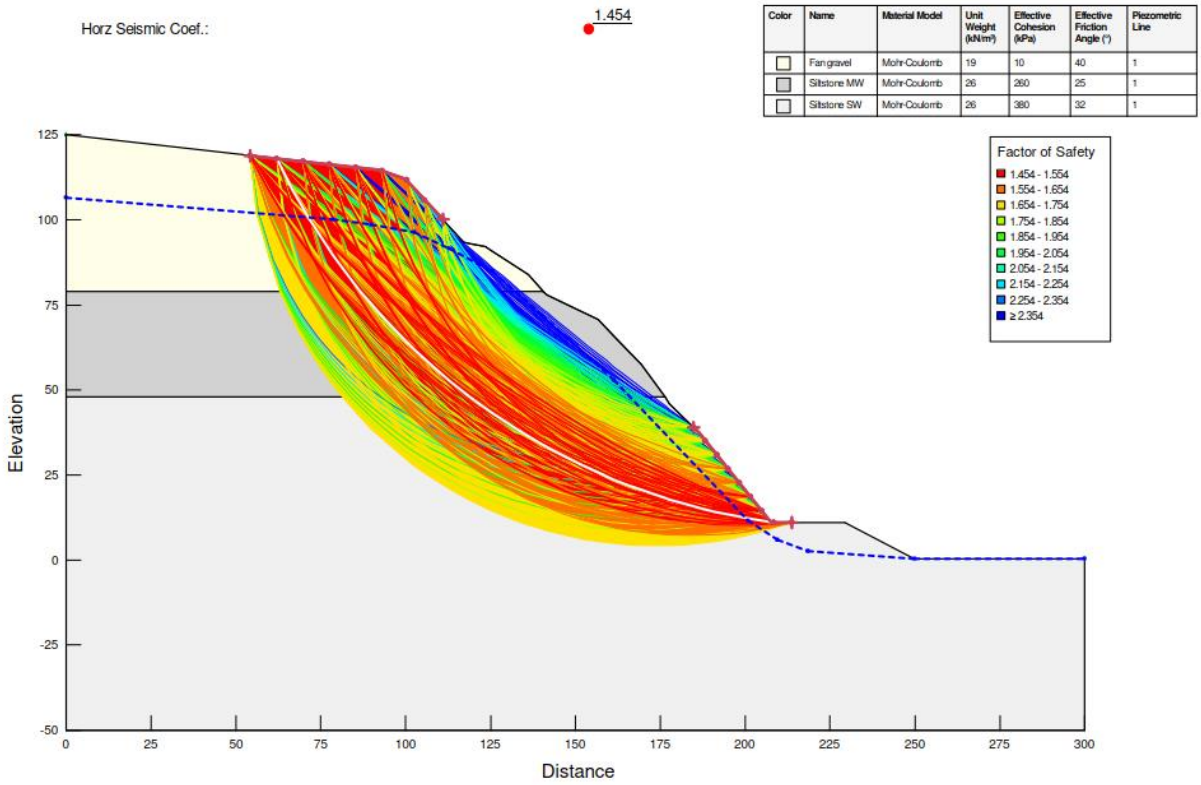

Okiwi Bay static stability analysis

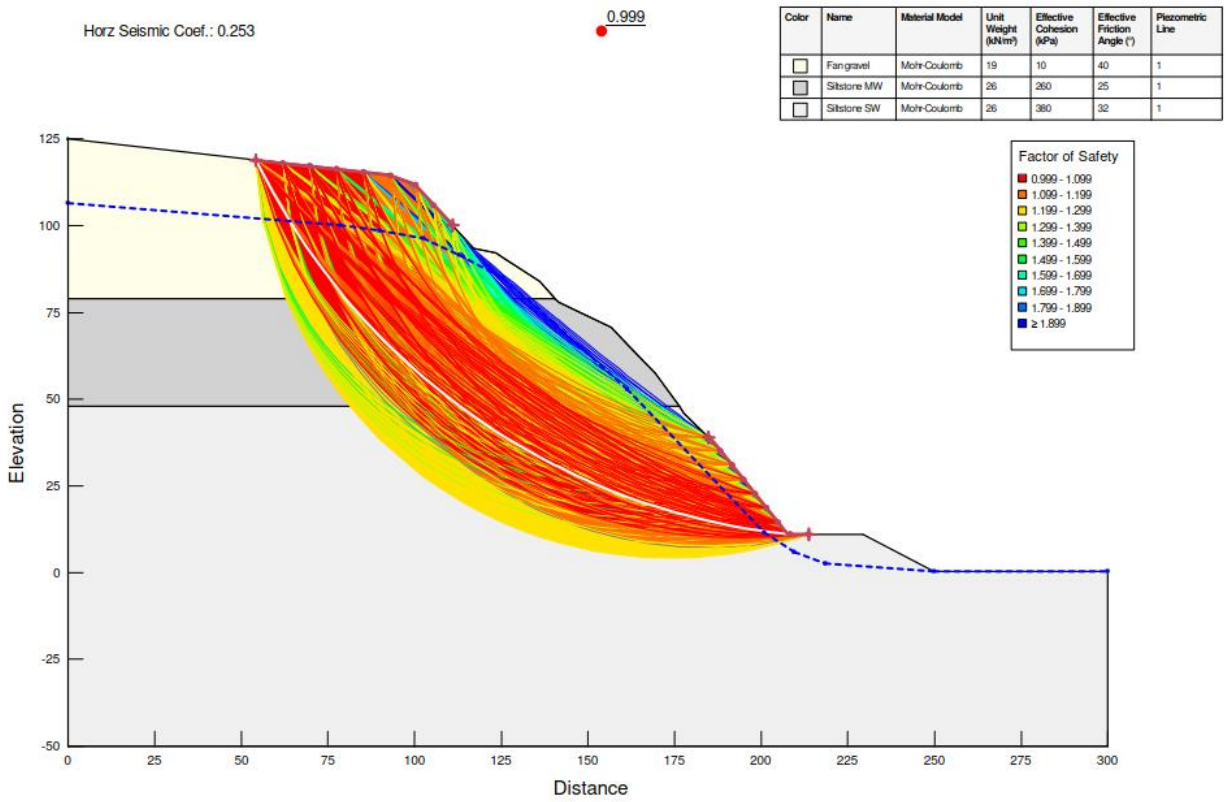

Okiwi Bay seismic back-analysis (critical acceleration = 0.25 g)

Color	Name	Material Model	Unit Weight (kN/m³)	Effective Poisson's Ratio	Effective Cohesion (kPa)	Effective Friction Angle (°)	Gmax Modulus (kPa)
	Fan gravels	Equivalent Linear	19	0.4	10	40	200,000
	Siltstone MW	Equivalent Linear	26	0.3	260	25	2,000,000
	Siltstone SW	Equivalent Linear	26	0.3	380	32	4,000,000

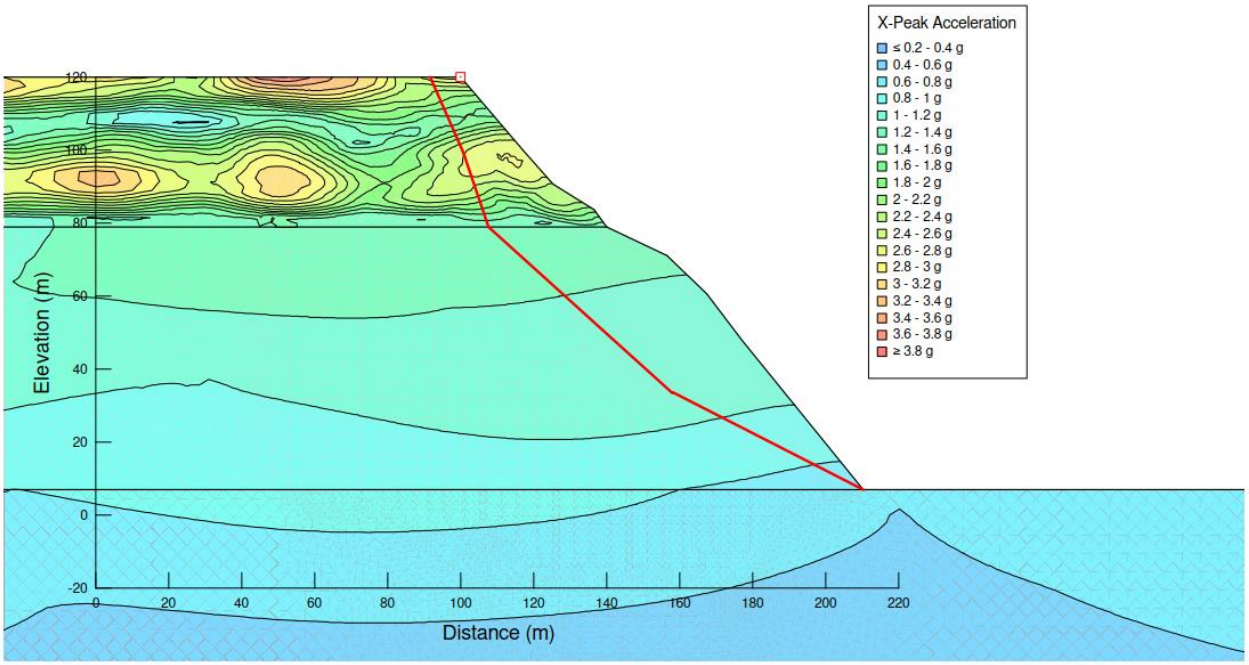

Okiwi Bay dynamic analysis, contours of peak horizontal acceleration

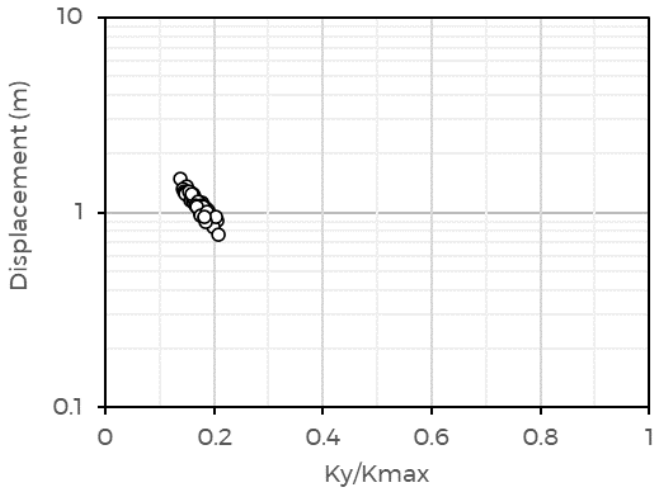

Okiwi Bay simulated Newmark ground displacements, shown as a function of the ratio of the yield acceleration (Ky) to the average acceleration of the landslide mass (Kmax) for the 50 slide surfaces with the lowest factors of safety.

Culvert 55

- The failure surface extended through the full height of the embankment, which is likely to be due to the strong ground shaking over a significant duration. Ground shaking recorded at the Cheviot station consisted of ~100 seconds of significant shaking, with peaks at ~20 seconds and ~85 seconds.
- Groundwater pressures within the fill materials were likely to be elevated as a result of blockage of the culvert pipe and a lack of effective subsoil drainage measures within the embankment fill. The failure surface was reasonably closely approximated by the slip circles with the lowest factors of safety in the limit equilibrium analysis.
- Similar magnitudes of displacement were predicted by the decoupled analysis and semi-empirical methods. The pseudostatic factor of safety and modelled coseismic displacements were outside the limits specified by the Bridge Manual, and the total (i.e. post-yield) displacement of the failed mass was 5.8 metres.
- The observed displacements of several metres is larger than predicted by the decoupled analyses and semi-empirical methods, and is likely to be due to degradation of the soil strength during large displacements along the failure surfaces, and possibly post-earthquake flow failure of the saturated soil mass in the lower part of the slope. If the coseismic displacements were limited to be of smaller magnitude, then reduction in strength along the failure surface and therefore large displacements may not have been observed.
- These observations reinforce that the semi-empirical methods suggested by the Bridge Manual for assessing slope stability and displacement provide a sound basis for design. In order to achieve resilience in the performance of fill embankments, provided resilience-based design approaches to limit displacements to small magnitudes, sound construction practices and proactive maintenance of drainage assets are important.
- Even with a modest 10 m height of embankment, the dynamic analyses suggested an amplification of PGA of the order of 1.4 times the free field acceleration.

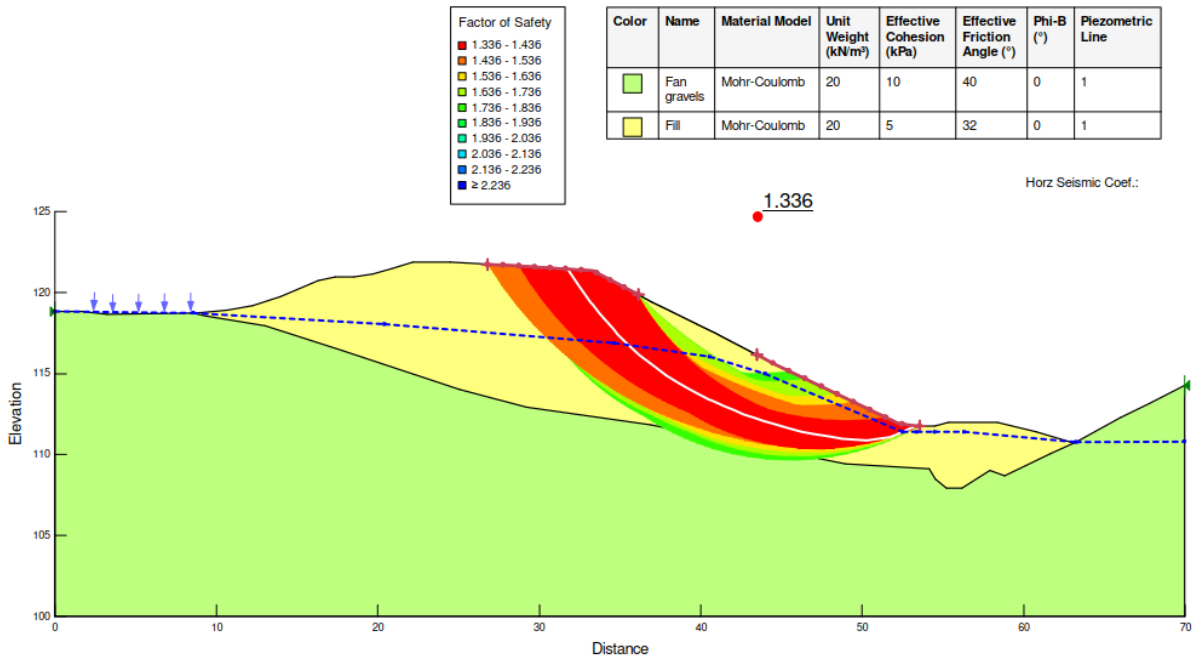

Culvert 55 static stability analysis

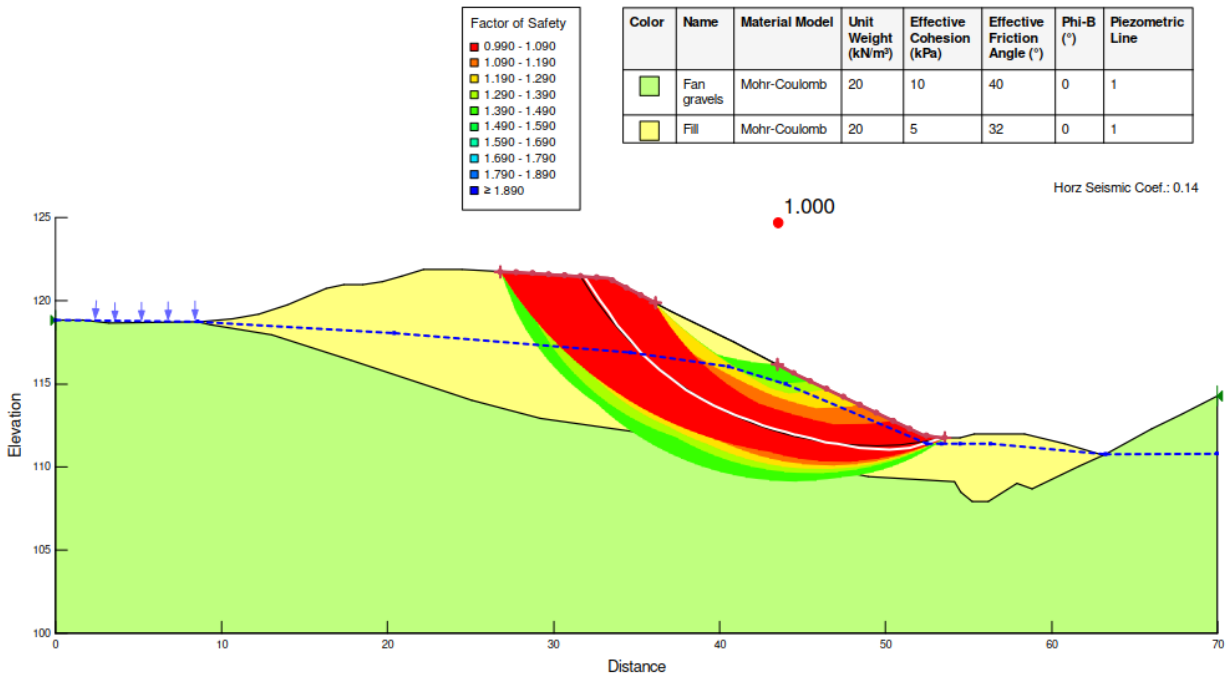

Culvert 55 seismic back-analysis (critical acceleration = 0.14 g)

Color	Name	Material Model	Unit Weight (kN/m³)	Effective Poisson's Ratio	Effective Cohesion (kPa)	Effective Friction Angle (°)	Gmax Modulus (kPa)
	Fan gravels	Equivalent Linear	19	0.4	10	40	300,000
	Fill	Equivalent Linear	20	0.4	5	32	200,000
	Siltstone	Equivalent Linear	21	0.35	30	30	2,000,000

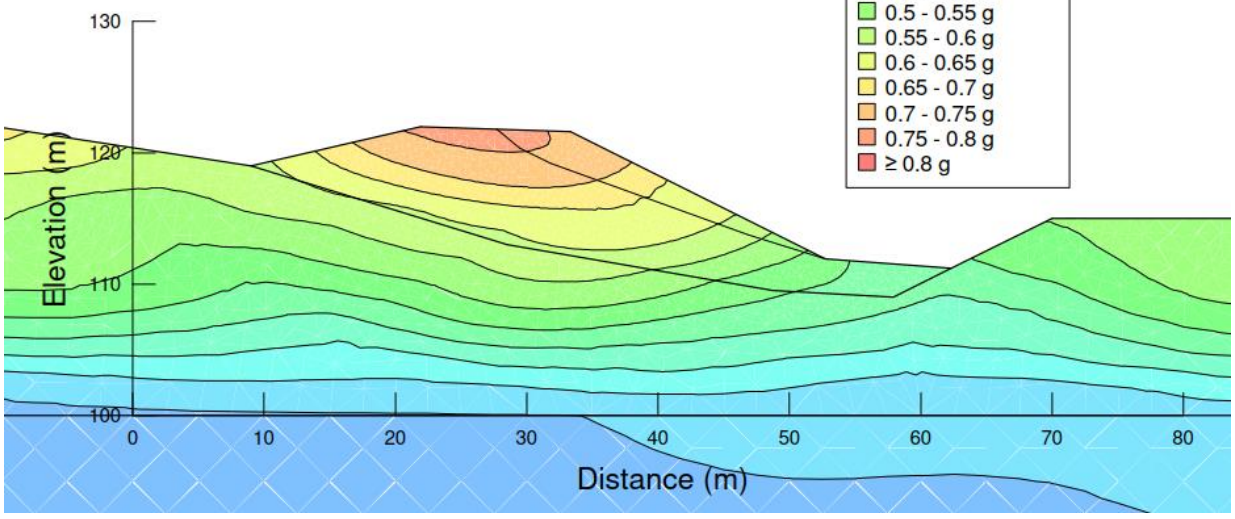

Culvert 55 dynamic analysis, contours of peak horizontal acceleration

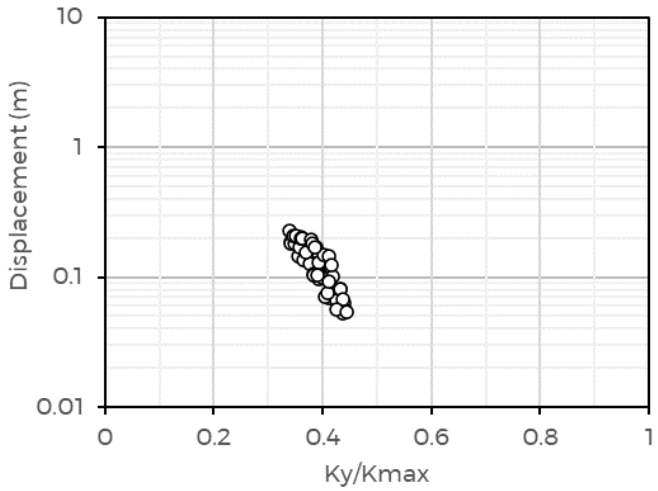

Culvert 55 simulated Newmark ground displacements, shown as a function of the ratio of the yield acceleration (Ky) to the average acceleration of the landslide mass (Kmax) for the 50 slide surfaces with the lowest factors of safety.

The Sandpit

- The failure surface extended through the full height of the slope, which is likely to be due to the strong ground shaking over a significant duration and the loose sand deposits in the near-surface ground. The failure was approximated closely by the slip circles with the lowest factors of safety in the limit equilibrium analysis.
- The sequence of loose to medium dense sands near to the ground surface result in a low static factor of safety and low yield acceleration. Variability in the modelled PGA between the Shakemap, Bradley and USGS models results in a wide range of predicted displacements using the semi-empirical methods suggested in the Bridge Manual. Similar ranges of magnitudes of displacement were predicted by the decoupled analysis. The pseudostatic factor of safety and modelled coseismic displacements were outside the limits specified by the Bridge Manual, and the total (i.e. post-yield) displacement of the failed mass was 7.8 metres.
- The PGA simulated by the dynamic slope analysis at the road level was approximately 1.1x higher than the free field PGA.

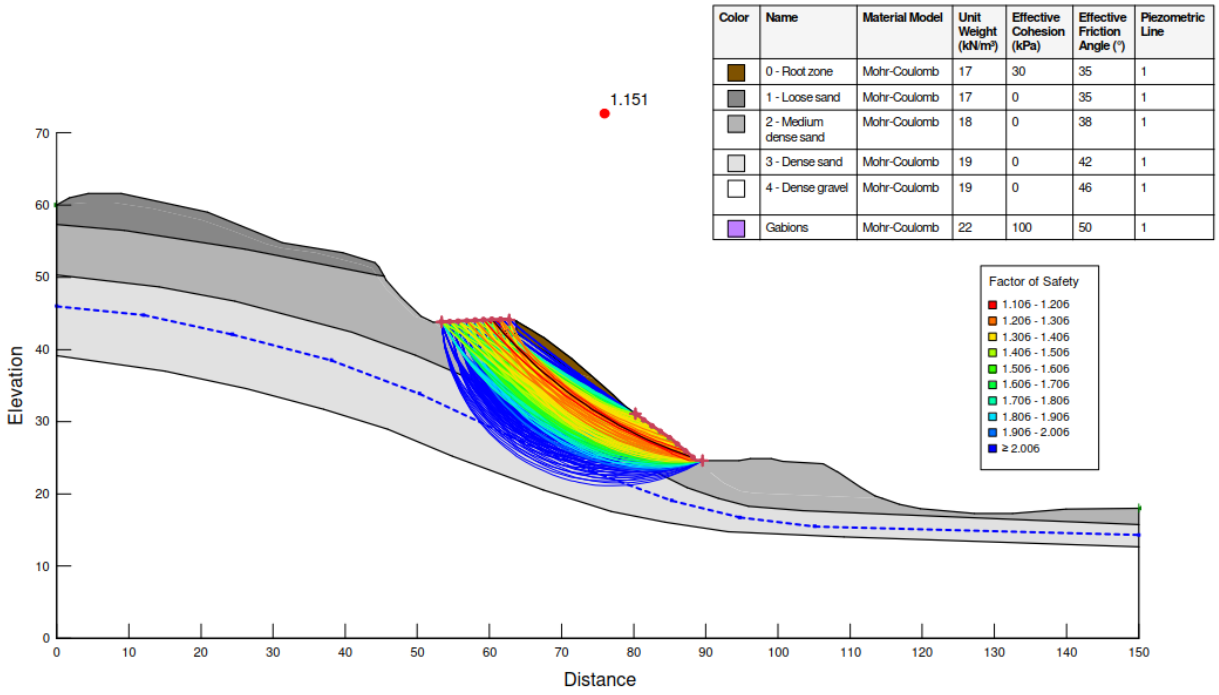

The Sandpit static stability analysis

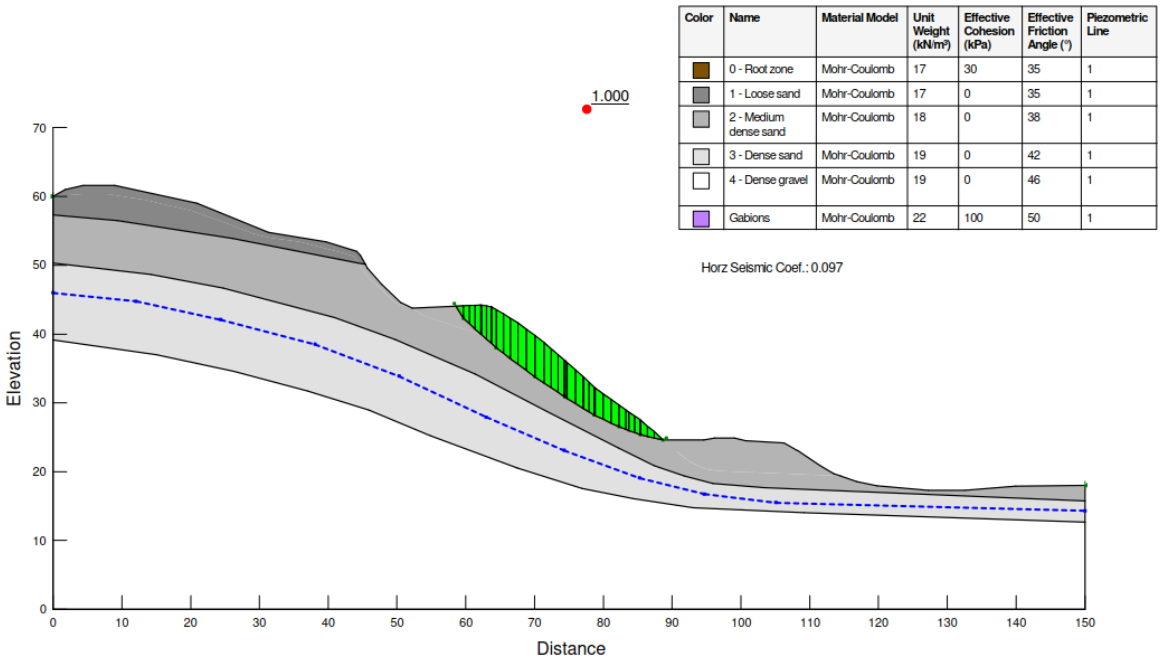

The Sandpit seismic back-analysis (critical acceleration = 0.1 g)

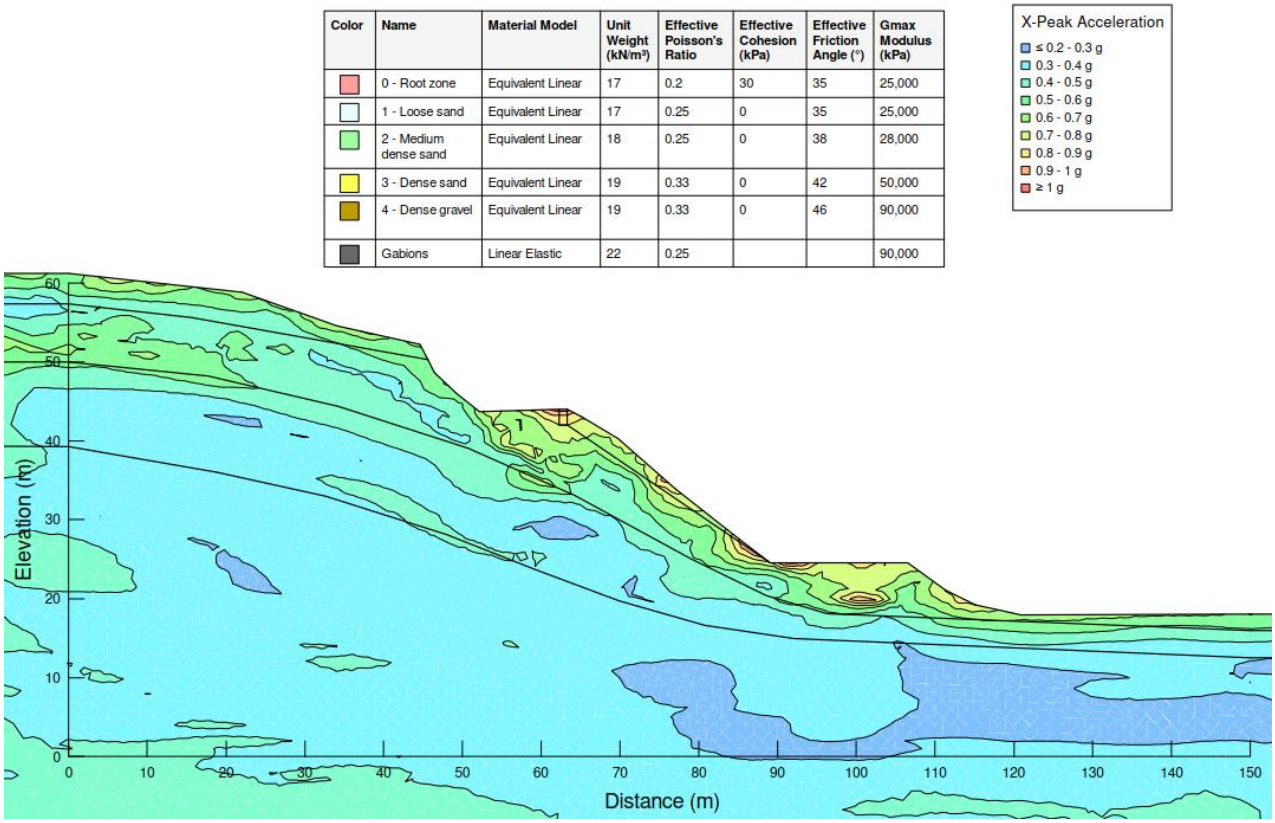

The Sandpit dynamic analysis, contours of peak horizontal acceleration

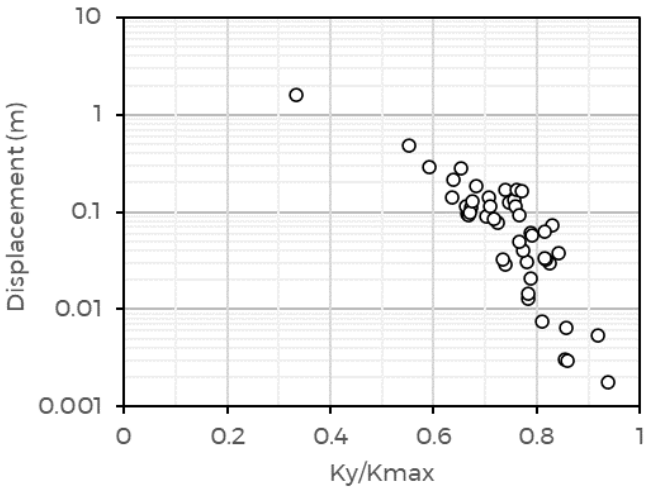

The Sandpit simulated Newmark ground displacements, shown as a function of the ratio of the yield acceleration (Ky) to the average acceleration of the landslide mass (Kmax) for the 50 slide surfaces with the lowest factors of safety.

wsp.com/nz